ABSTRACT

HIGH-SPIN ROTATIONAL BAND STRUCTURE OF ^{177}W AND ^{178}W

By

Carol Lynne Dors

The rotational band structure of ^{177}W and ^{178}W has been investigated using the techniques of in-beam gamma ray spectroscopy. Of particular interest in this region of deformed rare-earth nuclei is the anomalous behavior which occurs in *yrast* sequences at very large values of angular momentum, and the possible involvement of $i_{13/2}$ neutrons in this phenomenon. In the experiments discussed here, the $7/2^+[633]$ band in ^{177}W was populated to spin 33/2 and the ground band of neighboring ^{178}W to spin 16. The $i_{13/2}$ band in ^{177}W was compared with similar bands in other odd-A tungsten nuclei, and the results were applied to the systematics of the doubly even tungsten ground band structures.

Levels in ^{177}W were populated in the ^{177}Hf(α,$4n\gamma$) reaction. The ground state is assigned as $1/2^-[521]$; other low-lying bands which were seen include the $7/2^+[633]$, $5/2^-[512]$, and $7/2^-[514]$. The $7/2^+[633]$ band displays a highly perturbed structure which can be theoretically reproduced through Coriolis-induced mixing of higher energy positive parity bands.

The ^{177}Hf(α,$3n\gamma$) reaction was used to populate states in ^{178}W. The $K^\pi=0^+$ ground band was observed up to spin 16. On a plot of $(\hbar^2/2\mathcal{J})^{-1}$ vs. $(\hbar\omega)^2$ the band shows some deviation from normal

rotational behavior at high spin. The $K^{\pi}=2^{-}$ octupole band was located at 1045 keV and has an alternating energy sequence, with the odd spin members "favored". A pair of two-quasiparticle bands has been identified and is tentatively assigned as $K^{\pi}=6^{+}$ and $K^{\pi}=(6,7)^{-}$. The β-vibrational band was identified from spin 6 to spin 16.

A discussion of backbending and the $i_{13/2}$ neutron orbitals is made in the light of a systematic study of odd-even isotopic pairs. The result suggests a possible correlation in the tungsten nuclei between the amount of decoupling in the positive parity bands in the odd-*A* isotopes and the degree of backbending-type behavior observed in the neighboring even-even nucleus.

MSUNC-192

HIGH-SPIN ROTATIONAL BAND STRUCTURE OF ^{177}W AND ^{178}W

By

Carol Lynne Dors

A DISSERTATION

Submitted to
Michigan State University
in partial fulfillment of the requirements
for the degree of

DOCTOR OF PHILOSOPHY

Department of Chemistry
Program in Chemical Physics

1976

ACKNOWLEDGMENTS

I wish to thank Fred Bernthal for suggesting this project. His guidance on experiment details, interpretation of the results, and his assistance in preparation of this thesis are sincerely appreciated. I would also like to thank T. L. Khoo for his valuable advice and helpful time-consuming discussions.

Bill Kelly deserves my sincere gratitude for his never-ending words of encouragement and his special advice.

I would like to thank Ray Warner for the many hours he spent giving experimental assistance. His friendship and advice have been invaluable.

Thanks to Chuck King, Brian Jeltema, Clare Morgan, Larry Samuelson, and Mark Slaughter for giving of their time during the long hours of a cyclotron experiment.

I wish to thank the cyclotron engineering staff, especially Peter Miller and Harold Hilbert, for assistance in cyclotron set-up and trouble-shooting.

I would like to extend my thanks to the Nuclear Beer Group without whom Friday afternoons would not have been the same.

A special thanks to Alice Ridky for typing the final copy of this thesis under the usual pressure of a deadline.

Finally, I particularly wish to thank my parents for their encouragement, and my husband, Tim, for his perspiration, inspiration, and motivation.

TABLE OF CONTENTS

LIST OF TABLES

LIST OF FIGURES

CHAPTER I

INTRODUCTION

The purpose of this study was to elucidate the even-parity band structure of ^{177}W and to investigate any implications for the level structure of the *yrast* cascade in neighboring ^{178}W. The measurements on ^{178}W, an isotone of ^{176}Hf, were also intended to identify and characterize any high-K, multiparticle structures. The odd-even nuclear pair ^{177}W, ^{178}W was chosen on the basis of the available Nilsson deformed single-particle levels which would most likely be populated. The $7/2^+[633]$ level which originates from the spherical $i_{13/2}$ orbital would be low-lying, as should several high-Ω neutron and proton negative parity levels. The investigative technique, in-beam gamma-ray spectroscopy was chosen both because the product nuclei are not easily accessible to charged particle spectroscopy, and because the rotational bands that would be systematically populated should have characteristic "fingerprints" which would make their identification, and association with particular Nilsson levels quite unambiguous.

The experiments were performed using the Michigan State University sector-focused isochronous cyclotron running in the N=2 harmonic mode for the high energy (25-50 MeV) alpha-particle beams. When the experiments were begun, N=2 was a poorly developed mode of operation for the machine, and alpha beams were extracted largely by trial and error since the settings were not well calculated. Toward the conclusion of the experiments, state-of-the-art turn patterns could be easily

attained in about two hours, with up to 1-1/2 microamperes of beam impinging on the target. During this time also, a high voltage rf beam sweeper was built which uses deflecting plates to select only every second to eleventh beam burst, allowing timing in the range 100-500 nsec [Kh72]. In addition, a high voltage beam pulser was available to study states delayed by more than 1 μsec. Computer developments were also made in this time period to bring the Xerox Σ-7 computer perhaps to its limit of computing capability. The most useful computer development to γ-ray spectroscopists was the three parameter event recording and sorting programs. Up to three 4096-channel spectra in coincidence mode can be accumulated with data storage on magnetic tapes; "replaying" of the data with results stored on temporary disk files then allows fast, relatively efficient sorting with background subtraction included. A newer development involves installation of a CAMAC system interfaced to a PDP 11-40 computer, but for this work, only the Sigma-7 with a PDP 11-20 handling peripherals was available.

At the time the tungsten experiments were begun, Ge(Li) detectors were technically much the same as they are today. The decay studies which had been performed originally with NaI(Tl) detectors had already been redone to make use of the improved resolution of Ge(Li) detectors. The in-beam gamma-ray spectra which had originally been taken with NaI(Tl) detectors were seen to contain a profundity of supplementary data, and in fact, today the decay studies are viewed to be the supplementary ones.

The tungsten experiments that will be discussed partly involved the retaking of old data that had been obtained with NaI(Tl) detectors,

but with illuminating new results, a wealth of new states could now easily and quickly be sifted out of the pile of data, sorted into rotational bands, and included in the rapidly growing list of systematics. Ultimately the goal of nuclear experimentalists is to make the list of systematics form a simple and clear description of nuclear structure. With that goal in mind, this thesis is designed mainly to display the addition of a few more pieces of information to test the theories of deformed nuclei at moderately high spins.

The structure of the thesis will be: 1) a discussion of some of the relevant theory involving well deformed, rotating nuclei; 2) experimental data and level schemes for each nucleus; 3) a discussion of how the data fit into the applicable systematics, and any perturbation in the systematics due to this new data set.

CHAPTER II

THEORETICAL CONSIDERATIONS

In order to understand the features of spectra belonging to nuclei in the deformed rare earth region, one seeks an appropriate phenomenological model. The most successful model applicable in this region has been the Collective Model of Bohr and Mottelson which was introduced in 1952 [Bo52] to describe the rotational spectra and collective properties of deformed nuclei. The intrinsic states on which the collective properties are built, were described by Nilsson [Ni55], and the combined properties were summed up by Mottelson and Nilsson in a unified model [Mo59] which with some refinements and additions is widely used today in interpreting the level data in the mass region $150 < A < 190$.

2.1 Description of the Total Hamiltonian

The Hamiltonian for a system of nucleons moving in a non-spherical potential consists of two basic types of interactions, one which is associated with the collective motion of all nucleons and which gives rise to the rotational spectrum, the other an intrinsic motion of each nucleon in a deformed orbital giving rise to the single-particle spectrum. The Hamiltonian for a particle strongly coupled to a rotating core can be written (see e.g. Pr62 for further discussion):

$$H = H_{rot} + H_{int} \tag{1}$$

The rotational Hamiltonian may be written:

$$H_{rot} = \frac{\hbar^2}{2\mathcal{J}}(\vec{I}^2 - I_3^2) + \frac{\hbar^2}{2\mathcal{J}}(\vec{j}^2 - j_3^2) - \frac{\hbar^2}{2\mathcal{J}}(\vec{I}_+\vec{j}_- + \vec{I}_-\vec{j}_+) \qquad (2)$$

The last term in this expression contains the interaction between the particle and rotational motion, while the first and second terms refer to collective and particle motion, respectively. The total Hamiltonian may thus be reconstructed in the following way:

$$H = H_c(\text{collective variables}) + H_{int}(\text{intrinsic variables}) + H_{coup} \qquad (3)$$

with H_{coup} representing the particle-rotational coupling, and with the second term in H_{rot}, the so-called recoil term, incorporated in H_{int}.

Figure 2-1 shows a vector diagram of an odd-A deformed nucleus consisting of a single particle which is coupled to an axially-symmetric rotating core. Since the core rotates freely in space, the coordinate system using body-fixed axes (1,2,3) is chosen to simplify the description. For the axially-symmetric case, the 3-axis is the nuclear symmetry axis and the particle angular momentum, $\vec{j}$, precesses about the 3-axis with projection Ω. In the axially-symmetric case, the core angular momentum $\vec{R}$ is perpendicular to the 3-axis, and the total momentum $\vec{I}$ has a projection K equal to Ω. In a rotating system like this, it is easily verified that one influence of the rotation on the particle motion will be the familiar Coriolis effects [St72].

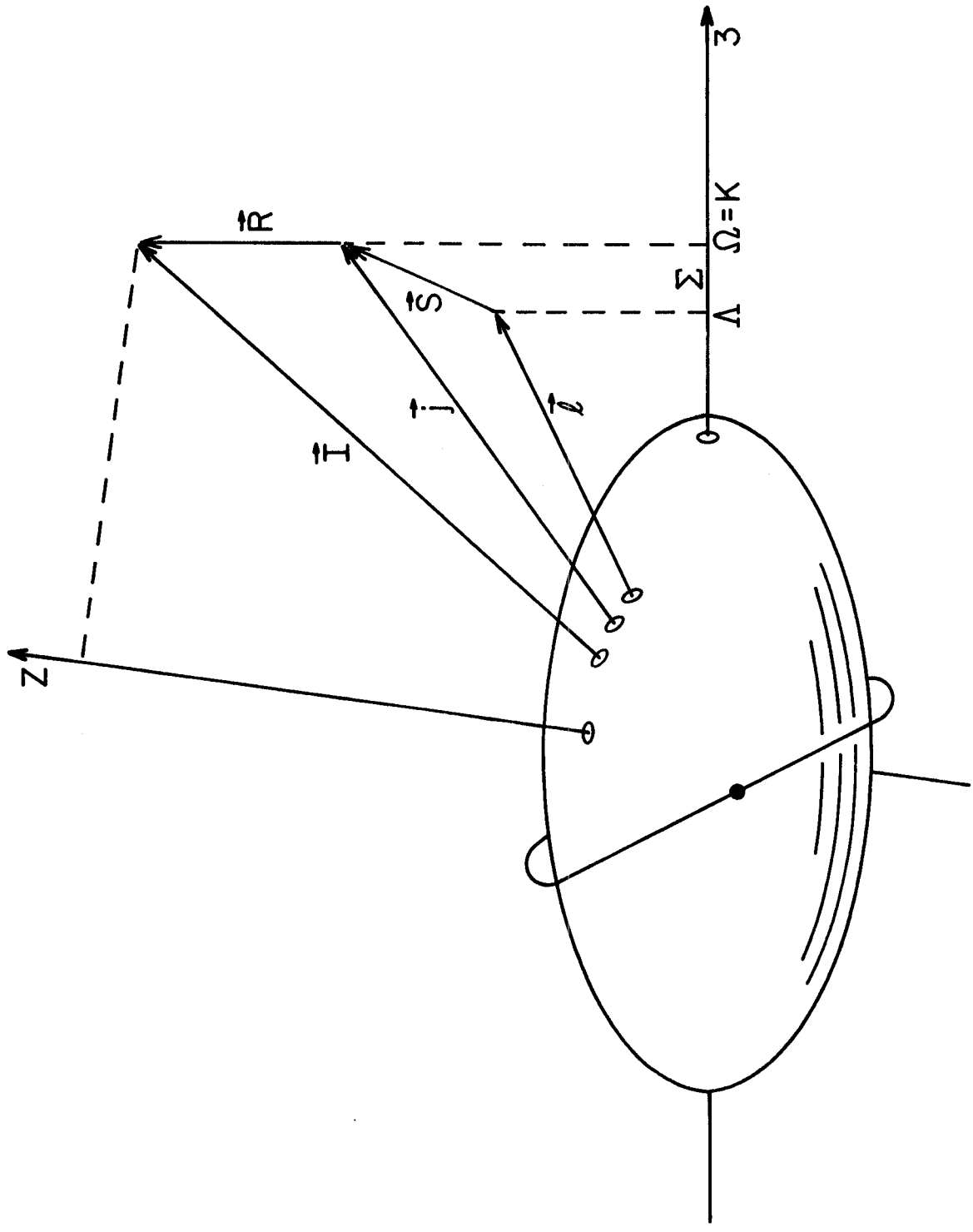

Figure 2-1. Vector diagram of a particle coupled to an axially symmetric rotating core.

2.2 Statement of the Wavefunction

In order to solve for the energy levels of the system, the wavefunction introduced is (see e.g. Pr75 for details):

$$\Psi = \chi_\Omega \mathcal{D}^I_{MK}, \tag{4}$$

a separable wavefunction consisting of the intrinsic and rotation coordinates. The wavefunction is normalized and symmetrized so that $\mathcal{D}$ gives unitary transformations from space-fixed to body-fixed coordinates, invariance with respect to 180° rotation of the 3-axis, and the total parity is the parity of the particle state:

$$\Psi = \sqrt{(2I+1)/16\pi^2}\left\{\chi_\Omega \mathcal{D}^I_{MK}(\Theta_i) + (-1)^{I-j}\chi_{-\Omega}\mathcal{D}^I_{M,-K}(\Theta_i)\right\} \tag{5}$$

2.3 Rotational and Particle-Rotation Eigenvalues

The first term in the total Hamiltonian, H_c, will yield the familiar rotational band energies:

$$E = \frac{\hbar^2}{2\mathfrak{J}}[I(I+1) - K^2] \tag{6}$$

Operating on the wavefunction with the rotation-particle coupling term in the Hamiltonian, H_{coup}, yields the following matrix elements:

$$\begin{aligned}\langle\Omega_2, K_2|-\frac{\hbar^2}{2\mathfrak{J}}(I_+j_- + I_-j_+)|\Omega_1, K_1\rangle &= -\frac{\hbar^2}{2\mathfrak{J}}\sqrt{(I\mp K_1)(I\pm K_1+1)} \\ &\times \langle\Omega_2|j_\pm|\Omega_1\rangle\, \delta_{K_1, K_2\pm 1}\, \delta_{\Omega_1, \Omega_2\pm 1}\end{aligned} \tag{7}$$

The eigenvalues of $\langle\Omega_2|j_\pm|\Omega_1\rangle$ must be evaluated using a specific particle wavefunction χ_Ω. If a Nilsson-type wavefunction is assumed, then one obtains:

$$\langle\Omega_2|j_\pm|\Omega_1\rangle = \sum_{j,\ell} C_{j\ell}^{\Omega_1} C_{j\ell}^{\Omega_2} \sqrt{(j\pm\Omega_1)(j\mp\Omega_1+1)}\ \delta_{\Omega_1,\Omega_2\pm1} \tag{8}$$

where C_j's are coefficients used to expand spherical harmonic-oscillator wavefunctions to account for the fact that in a non-spherical basis $\vec{j}$ is not a conserved quantity. For the special case where j can be considered to be a good quantum number, the simple result may be added to the Coriolis energies giving:

$$\langle\Omega_2,K_2|-\frac{\hbar^2}{2\mathcal{J}}(\vec{I}_+\vec{j}_-+\vec{I}_-\vec{j}_+)|\Omega_1,K_1\rangle = -\frac{\hbar^2}{2\mathcal{J}}\sqrt{(I\mp K_1)(I\pm K_1+1)} \times \sqrt{(j\mp\Omega_1)(j\pm\Omega_1+1)}\ \delta_{K_1,K_2\pm1}\ \delta_{\Omega_1,\Omega_2\pm1} \tag{9}$$

The first term in this Hamiltonian steps down both K and Ω, the second will step them up, mixing states differing by one K-unit via non-diagonal matrix elements. The Coriolis effect can easily be seen to be largest for states of small Ω projections in high-j orbitals. Due to pairing correlations between nucleons, these matrix elements are found to be too large and a pairing reduction factor which will be discussed later in this chapter must be included.

For $K = \Omega = \frac{1}{2}$ there will be diagonal matrix elements which have the form:

$$\langle K=\tfrac{1}{2},\ \Omega=\tfrac{1}{2}|-\frac{\hbar^2}{2\mathcal{J}}(I_+j_-+I_-j_+)|\tfrac{1}{2},\tfrac{1}{2}\rangle = \frac{\hbar^2}{2\mathcal{J}}(-1)^{I+\frac{1}{2}}(I+\tfrac{1}{2})a \tag{10}$$

where a, the decoupling parameter is given by [Og71]:

$$a = -\langle \tfrac{1}{2}|j_-|\tfrac{1}{2}\rangle = -\langle \tfrac{1}{2}|j_+|-\tfrac{1}{2}\rangle \qquad (11)$$

and is evaluated using a specific particle wavefunction χ_Ω. If again a Nilsson-type wavefunction is assumed, then a takes the form:

$$a = -\sum_j (-1)^{j+\frac{1}{2}} (j+\tfrac{1}{2}) \; |C_{j(\frac{1}{2})}|^2 \qquad (12)$$

Thus, $K = \frac{1}{2}$ bands have a perturbed structure with alternating levels lowered in energy from the normal I(I+1) energy dependence. The sign of a determines whether $(I+\frac{1}{2})$ = *even* or *odd* spin levels will be decreased in energy. In [Bu71] there is a tabulation of values of the decoupling parameters for neutron and proton $K = \frac{1}{2}$ orbitals in the N=5 and 6 shells. Experimentally, these bands are easy to locate due to the strong alternating energy sequence of levels, and they can usually be assigned to a particular orbital by studying the sense of the perturbation.

2.4 Intrinsic Wavefunctions and Nilsson Single-Particle Energies

To solve the eigenvalue problem for the single particle or intrinsic energies, a wavefunction χ_Ω with convenient particle coordinates is chosen. In the Hamiltonian, the potential used by Nilsson [Ni55] for the single particle problem consists of the following terms:

$$H_o + 2\kappa\hbar\omega(\vec{\ell}\cdot\vec{s} - \mu\vec{\ell}^2) \qquad (13)$$

where H_o is the deformed harmonic oscillator potential and may be separated into an isotropic part and a part which depends on the deformation: $H_o = H_o^o + H_\delta$. The parameters (κ,μ) are adjusted so that at zero deformation the solution will yield the empirically determined energies of the spherical shell model.

The wavefunctions formulated by Nilsson [Ni55] are linear combinations of cylindrical harmonic-oscillator functions. The lack of spherical symmetry causes j to no longer be a good quantum number; however, j_z commutes with the total Hamiltonian so that Ω is still a strictly good quantum number in this representation. Since ℓ_z and s_z commute only with H_o and not the total Hamiltonian, the eigenvectors for each Ω are, then, composed of a sum of terms each characterized by N,ℓ,Λ,Σ. N is the total number of oscillator quanta, and the other quantities are shown on the vector diagram, Figure 2-1.

Operating on the Nilsson wavefunctions with the above Hamiltonian yields eigenstates having energies which are a function of deformation. Each Nilsson level which can hold two paired nucleons is then labeled with the asymptotic quantum numbers $\Omega^\pi[Nn_z\Lambda]$. For large deformations, the $\vec{\ell}\cdot\vec{s}$ and $\vec{\ell}^2$ terms in the Hamiltonian are treated as perturbations in which case Λ, Σ and n_z (the number of nodal planes along the symmetry axis) become good quantum numbers. Levels can be calculated incorporating both quadrupole (ε_2) and hexadecapole (ε_4) deformations [Ni69] where the deformation parameter $\varepsilon_2 = \delta + \frac{1}{6}\delta^2$.

For the nuclei ^{177}W and ^{178}W, the deformation is estimated to be about $\varepsilon_2 = 0.23$, $\varepsilon_4 = 0.05$. Using a code from the University of Rochester [NILS], the Nilsson levels for this deformation were calculated for both neutrons and protons and are displayed in Figures 2-2 and 2-3.

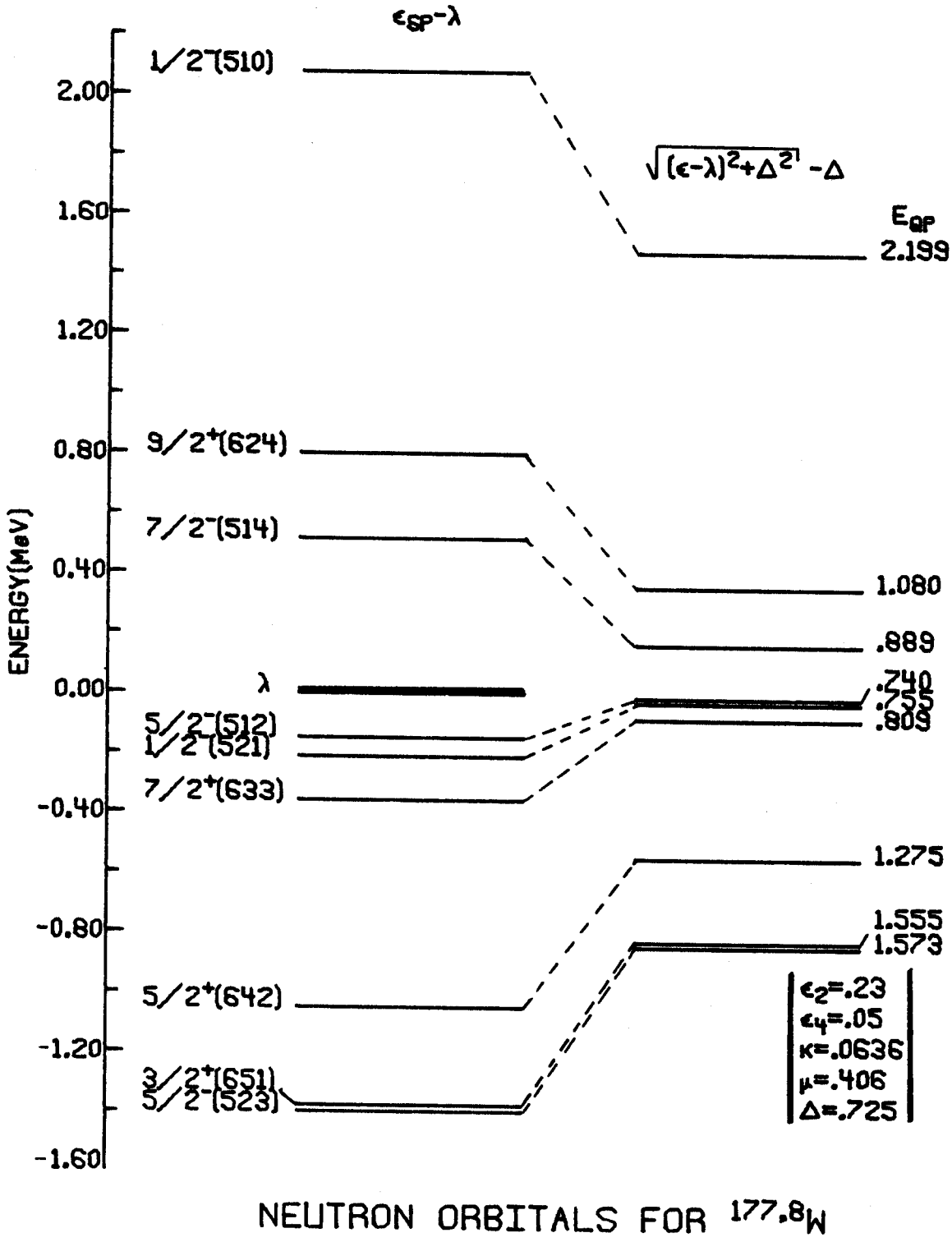

Figure 2-2. Single particle deformed neutron orbitals and quasi-particle energies for N=103, calculated with the values of the parameters which are listed above.

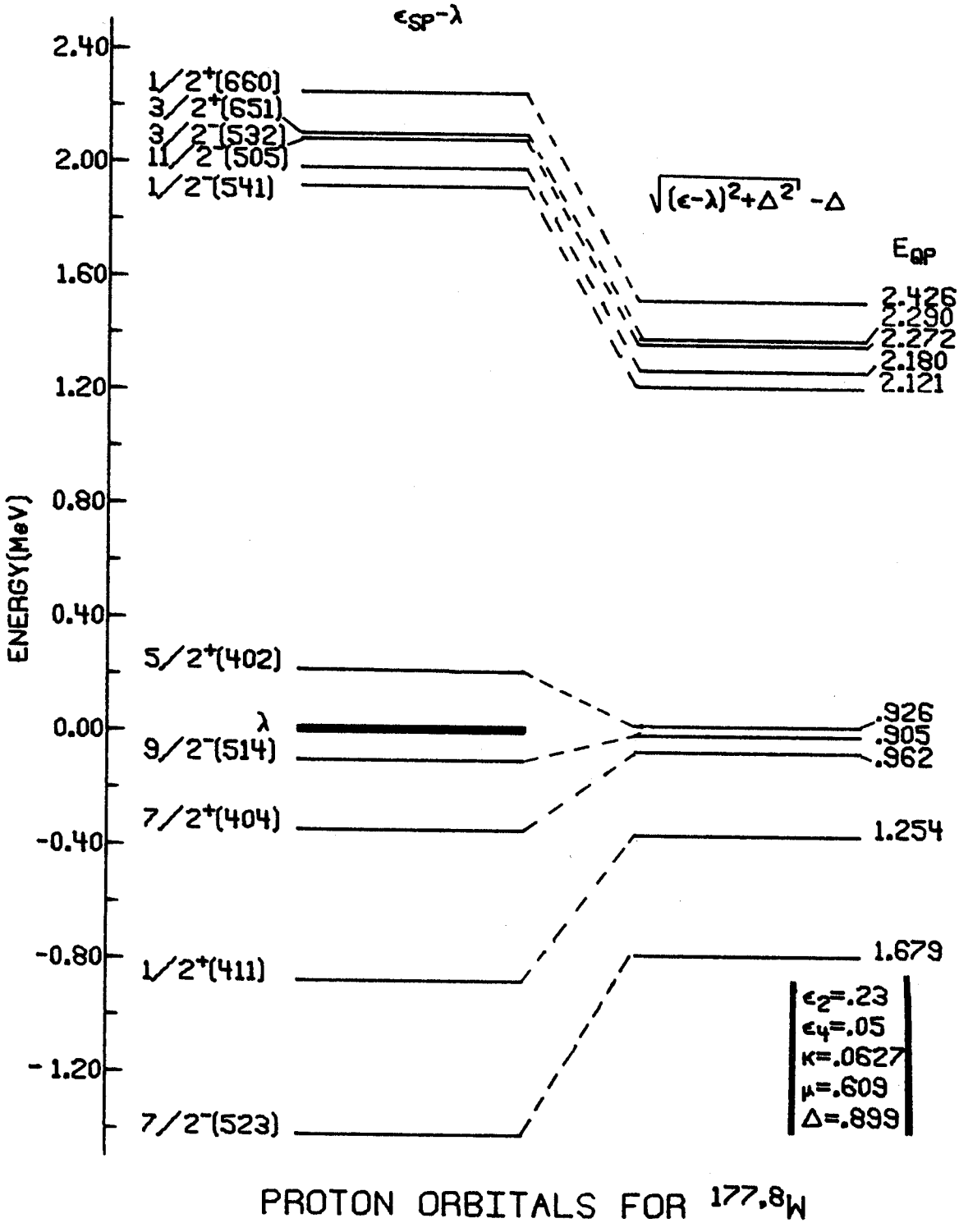

Figure 2-3. Single particle deformed proton orbitals and quasi-particle energies for Z=74 calculated with the values of the parameters which are listed above.

The most noticeable feature of the neutron orbitals is the absence of positive parity states other than those which originate in the $i_{13/2}$ spherical state. These states will have a relatively pure j-value, 13/2, since the nearest positive parity states which can easily mix with them are the $g_{9/2}$ which are about 2 MeV higher in excitation. Thus, for mixing calculations involving bands associated with the $i_{13/2}$ states, only the set of orbitals in the $i_{13/2}$ family need be included.

In Section 2.1, it was mentioned that the recoil term, $\frac{\hbar^2}{2\mathcal{J}}(\vec{j}^2-j_3^2)$, was commonly assumed to be included in the intrinsic Hamiltonian. It has recently been shown [Os75] that the Nilsson Hamiltonian in its usual form does not incorporate this term unless the model parameters κ and μ are made to be deformation dependent. A calculation of the single particle energies taking the recoil term into account explicitly has been attempted [Re76], and the authors found that the values of the potential parameters, κ and μ, obtained in their procedure gave better experimental agreement to the levels in N=89 nuclei. In general, inclusion of this term may cause a several hundred keV shift in the bandhead energies - with the largest effect occurring for bands having large values of the inertial parameter, $\frac{\hbar^2}{2\mathcal{J}}$, and for high-j low-$\Omega$ orbitals. A preliminary calculation of the positions of the $i_{13/2}$ orbitals using a Woods-Saxon potential and taking the recoil term into account [Li72] showed shifts of only about 100 keV from the positions of these states calculated with the standard Nilsson model. Until recently there was little agreement on how to handle the term correctly although a few attempts have been made (e.g. Og71), so all the calculations of intrinsic states in this thesis were done without taking the recoil term into consideration.

2.5 Treatment of Pairing Correlations

The theory of superfluidity introduced by Bardeen, Cooper, and Schreiffer in 1957 [Ba57] describes long range pairing correlations in an electron gas. A similar pairing phenomenon occurs in nuclei and the BCS model has been successfully used [Bo58] to correct Nilsson single-particle energies for this effect.

A pair of nucleons which occupy identical time-reversed orbitals interact with each other through a pairing force; a consideration of all such pairs, then, gives an energy level which is lower than the normal ground state of the nucleus. Excited states of this system are quasiparticle excitations, where a quasiparticle is a fractional (V_j^2) hole state mixed with a fractional (U_j^2) particle state. The occupation parameters U_j and V_j can be obtained from the expression [Og71]:

$$\left.\begin{matrix} U_j^2 \\ V_j^2 \end{matrix}\right\} = \frac{1}{2}\left[1 \pm \frac{\varepsilon_{sp}-\lambda}{E_{qp}}\right] \tag{14}$$

And, finally, the energies of excited states, E_{qp}, can be found from:

$$E_{qp} = \sqrt{(\varepsilon_{sp}-\lambda)^2 + \Delta^2} \tag{15}$$

where ε_{sp} are the average field single-particle energies, λ is the energy of the Fermi surface which is normally close to the last filled level in the ground state of the nucleus, and 2Δ is the energy difference between the normal and paired ground state. A value for Δ, the gap parameter, can be obtained from the experimental odd-even mass

differences, and is found to be larger, in general, for protons than for neutrons [Ni69]. The gap parameter can be suitably approximated [Ni69] by:

$$\Delta = \frac{12}{\sqrt{A}} \text{ MeV}. \tag{16}$$

The ground state of an odd-A nucleus can be shown to be a one-quasiparticle state, while the lowest intrinsic states of an even-even nucleus are two quasiparticle excitations, the ground state being a quasiparticle vacuum. Quasiparticle energies which have been calculated from the Nilsson levels shown in Figures 2-2 and 2-3 are also displayed in those figures.

It should be noted that in the BCS model, the number of nucleons is not a conserved quantity, so applicability is limited to systems with large numbers of nucleons. Also, a more sophisticated treatment should include the effects of blocking [Og71] in odd-A nuclei, i.e. pairs are hindered from occupying orbitals that are blocked by the single particle.

2.6 Summary of Eigenvalues and Discussion of Correction Terms

Thus, the total Hamiltonian for the strong coupling problem has been discussed term by term, and the matrix elements may be written, in summary:

$$E_I^{diag} = E_{qp} + \left\{\frac{\hbar^2}{2\mathfrak{J}} + B[I(I+1)-K^2]\right\}[I(I+1)-K^2+\delta_{K,\frac{1}{2}} a(-1)^{I+\frac{1}{2}}(I+\tfrac{1}{2})] \tag{17}$$

$$E_I^{coup} = -[\frac{\hbar^2}{2\mathfrak{J}} + BI(I+1)]\sqrt{(I\mp K_1)(I\pm K_1+1)}\ \sqrt{(j\mp\Omega_1)(j\pm\Omega_1+1)} \times \delta_{K_1,K_2\pm1}\ \delta_{\Omega_1,\Omega_2\pm1} \times (U_1U_2 + V_1V_2) \quad (18)$$

where the "B" terms are added according to the prescription in Li73 to account for second order effects such as rotation-vibration interactions by inclusion of a spin-dependent variable moment of inertia. The pairing reduction factor f(U,V) is written here explicitly in terms of the occupation parameters U and V.

From equation (17), it is seen that the experimental levels will consist of quasiparticle excitations, each with an associated rotational band having energy level spacings characteristic of the K-value of the orbital. The deviations from the simple I(I+1) rule will come directly from the a term for K=1/2 bands, through Coriolis mixing of the bands propagated by K,K±1 interactions, and from effects which require a variable moment of inertia description (B-term).

In even nuclei, the lowest intrinsic excitations will consist of two-quasiparticle states. They are separated in energy from the ground state by a gap of order 2Δ. Collective vibrational modes of excitation (which have not been covered in this discussion - see e.g. Pr62) may, in the even-even case, appear at lower excitations than the intrinsic two-quasiparticle levels. The simplest vibrational states, which will have rotational bands built on them, are expected at about 1 MeV excitation. The lowest energy vibrational modes which have been

identified in even-even nuclei in the rare earth deformed region are the following:

1. The β-vibration which corresponds to an axially-symmetric single quadrupole - (λ=2) phonon excitation, and which carries zero units of angular momentum along the symmetry axis.
2. The γ-vibration which is an axially non-symmetric λ=2 phonon excitation which carries two units of angular momentum along the symmetry axis.
3. The octupole vibration which is an odd parity λ=3 phonon excitation and may carry 0-3 units of angular momentum along the symmetry axis.

Usually, the γ , or one of the octupole bands will lie at the lowest energy with the β-band somewhat higher in this region. Since these bands are within the gap expected for two-quasiparticle excitations, they are relatively easy to identify.

To summarize: Both odd and even-even rare earth deformed nuclei can be discussed in the light of Nilsson-type single-quasiparticle orbitals, with the extra-core particle or pair of particles usually coupled to the rotating core. The Coriolis force will affect the coupling of the core and particle angular momenta to varying extents [St74] which is then reflected in the experimental energy levels of the system.

CHAPTER III

^{177}W EXPERIMENTAL DETERMINATIONS

3.1 Gamma-Ray Singles Spectra

The ^{177}W nuclei for all the experimental determinations were produced by the bombardment of a thin foil of ^{177}Hf by 43-50 MeV alpha particles inducing the reaction ^{177}Hf(α,4n)^{177}W. The targets were self-supporting foils of ^{177}Hf made at the Niels Bohr Institute by G. Sletten [S172]. The targets were about 1 mg/cm^2 of 91.7% isotopically enriched ^{177}Hf. The targets could be placed in one of two interchangeable chambers. The chamber which was used for the singles spectra was cylindrical allowing a detector to be positioned at any angle from 90° to 155° with respect to the beam direction.

The alpha particle beam was produced in the MSU sector-focused isochronous cyclotron. The beam current required for these experiments was >10 na for most experiments and was readily obtainable for the runs. The energy resolution of the beam was at least 0.1%, with alpha particle energies of 24 to 50 MeV available in the N=2 mode of operation. The reaction cross sections for (α,xn) reactions as a function of alpha particle energy were calculated using the code CS8N [CS8N]. The maximum cross sections for (α,2n) through (α,5n) reactions are spaced about 10 MeV apart, and the curves are broadly peaked with some overlap between them. On the peaks of the cross-section curves, the amount of contaminant production is about 3% of the total cross section. The reactions are thus moderately selective, and the optimum

alpha particle energy for a desired product nucleus could be found experimentally by minimizing production of the contaminant gamma rays.

The optimum excitation energy required to induce the (α,4n) reaction is close to 50 MeV, so the highest energy alpha beam which could be obtained by the cyclotron was used for the ^{177}W experiments. The (α,5n) product gamma rays can be seen in some of the spectra as intensely as the (α,3n) product, but in most of the runs the (α,3n) products were the main contaminants. The contaminant gamma rays were readily identifiable from the ^{178}W experiments, especially from the excitation function data.

Most of the gamma rays which are of interest in ^{177}W are below 650 keV. There is a heavy population of gamma rays below 200 keV. Therefore, the detector which was chosen for the singles experiments was a LEPS (Low Energy Photon Spectrometer). This detector is a small volume(2.5cm^3) planar Ge(Li) crystal having 0.7 keV resolution at 122 keV.

In Figure 3-1 a spectrum of the gamma rays produced by bombarding ^{177}Hf with 50.2-MeV alpha particles is shown. The LEPS was placed at 125° with respect to the beam and the counting period for this and all the singles spectra was typically about 100 minutes at counting rates of 4-8$\times$10^3 counts/sec. A copper-cadmium absorber was always used to shield the detector from X-rays which would otherwise dominate the spectrum.

The EC/β^+-decay half-life of ^{177}W is 2.2 hrs, so that in a long experiment the radioactivity from this decay is seen quite strongly. The two most prominent decay peaks in ^{177}Ta are the 115-keV and 186-keV gamma rays - the former is a triplet and the latter a doublet

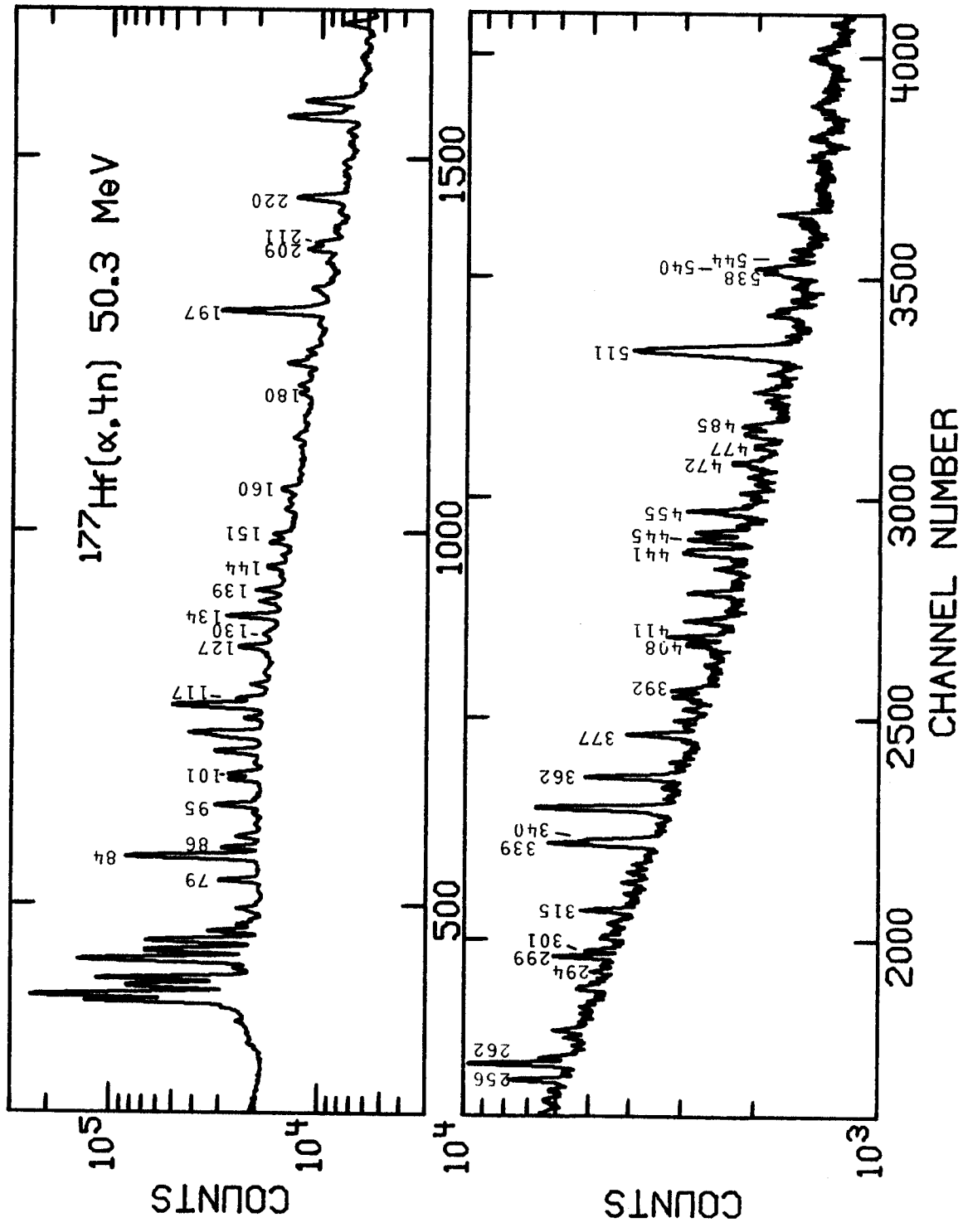

Figure 3-1. Spectrum of ^{177}Hf(α,4*n*) taken with the LEPS placed at 125°.

[A172]. A consistent analysis of these two peaks in particular using the analysis routine SAMPO [Ro69] indicated the "goodness" of the shape parameters used in the analysis from experiment to experiment. The second most prominent contaminant lines belong to the neighboring even-even tungsten isotopes ^{178}W and ^{176}W. Since the *yrast* sequences in the even-even nuclei get most of the feeding, these transitions are quite intense.

An efficiency curve for the detector was measured and the relative intensities of the gamma rays could be determined with 6-8% accuracy. In many cases the limitations on the accuracy was the stripping of the parts of peaks that were multiplets. An internal energy calibration was performed allowing the peak energies to be determined with 0.05 keV accuracy for the best cases, and within 0.1 keV accuracy for the close multiplet components. Table 3-1 contains a list of all the gamma rays seen in this experiment with the energies and relative intensities of the transitions in ^{177}W indicated along with angular distribution coefficients and transition assignments which will be discussed in later sections.

A low energy gamma-ray singles spectrum was taken with only a thin copper absorber on the LEPS in order to detect any low energy gamma rays not previously observed. The gamma ray of particular interest was the 34.1-keV transition which had been seen in the conversion electron decay spectrum [Ha74] but in none of the in-beam γ-ray spectra. The main purposes of this experiment were to determine whether the same gamma ray was strongly populated in-beam and to see if it had the appropriate relative intensity to be the intraband

Table 3-1. Energies (E_γ), relative intensities (I_γ), angular distribution coefficients, multipolarities, and spin assignments for transitions in ^{177}W. In the cases where no A_4/A_0 is listed, the angular distribution data for those transitions were fit with A_4/A_0 constrained to zero. The transitions labeled with an asterisk are components of closely spaced (<0.5 keV) doublets.

Table 3-1

E_γ (keV)	I_γ (rel. int.)	Angular Distribution Coeff.		Assignment	
		A_2/A_0	A_4/A_0		
34.09(5)	no calibration				$(\frac{9+}{2}\rightarrow\frac{7+}{2}[633])$
63.08(5)	masked by HfK_{β_1}				$\frac{11+}{2}\rightarrow\frac{9+}{2}[633]$
79.60(5)	17(1)	-0.03 ±0.02		*M*1, *E*2	$\frac{3-}{2}\rightarrow\frac{1-}{2}[521]$
84.44(5)	100(6)	-0.03 ±0.01	0.01 ±0.02	*E*1	$\frac{7+}{2}[633]\rightarrow\frac{5-}{2}[521]$
86.30(5)	14.9(9)	-0.48 ±0.01	-0.03 ±0.02	*M*1, *E*2	$\frac{13+}{2}\rightarrow\frac{11+}{2}[633]$
94.93(5)	20(1)	-0.04 ±0.07	-0.06 ±0.10		$\frac{5-}{2}\rightarrow\frac{1-}{2}[521]$
101.42*(5)	7(1)				$\frac{7-}{2}\rightarrow\frac{5-}{2}[512]$
116.91(5)	12.0(7)	-0.66 ±0.06	-0.00 ±0.09	*M*1, *E*2	$\frac{9-}{2}\rightarrow\frac{7-}{2}[514]$
127.68(5)	15.7(9)	-0.56 ±0.03	-0.08 ±0.05	*M*1, *E*2	$\frac{17+}{2}\rightarrow\frac{15+}{2}[633]$

Table 3-1 (cont'd.)

E_γ (keV)	I_γ (rel. int.)	Angular Distribution Coeff.			Assignment
		A_2/A_0	A_4/A_0		
130.29(6)	3.6(4)				$\frac{9-}{2}\rightarrow\frac{7-}{2}$[512]
134.08(5)	28(2)	-0.55 ±0.01	0.02 ±0.02	*M*1, *E*2	$\frac{15+}{2}\rightarrow\frac{13+}{2}$[633]
139.49(5)	11.5(7)	-0.67 ±0.05	-0.13 ±0.09	*M*1, *E*2	$\frac{11-}{2}\rightarrow\frac{9-}{2}$[514]
144.31(5)	8.5(6)	-0.72 ±0.01	0.18 ±0.01	*M*1, *E*2	$(\frac{23}{2})\rightarrow\frac{21+}{2}$[633]
149.28(5)	9.7(6)	0.2 ±0.1		*E*2	$\frac{13+}{2}\rightarrow\frac{9+}{2}$[633]
150.90(5)	8.1(5)	0.29 ±0.07	0.03 ±0.09		$\frac{21+}{2}\rightarrow\frac{19+}{2}$[633]
157.88(5)	4.1(3)				$\frac{11-}{2}\rightarrow\frac{9-}{2}$[512]
160.25(5)	6(1)				$\frac{13-}{2}\rightarrow\frac{11-}{2}$[514]
179.98(5)	7.7(5)	-0.82 ±0.07	-0.23 ±0.09	*M*1, *E*2	$\frac{15-}{2}\rightarrow\frac{13-}{2}$[514]

Table 3-1 (cont'd.)

E_γ (keV)	I_γ (rel. int.)	Angular Distribution Coeff.			Assignment
		A_2/A_0	A_4/A_0		
187.41(5)	6.7(5)	-0.85 ±0.07	0.0 ±0.1	*M*1, *E*2	$(\frac{25}{2})\rightarrow(\frac{23}{2})$
196.87*(5)	17(5)	0.2 ±0.1			$\frac{17^-}{2}\rightarrow\frac{15^-}{2}$[514]; ^{19}F
197.16(5)	49(3)	0.18 ±0.1		*E*2	$\frac{7^-}{2}\rightarrow\frac{3^-}{2}$[521]
209.95(5)	19(1)	0.26 ±0.03	-0.02 ±0.04	*E*2	$\frac{9^-}{2}\rightarrow\frac{5^-}{2}$[521]
211.19(5)	16.2(1)	-0.69 ±0.01	-0.03 ±0.02	*M*1, *E*2	$\frac{19^+}{2}\rightarrow\frac{17^+}{2}$[633]
213.42(5)	7.6(6)				
214.53(5)	5.4(6)	-0.5 ±0.1		*M*1, *E*2	$\frac{19^-}{2}\rightarrow\frac{17^-}{2}$[514]
217.55(5)	3.8(4)				$(\frac{27}{2})\rightarrow(\frac{25}{2})$
220.35(5)	37(2)	0.14 ±0.07	-0.1 ±0.1	*E*2	$\frac{15^+}{2}\rightarrow\frac{11^+}{2}$[633]

Table 3-1 (cont'd.)

E_γ (keV)	I_γ (rel. int.)	Angular Distribution Coeff.			Assignment
		A_2/A_0	A_4/A_0		
241.6(1)	4.2(5)				$(\frac{29}{2})\rightarrow(\frac{27}{2})$
256.23(5)	21(1)	0.21 ±0.09	-0.1 ±0.1		$\frac{11-}{2}\rightarrow\frac{7-}{2}$[514]
261.79(5)	44(3)	0.02 ±0.1			$\frac{17+}{2}\rightarrow\frac{13+}{2}$[633]
294.35(5)	5.7(5)	-1.2 ±0.1		*M*1, *E*2	$\frac{23+}{2}\rightarrow\frac{21+}{2}$[633]
299.52(5)	25(2)	0.17 ±0.02	-0.06 ±0.03	*E*2	$\frac{13-}{2}\rightarrow\frac{9-}{2}$[514]
301.72(5)	11.0(8)	0.15 ±0.07	0.00 ±0.00	*E*2	$\frac{11-}{2}\rightarrow\frac{7-}{2}$[521]
315.84(5)	21(1)	0.20 ±0.06	-0.10 ±0.07	*E*2	$\frac{13-}{2}\rightarrow\frac{9-}{2}$[521]
338.97(5)	48(3)	0.28 ±0.04	-0.04 ±0.04	*E*2	$\frac{19+}{2}\rightarrow\frac{15+}{2}$[633]
340.19(5)	31(2)	0.17 ±0.08	-0.2 ±0.1	*E*2	$\frac{15-}{2}\rightarrow\frac{11-}{2}$[514]

Table 3-1 (cont'd.)

E_γ (keV)	I_γ (rel. int.)	Angular Distribution Coeff.			Assignment
		A_2/A_0	A_4/A_0		
362.08(5)	51(3)	0.26 ±0.03	-0.04 ±0.04	*E*2	$\frac{21+}{2}\rightarrow\frac{17+}{2}$[633]
376.98*(5)	39(2)				$\frac{17-}{2}\rightarrow\frac{13-}{2}$[514]; ^{177}Ta
392.44(5)	12.9(9)	0.20 ±0.04	0.02 ±0.05	*E*2	$\frac{15-}{2}\rightarrow\frac{11-}{2}$[521]
404.96(6)	3.6(4)				$(\frac{27}{2})\rightarrow(\frac{23}{2})$
408.62(5)	20(1)	0.18 ±0.05	0.00 ±0.09	*E*2	$\frac{17-}{2}\rightarrow\frac{13-}{2}$[521]
411.27(5)	27.4(2)	0.12 ±0.04	-0.07 ±0.05	*E*2	$\frac{19-}{2}\rightarrow\frac{15-}{2}$[514]
441.32(6)	34(2)	0.2 ±0.2		*E*2	$\frac{21-}{2}\rightarrow\frac{17-}{2}$[514]
445.17(5)	31(3)	0.26 ±0.05		*E*2	$\frac{23+}{2}\rightarrow\frac{19+}{2}$[633]
454.98(6)	37.8(2)	0.29 ±0.03	-0.02 ±0.03	*E*2	$\frac{25+}{2}\rightarrow\frac{21+}{2}$[633]

Table 3-1 (cont'd.)

E_γ (keV)	I_γ (rel. int.)	Angular Distribution Coeff.			Assignment
		A_2/A_0	A_4/A_0		
466.95(6)	10(1)	0.2 ±0.1		*E*2	$\frac{19-}{2} \rightarrow \frac{15-}{2}$ [521]
471.64(6)	22(2)	0.22 ±0.03	-0.06 ±0.04	*E*2	$\frac{23-}{2} \rightarrow \frac{19-}{2}$ [514]
484.82(7)	15(2)				$\frac{21-}{2} \rightarrow \frac{17-}{2}$ [521]
496.82(7)	17.1(1)	0.3 ±0.2			$\frac{25-}{2} \rightarrow \frac{21-}{2}$ [514]
525.59(7)	13(1)				$\frac{27-}{2} \rightarrow \frac{23-}{2}$ [514]
538.42(8)	25(2)	0.3 ±0.1		*E*2	$\frac{27+}{2} \rightarrow \frac{23+}{2}$ [633]
540.10(9)	29(2)	0.27 ±0.08		*E*2	$\frac{29+}{2} \rightarrow \frac{25+}{2}$ [633]
543.7(1)	11(1)				$\frac{25-}{2} \rightarrow \frac{21-}{2}$ [521]
546.3(1)	10(1)	0.4 ±0.3			$\frac{29-}{2} \rightarrow \frac{25-}{2}$ [514]

Table 3-1 (cont'd.)

E_γ (keV)	I_γ (rel. int.)	Angular Distribution Coeff.		Assignment	
		A_2/A_0	A_4/A_0		
612.1(2)	16(2)	0.7 ±0.5		*E*2	$\frac{33+}{2} \rightarrow \frac{29+}{2}$ [633]
613.6(1)	14(2)				$\frac{31+}{2} \rightarrow \frac{27+}{2}$ [633]

$9/2^+ \rightarrow 7/2^+$ cascade transition. Indeed, it was seen and the energy was well measured. The intensity, however, could not be accurately determined since there were no calibration sources available having more than one peak in the range that was being studied. The efficiency curve for the detector is well-known above about 50 keV, but below this value the curve is changing so rapidly that accurate extrapolation is not possible.

A portion of the low-energy spectrum is shown in Figure 3-2. From this spectrum, it is evident that there is no prominent low energy gamma ray besides the 34-keV gamma, and that, although it is relatively weak, further in-beam experiments could be carried out on the 34-keV transition in order to determine its placement.

3.2 Angular Distributions

When the incoming alpha particles impinge upon the target nuclei with velocity $\vec{v}$, they align the nuclei such that the angular momentum vectors $(\vec{r}\times\vec{v})$ are all predominantly in a plane perpendicular to the beam. As these nuclei decay by emitting electromagnetic radiation, they lose some of the original alignment with each transition. In [Jo73] it is noted that the lowest members of a band will have only 20-50% of the original alignment. Although the mixing ratios of dipole and quadrupole radiation cannot be very accurately determined using these distributions, the qualitative information contained in the shapes of the curves can be helpful in confirming placements of gamma rays in the level scheme.

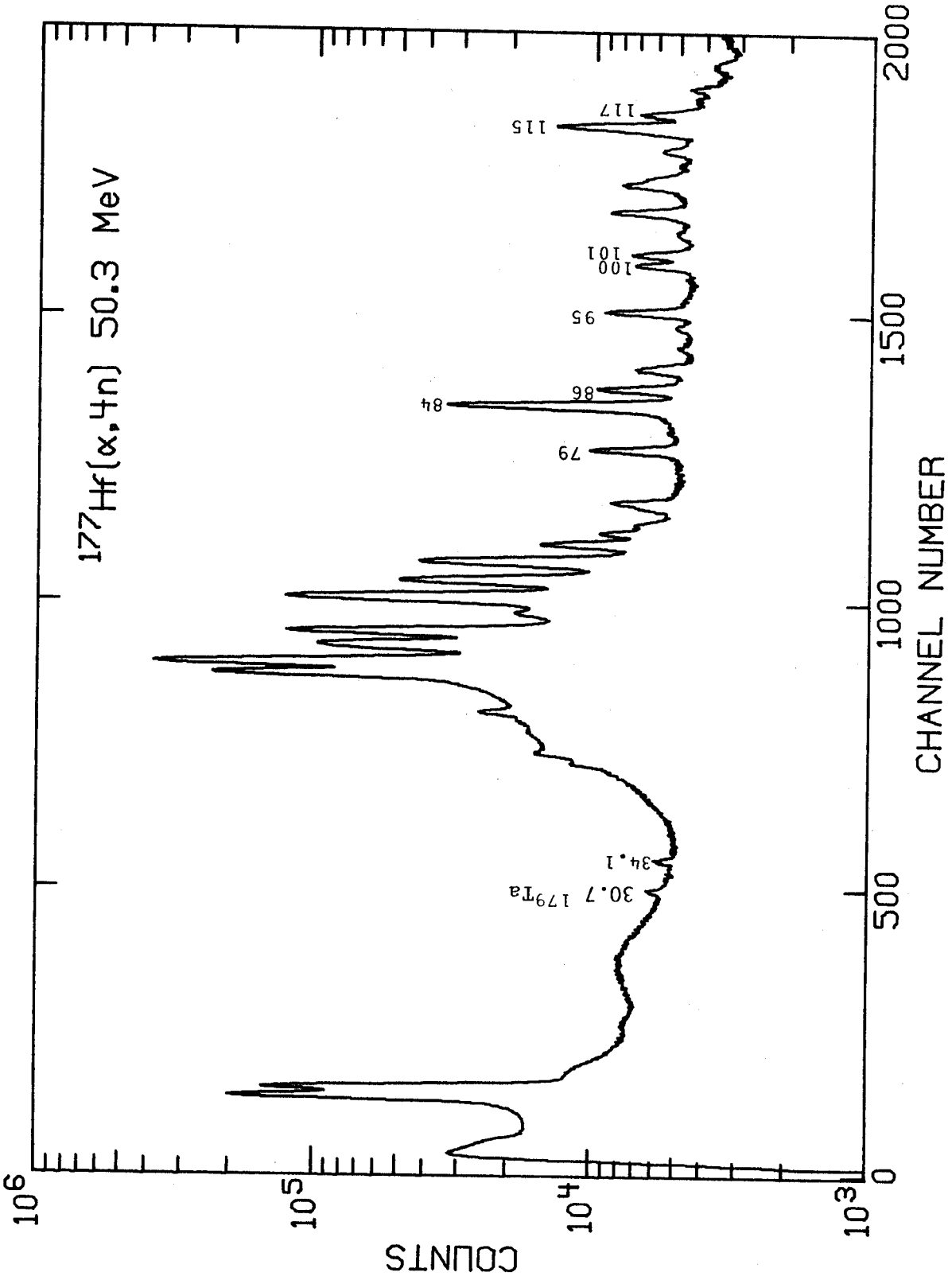

Figure 3-2. The low energy portion of the high gain spectrum taken with the LEPS.

In order to measure the anisotropies of the gamma rays, the LEPS was placed about 3" from the target on a moveable arm and singles spectra were taken at 90°, 105°, 125°, and 145° with respect to the beam direction. Since the X-rays are emitted isotropically, the X-ray intensity can be used to normalize the runs. The normalized intensities are fitted to the equation

$$I = 1 + (A_2/A_0)P_2(\cos\theta) + (A_4/A_0)P_4(\cos\theta)$$

The data along with the fitted curves for some of the gamma rays in ^{177}W are shown in Appendix D. Angular distributions of a few gamma rays from each band are displayed, with the data transposed to the 0-90° quadrant which is plotted. Since the distributions are symmetrical about 90°, only one quadrant is shown. The angular distributions that are not shown in these figures were either very weak, or parts of multiplets and so had very large error bars on the values of the transition intensities. The values of A_2/A_0 and A_4/A_0 from this experiment are also listed in Table 3-1 along with the multipolarities deduced from these values. Where a good value for A_4/A_0 could not be obtained, the data were refit with values for A_4/A_0 set equal to zero. These are shown in the table with no A_4/A_0 indicated.

3.3 Gamma-Ray Lifetimes

The measurement of the half-lives of gamma-rays can provide a valuable tool in the placement of some intraband transitions and the confirmation of K-values for the bands. In ^{177}W, the gamma-ray

lifetimes in the range of 5 nsec to 500 nsec were measured by performing two timing experiments. The first utilized the time bunching of particles in a cyclotron, each bunch being associated with an rf cycle. In the second experiment, 8 of every 9 of the bunches was swept away by a pair of deflecting plates. In both cases, the decay of the gamma rays between the beam bursts was studied.

Two parameter (E_γ-t) data are acquired by the data acquisition program TOOTSIE written by D. Bayer [TOOTS]. The program allows for 10 time bands to be set and the appropriate gamma spectra are channeled into these bands. One band is set on the prompt portion of the TAC for energy identification, while the other 9 are evenly spaced between beam bursts.

Using the LEPS as a start and the cyclotron RF for the stop signal, a TAC peak with 9 nsec FWHM can be easily obtained. Thus it is possible to measure the half-lives of some γ-rays decaying between beam bursts. For 50 MeV alpha particles, since the time between bursts is about 49 nsec, lifetimes as short as 5 nsec can be readily measured. In Figure 3-3, nine spectra taken between beam bursts during the $^{177}Hf(\alpha,4n)$ reaction are shown. The spectrum at the top of the page is the least delayed, the spectrum at the bottom is the most delayed. The most prominent delayed transitions which were seen in this experiment were the 84-keV line, the 79-, 95-, 101-keV lines, and the 106-, 237-, and 352-keV lines. The latter three transitions belong to the ground band of ^{178}W and have a measured half-life of 10 nsec. The 197-keV transition of ^{19}F having a half-life of 87 nsec is seen in these spectra to show little measurable decay. The 79-, 95-, and 101-keV

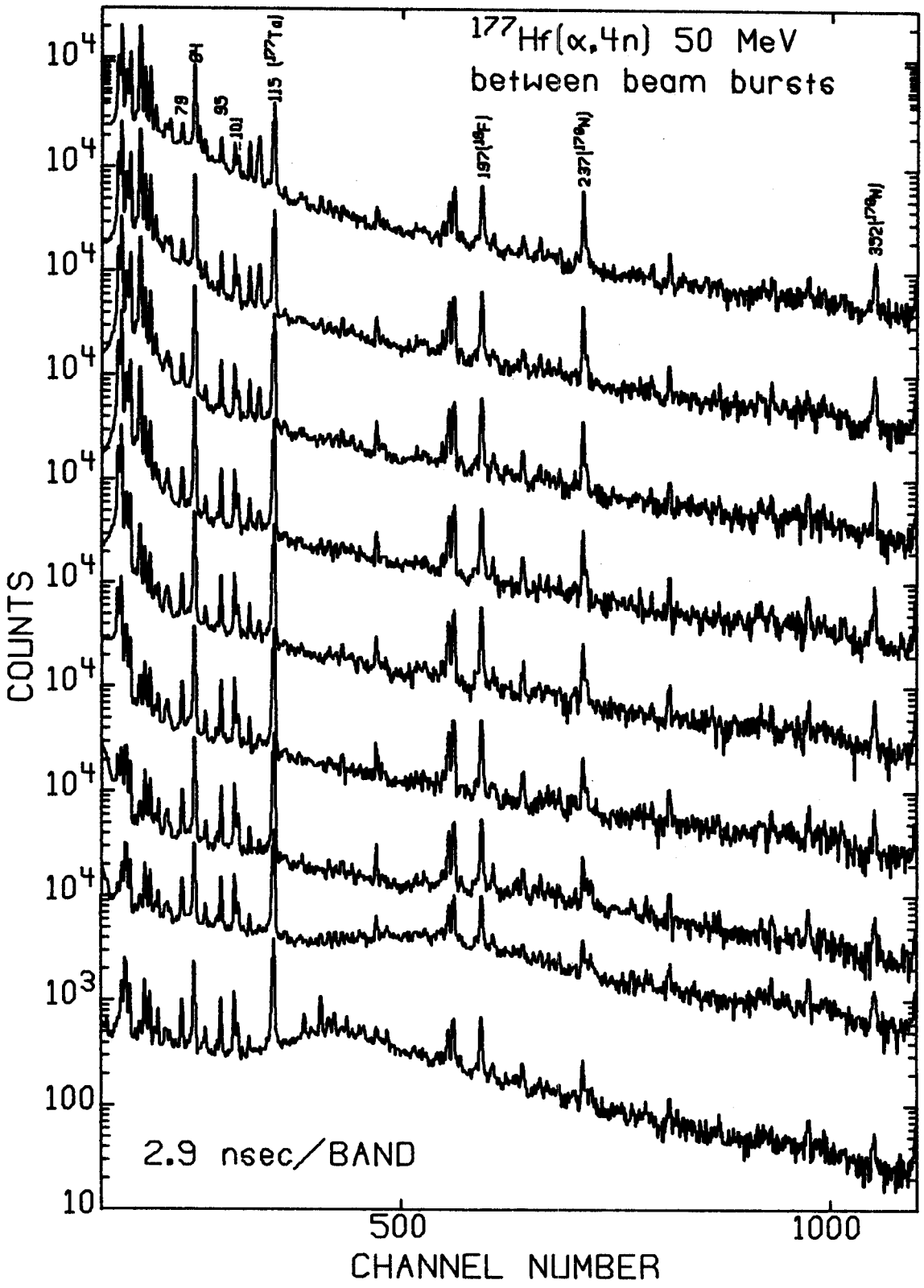

Figure 3-3. Spectra taken between beam bursts during the ^{177}Hf(α,4n) reaction. Delay time increases with each spectrum from top to bottom.

peaks decay to some extent in the course of 27 nsec but a further sweeping experiment was performed to accurately measure their lifetimes. The half-life of the 84-keV transition was measured in this experiment to be 9.7±0.7 nsec. The relevant data for the 84-keV half-life are plotted in Figure 3-4.

In the 1 of 9 sweeper experiment, the 101-keV gamma ray was seen with a lifetime at 40±3 nsec. The 79- and 95-keV states also had components with the same half-life. The data from this experiment are plotted in Figure 3-5.

3.4 Excitation Functions

For a description of the process by which levels in a (particle,xn) reaction are populated see for example New70. Here, it will be sufficient to note that as the energy of the incoming particle is increased, the population shifts to higher spin levels. Thus, at least within a band, another confirmation of the correct placement of a gamma ray can be made by comparing the change in relative intensity with an increase in beam energy, normalizing to an intense gamma ray either at the bottom or top of the band.

The excitation function data set for ^{177}W was taken as part of a study for ^{178}W. Singles spectra were taken with an 8% efficient detector (detector efficiencies are relative to the efficiency at 1.33 MeV of a 3"x3" NaI(Tl) detector 25cm from target) at beam energies of 34, 38, 43 and 46 MeV. The (α,4n) reaction cross section peaks at an alpha particle energy of 50 MeV. The 43 and 46 MeV beams were well below

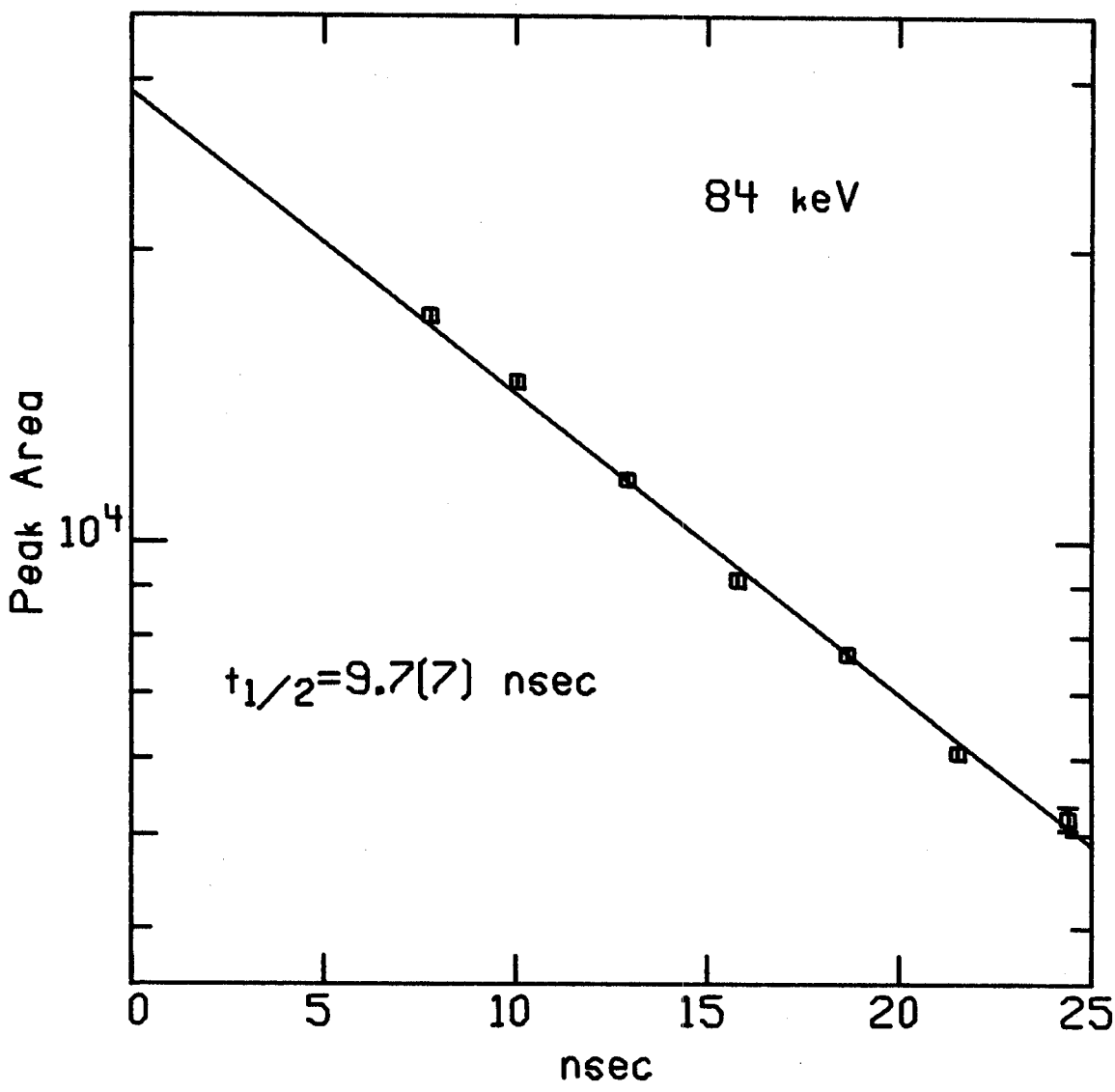

Figure 3-4. The half-life data for the 84-keV transition in ^{177}W.

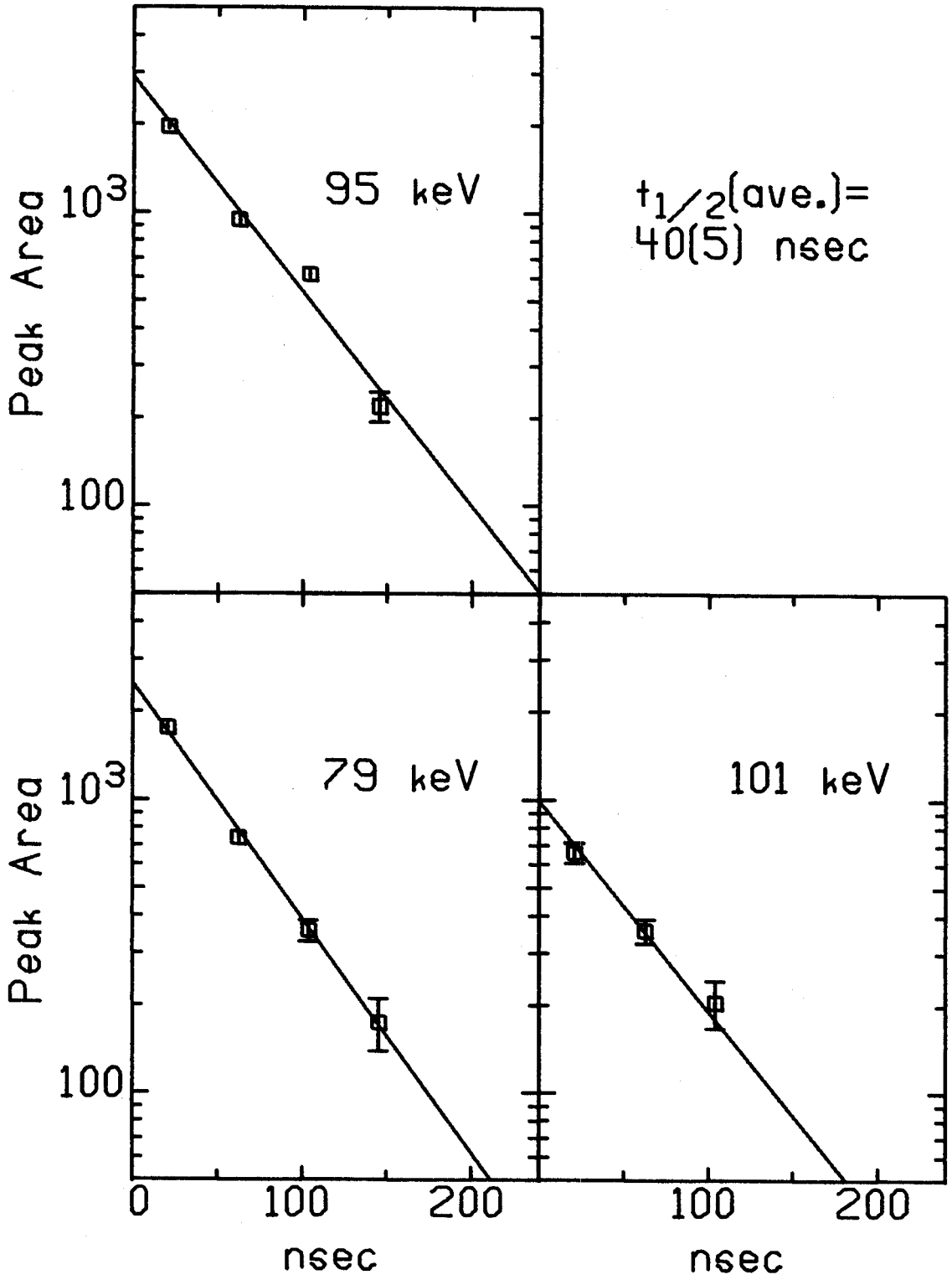

Figure 3-5. The half-life data for the 101-, 79-, and 95-keV transitions in ^{177}W.

this maximum, but the $(\alpha,4n)$ gamma rays are strong enough in these spectra to obtain some information about the relative spins of the more intense transitions. The spin assignments for ^{177}W were confirmed by the excitation function data, but no placements were made entirely on the basis of these data.

3.5 Gamma-Gamma-Time Coincidences

The most important and most extensive type of experimental data which were taken for this study consisted of three parameter-γ-γ-t-coincidences. In this experiment two detectors were placed about 2" away from the target at 180° with respect to each other. The energies of gamma rays from each detector, as well as the time between them are recorded as a word on magnetic tape. A typical experiment consists of recording about 3×10^7 events.

The prompt gamma rays which form a cascade will occur within 100 psec of each other. Using a 10% detector with a closed end coaxial shape, and a 7% efficient detector of the same shape, a time resolution of 15 nsec FWHM was obtained. Due to walk in the timing information of the low energy signals, the TAC peak generally had an asymmetric shape with the low energy gammas producing a tail which had to be included when setting a prompt time gate. By sorting the gamma rays into sequential time intervals, the prompt gammas as well as the delayed gamma rays could be studied with chance or random background subtracted.

As well as sorting gamma ray spectra according to the time when they occurred, the spectra were sorted according to energy gates set on either detector while displaying everything that was in coincidence in the other detector. The displayed spectra were also background subtracted. Using the program KKRECOVERY by C. B. Morgan [KKREC], up to 120 2048-channel spectra may be generated in the sorting process. The sorting process takes about 30 minutes per tape (3 million events) on the Xerox Σ7 and thus it is feasible to set gates on every peak, in both detectors.

After performing the experiment with the two detectors mentioned above, it became clear that the large density of low energy gamma rays required a coincidence experiment with the high resolution LEPS detector. The LEPS is such a small volume detector that only 9 million events were acquired in 24 hours, but the data were highly resolved and many of the level assignments were made on the basis of these data.

In Appendix C important coincidence gates that were used to make the level assignments are shown. In order to display the high energy coincidences, spectra taken from the first coincidence experiment are shown. To display low energy coincidences, spectra, or parts of spectra taken from the LEPS high resolution experiment are shown. The spectra are arranged according to increasing energy within a band with the cascades first, then the crossovers.

The coincidence information was used to construct a tentative level scheme. The data from the angular distributions, excitation functions, and singles spectra were then used to lend support to the

scheme. The rotational structure of ^{177}W which was generated from these experiments is shown in Figure 3-6. Three bands, the $7/2^{+}[633]$, $1/2^{-}[521]$, $7/2^{-}[514]$ are strongly populated. The identification and characteristics of the three prominent bands, and the tentatively assigned $5/2^{-}[512]$ band will be discussed in the next chapter.

Figure 3-6. Level scheme of ^{177}W. Except for the members of the $1/2^{-}[521]$ ground band, every level should have added to it an energy Δ. Transitions labeled with an asterisk are members of close-spaced (<0.5 keV) doublets.

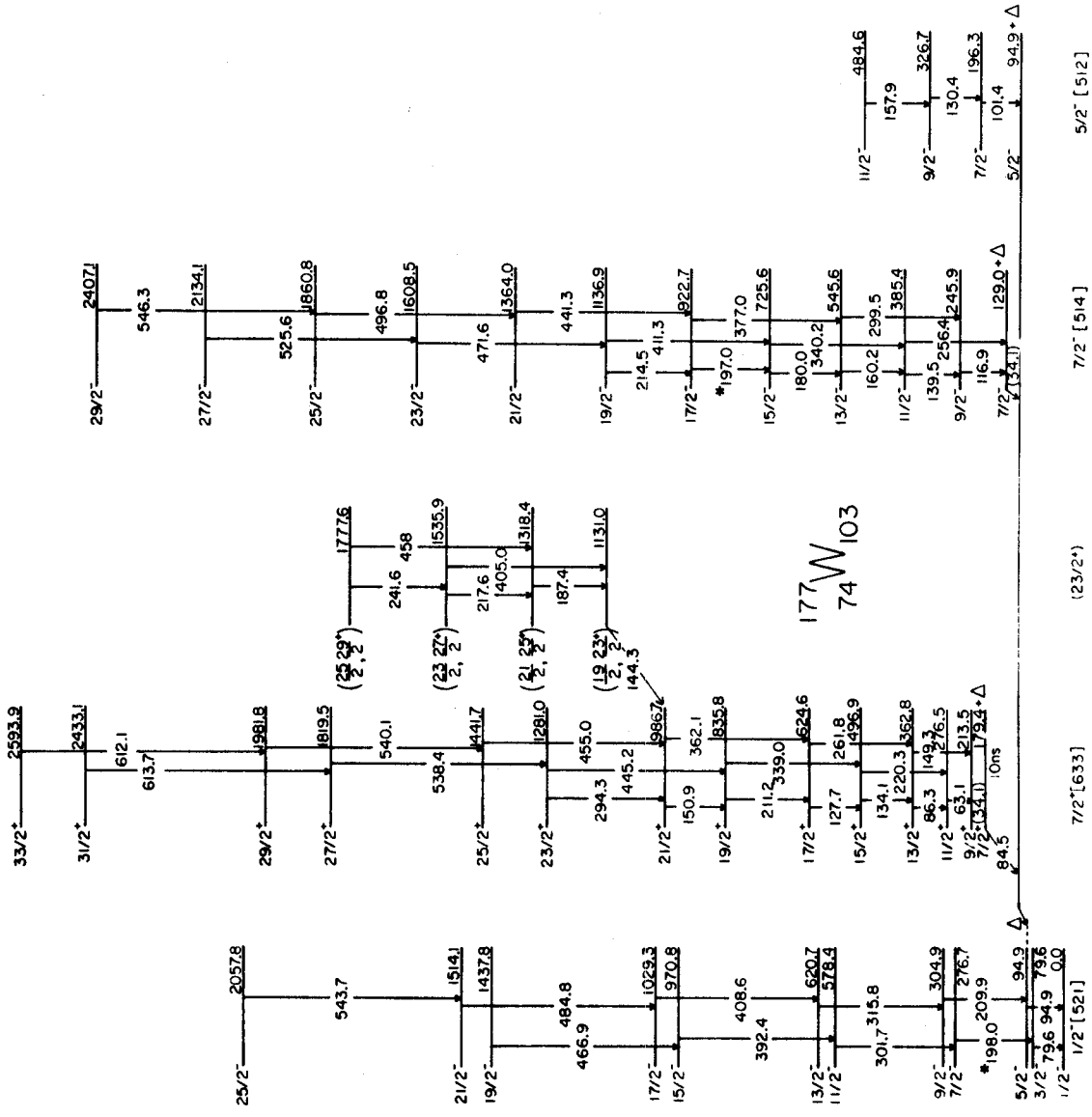
177 74W 103
7/2⁻[633]
(23/2⁺)
7/2⁻[514]
5/2⁻[512]
1/2⁻[521]
33/2⁺
31/2⁺
29/2⁺
27/2⁺
25/2⁺
23/2⁺
21/2⁺
19/2⁺
17/2⁺
15/2⁺
13/2⁺
11/2⁺
9/2⁺
7/2⁺
29/2⁻
27/2⁻
25/2⁻
23/2⁻
21/2⁻
19/2⁻
17/2⁻
15/2⁻
13/2⁻
11/2⁻
9/2⁻
7/2⁻
5/2⁻
3/2⁻
1/2⁻
25/2⁻
21/2⁻
19/2⁻
17/2⁻
15/2⁻
13/2⁻
11/2⁻
9/2⁻
7/2⁻
5/2⁻
2593.9
2433.1
2407.1
2134.1
1860.8
1608.5
1364.0
1136.9
922.7
725.6
545.6
385.4
245.9
129.0
94.9
0.0
612.1
613.7
546.3
525.6
496.8
471.6
441.3
411.3
377.0
340.2
299.5
256.4
198.0
981.8
819.5
540.1
538.4
441.7
281.0
455.0
294.3
445.2
986.7
362.1
835.8
339.0
624.6
261.8
496.9
220.3
362.8
149.3
276.5
213.5
179.4
84.5
1777.6
1535.9
1318.4
1131.0
458
241.6
217.6
405.0
187.4
144.3
2057.8
1514.1
1437.8
1029.3
970.8
620.7
578.4
304.9
276.7
543.7
484.8
466.9
408.6
392.4
315.8
301.7
209.9
94.9
79.6
0.0
484.6
326.7
196.3
157.9
130.4
101.4
*197.0
180.0
160.2
139.5
116.9
(134.1)
*198.0
150.9
211.2
127.7
134.1
86.3
63.1
(34.0)
(25 29⁺ / 2, 2)
(23 27⁺ / 2, 2)
(21 25⁺ / 2, 2)
(19 23⁺ / 2, 2)

Figure 3-6.

CHAPTER IV

^{177}W EXPERIMENTAL RESULTS

4.1 The 1/2$^-$[521] Band

The first 4 members of this band were previously seen in the decay of ^{177}Re which was studied using conversion electron [Ha75] and gamma ray [Go70] techniques. The conversion electron study indicated that the 1/2$^-$[521] is the ground state in ^{177}W. The transition between the 7/2$^-$ and 5/2$^-$ band members was seen in decay, but not in the present study.

In the (α,4n) reaction, the band was populated up to spin 25/2. Only crossover transitions were seen, as is usually the case for a strongly decoupled K=1/2 band. The rotational constant, $\frac{\hbar^2}{2\mathcal{J}}$, calculated by fitting the first 3 energy levels to the equation

$$E = E_o + \frac{\hbar^2}{2\mathcal{J}}[I(I+1) + a(-1)^{I+1/2}(I+\tfrac{1}{2})]$$

has the value 14.91 keV for this band, while the decoupling parameter, a, is +0.70. As expected,the value of $\frac{\hbar^2}{2\mathcal{J}}$ decreases higher in the band, while second order effects e.g. breakdown of pairing correlations due to Coriolis-induced decoupling, increase with spin - a fact reflected in an increase in the calculated value for the decoupling constant if higher levels in the band are used in the computation. To account for these effects, a third parameter, B, which is second order in I(I+1) could be included to incorporate the variable moment of inertia, thus

giving a better fit to the data. This parameter was used in identifying the other negative parity bands, but a two parameter fit was sufficient for identification of the $1/2^-[521]$ band. Bu71 contains a tabulation of these parameters for various bands in odd proton and odd neutron nuclei in the deformed region. The values for the $1/2^-[521]$ band in ^{177}W are consistent with the same band in other nuclei with $\varepsilon_2 = 0.2\text{-}0.3$.

4.2 The $7/2^+[633]$ Band

The $7/2^+[633]$ bandhead appears to feed either directly into the $1/2^-[512]$ ground band, or, in accordance with the coincidence data taken by Griffin in the decay of ^{177}Re [Gr76], into the $5/2^-[512]$ bandhead whose location above the 95-keV level is not known and is designated as Δ. The $7/2^+[633]$ band deexcites through a very strong $E1$ transition, the 84.3-keV gamma ray. The bandhead has a half-life of $\simeq$10 nsec. Both in ^{173}Hf and ^{175}Hf a corresponding situation exists [Hu73]. A comparison of the gamma-ray transition rates compared to the Weisskopf estimates, F_w, given in Table 4-1 shows that the [633]$\rightarrow$[512] transition in ^{177}W is $\approx$14 times faster than the corresponding one in ^{177}Hf, and proceeds $\approx$6 times faster than the same transition in ^{175}Hf.

Table 4-1. Hindrance Factors for [633]$\rightarrow$[512] Transitions

	E_γ (keV)	$(T_{1/2})_\gamma$(exp)($\times 10^9$sec)	$F_w=(T_{1/2})_\gamma(\text{exp})/(T_{1/2})_\gamma(\text{Weiss})$
^{173}Hf	90.5	54.2	3.1×10^5
^{175}Hf	207.4	2.5	1.5×10^5
^{177}W	84.4	5.7	2.3×10^4

The rotational band which is built on this Ω=7/2 member of the $i_{13/2}$ group of orbitals is a highly perturbed structure. Figure 4-1 shows the band plotted in the usual way, E_I-$E_{I-1}/2I$ versus $2I^2$. On a graph like this, a well-behaved rotational band which follows the prescription

$$E_I = E_o + \frac{\hbar^2}{2\mathcal{J}} I(I+1) + BI^2(I+1)^2$$

will fall on a straight line with the rotational parameter $\frac{\hbar^2}{2\mathcal{J}}$ as the intercept and the slope equal to the second order rotational parameter, B. For a deformed nucleus with a single particle strongly coupled to a rotating core, this simple two parameter rotational equation should approximately hold. In the case of high-j ($i_{13/2}$,$h_{11/2}$ or $h_{9/2}$) orbitals, the Coriolis force will be large and the off-diagonal elements of the Hamiltonian will produce a highly distorted set of energy levels as shown in Figure 4-1.

In order to analyze this band, a bandfitting procedure as outlined in Be74 was used, proceeding in the following manner: First, the positions of the unperturbed average-field single-particle levels that originate in the $i_{13/2}$ spherical state were estimated for the appropriate deformation using the computer code of Nilsson [Ni69]. The parameters necessary for this calculation are ε_2, ε_4, κ_n, and μ_n. The deformation parameters, ε_2 and ε_4, were extrapolated from a plot of theoretical predictions for rare earth nuclear deformations found in Nilsson's paper [op. cit.], and κ_n and μ_n were obtained from equations

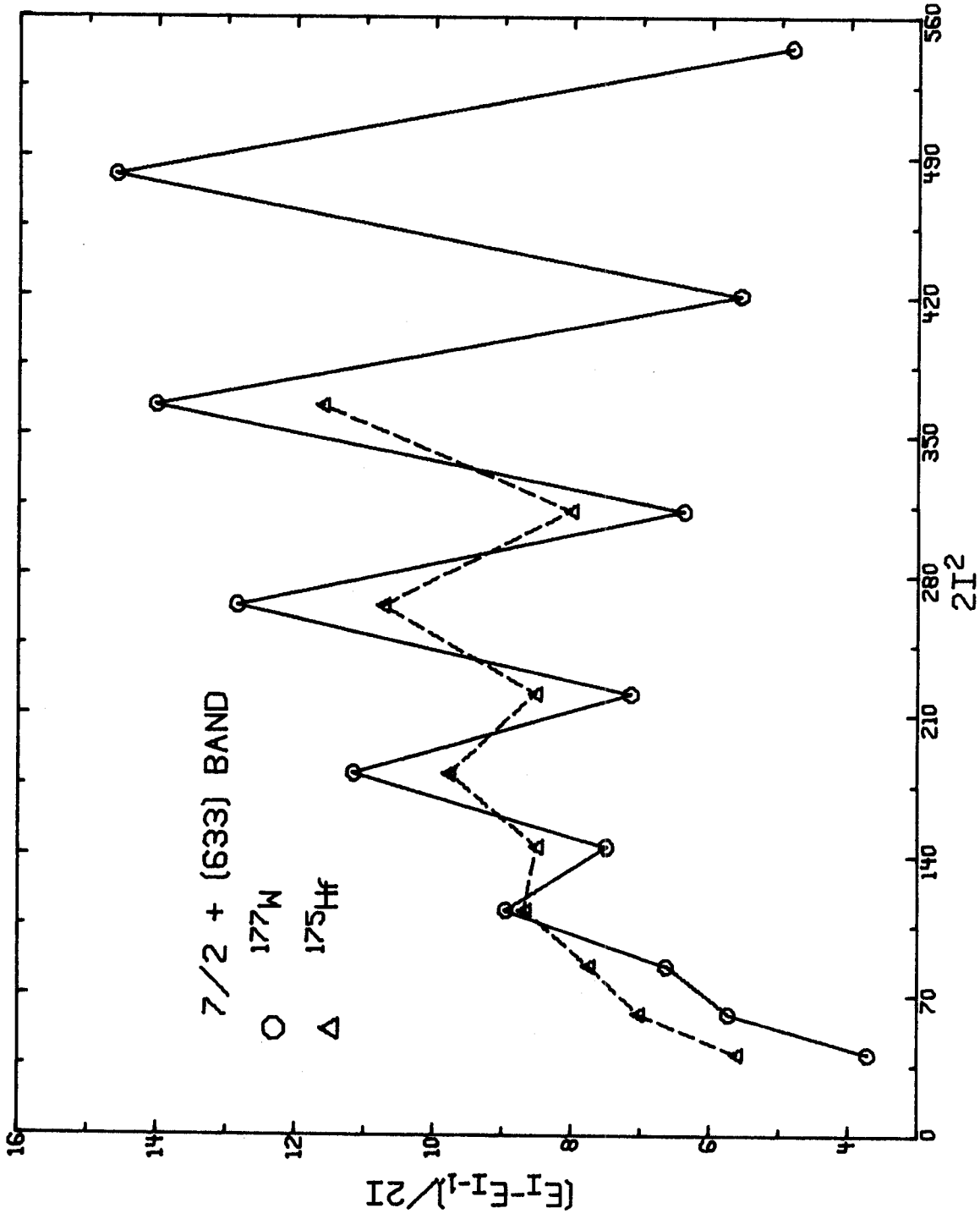

Figure 4-1. A plot of the $7/2^{+}[633]$ bands in ^{177}W and in ^{175}Hf.

given in the same reference -

$$\kappa_n = 0.0641 - 0.0026 \frac{A}{1000}, \quad \mu_n = 0.624 - 1.234 \frac{A}{1000} .$$

The single particle energies were then corrected for pairing correlations using the BCS formalism described in Chapter II. The necessary parameters for this calculation were Δ, the pairing gap parameter, which was estimated from the systematics of odd-even mass differences in the W nuclei [op. cit.], and the position of the Fermi surface, λ, which was extrapolated from calculations in Og71 of λ for similar N=103 nuclei.

The quasiparticle energies, plus the decoupling parameter, $a = -\langle \frac{1}{2} | j_+ | -\frac{1}{2} \rangle$, and the appropriate Coriolis interaction strengths, $\langle K+1 | j_+ | K \rangle$, which were calculated by the Nilsson code, were used to set up, for each spin state, the appropriate Coriolis interaction matrix. The rotational Hamiltonian, then, consists of the following elements:

$$H_{KK} = E_{qp} + \left\{ \frac{\hbar^2}{2\mathfrak{I}} + B(I(I+1)-K^2) \right\} \left\{ I(I+1)-K^2+(-1)^{I-1/2} a \delta_{K,1/2} \right\}$$

$$H_{K,K+1} = -\left\{ \frac{\hbar^2}{2\mathfrak{I}} + BI(I+1) \right\} \sqrt{(I-K)(I+K+1)} \langle K+1 | j_+ | K \rangle (U_K U_{K+1} + V_K V_{K+1}) \times g_{K,K+1}$$

This interaction matrix is then diagonalized in the space of the $i_{13/2}$ orbitals. The factors $g_{K,K+1}$ are attenuation coefficients which are necessary to reproduce the experimental energies. In general, the attenuation is found to be greater for states close to the Fermi surface, so some calculations [e.g. Li73, Hu73] have successfully

assumed a parameterization of a gaussian form for this factor. It has been claimed [Ri74] that if the calculation is done in the framework of the self-consistent cranking model, then no attenuation of the Coriolis matrix elements is necessary.

The experimental energies were fit by adjusting up to 10 variables - the $g_{K,K+1}$, $\frac{\hbar^2}{2\mathcal{J}}$, B, and one quasiparticle energy - in a least-squares fitting routine BETABLE [BETA] which minimizes the differences between the calculated and experimental energies. The rotational parameters, $\frac{\hbar^2}{2\mathcal{J}}$ and B, were initialized at the average values taken from the *yrast* sequences in the neighboring even-even nuclei. The results of the bandfitting procedure for the $7/2^+[633]$ band are summarized in Table 4-2. The only $i_{13/2}$ state which has been experimentally located in ^{177}W is the $7/2^+[633]$; positions of the other members of the family are not yet known. The fitting routine, then, has too many degrees of freedom, and a reasonably good fit to the known energy levels may be obtained with a wide variety of parameter sets. Most of these sets are not physically realistic, however. If a member of another low-lying $i_{13/2}$ band could be experimentally located, the position of the Fermi surface would then be constrained such that the quasiparticle energies could only vary within much smaller limits, yielding more believable results. In view of the attenuation coefficients calculated for positive-parity bands in other nuclei [cf. Be75], the most reasonable parameter set obtained here is the one given in Table 4-2.

One important conclusion of the fitting is that the energy of the $9/2^+ \rightarrow 7/2^+$ transition must be very small, about 30-35 keV. The transition will be a highly converted *M*1+*E*2 similar to that of the 86-keV

Table 4-2. Input parameters for the Coriolis bandmixing procedure, calculated energies and amplitudes of the resulting mixed wavefunctions.

Table 4-2.

$\frac{\hbar^2}{2\mathfrak{J}}$ = 17.24 keV B = -9.7 eV $\langle\frac{1}{2}|j_+|-\frac{1}{2}\rangle$ = 6.748 Δ = 850 keV λ = 150 keV+$E_{qp}(5/2^-[512])$

Orbital	$E_{qp}-E_{qp}^{7/2}$(keV)	$\langle K+1\|j_+\|K\rangle$	$g_{K,K+1}$	$(U_K U_{K+1}+V_K V_{K+1})$
$1/2^+[660]$	719	6.674	0.72	1.000
$3/2^+[651]$	634	6.464	0.98	0.998
$5/2^+[642]$	387	6.117	0.74	0.970
$7/2^+[633]$	0	5.601	0.82	0.839
$9/2^+[624]$	1026	4.830	0.75	0.970
$11/2^+[615]$	1611	3.606	not varied	0.997
$13/2^+[606]$	3890			

Level Energies (keV)			f_I^Ω						
Spin	E_{exp}	E_{calc}	$1/2^+[660]$	$3/2^+[651]$	$5/2^+[642]$	$7/2^+[633]$	$9/2^+[624]$	$11/2^+[615]$	$13/2^+[606]$
7/2	179.4	180.2	0.013	0.074	0.237	0.969			
9/2	213.5	211.2	0.057	0.132	0.318	0.897	0.273		
11/2	276.5	277.4	0.035	0.162	0.367	0.852	0.334	0.032	
13/2	362.8	363.2	0.135	0.233	0.416	0.795	0.347	0.046	0.002
15/2	496.9	498.2	0.054	0.231	0.438	0.782	0.369	0.060	0.004
17/2	623.0	623.7	0.227	0.323	0.475	0.707	0.339	0.061	0.005
19/2	835.8	835.5	0.071	0.284	0.485	0.732	0.371	0.074	0.008
21/2	986.7	985.6	0.310	0.392	0.505	0.629	0.310	0.065	0.007

Table 4-2 (cont'd.)

Spin	E_{exp}	E_{calc}	$1/2^+[660]$	$3/2^+[651]$	$5/2^+[642]$	$7/2^+[633]$	$9/2^+[624]$	$11/2^+[615]$	$13/2^+[606]$
23/2	1281.0	1280.1	0.084	0.325	0.516	0.695	0.363	0.082	0.010
25/2	1441.7	1442.2	0.374	0.439	0.517	0.564	0.278	0.063	0.008
27/2	1819.5	1818.9	0.094	0.357	0.538	0.665	0.352	0.085	0.012
29/2	1981.8	1983.3	0.421	0.470	0.521	0.514	0.251	0.060	0.008
31/2	2433.1	2433.9	0.101	0.381	0.554	0.642	0.341	0.086	0.013
33/2	2593.9	2592.8	0.453	0.490	0.521	0.476	0.229	0.056	0.008

transition with mixing ratio $\delta = -0.45$, where δ is the ratio of the L=2 amplitude to the L=1 amplitude. There is a 34.1-keV conversion electron peak with $E2/M1 = 0.0066$ [Ha75] seen also in the gamma decay [Gr75] and in in-beam spectra which is a possible candidate for the lowest $7/2^+[633]$ band cascade transition.

In order to resolve the placement of the 34-keV gamma ray, an accurate intensity measurement of the gamma ray which is seen in the $(\alpha,4n)$ spectrum, and perhaps even a coincidence experiment would be necessary. The difficulties involved in the determination of the intensity of this gamma ray were discussed in Chapter 3.1. The coincidence experiment would entail the problem of getting good timing signals from very low-energy detector pulses. The peak is also weak, as seen in Figure 3-2, but if the transition cascades into the very intense 84-keV line, then the coincidence relationship would be easily verified. In the level scheme shown in Figure 3-6, the 34.1-keV gamma ray is given two tentative placements - as the interband transition deexciting the $7/2^-[514]$ band, and as the lowest cascade member of the $7/2^+[633]$ band. The theoretical bandfitting prediction suggests the second placement, while preliminary gamma-decay coincidence results [Gr75] suggest the first.

4.3 The $7/2^-[514]$ Band

A third rotational band which was strongly populated in this experiment is believed to be built on the $7/2^-[514]$ single particle state. Twelve members of the band are seen and are plotted in the

usual way in Figure 4-2. Using the standard rotational equation given in section 2 of this chapter, and the energies of the first three levels, the calculated parameters of the band are $\hbar^2/2\mathcal{J}$ = 13.62 keV and B = -0.0155 keV. The corresponding $7/2^-[514]$ bands in ^{179}W and ^{181}W are also plotted in Figure 4-2 for comparison. The small perturbations at high spins in these bands arise from a propagation of $\langle I,K|V_{Coriolis}|I,K+1\rangle$ interactions which mix highly decoupled K=1/2 bands with K=3/2 bands, K=5/2, etc. until the K=7/2 bands are reached. In this deformation region, the presence of many negative parity states which can interact with each other accounts for the impurity of the K-quantum number, and also for the complexity of the mixture involved. The $7/2^-[514]$ bands shown here all have (I+1/2 = *odd*) spin levels as the favored ones, that is, these levels are lowered in energy as a result of mixing with a $K=1/2^-$ band which has the same sequence of levels depressed. Since the effect of decoupling in a K=1/2 band is to add the term $\delta_{K,1/2}\, a(-1)^{I+1/2}(I+1/2)$ to the level energies, then clearly a band having a negative decoupling factor, a, is causing the perturbations which are seen in the $7/2^-[514]$ bands. A tabulation of decoupling factors and Coriolis interaction matrix elements is given in Bu71 for N=5 neutron orbitals and from these values, the $1/2^-[530]$ can be seen to be the most likely cause of the perturbations observed in the $7/2^-[514]$ sequences.

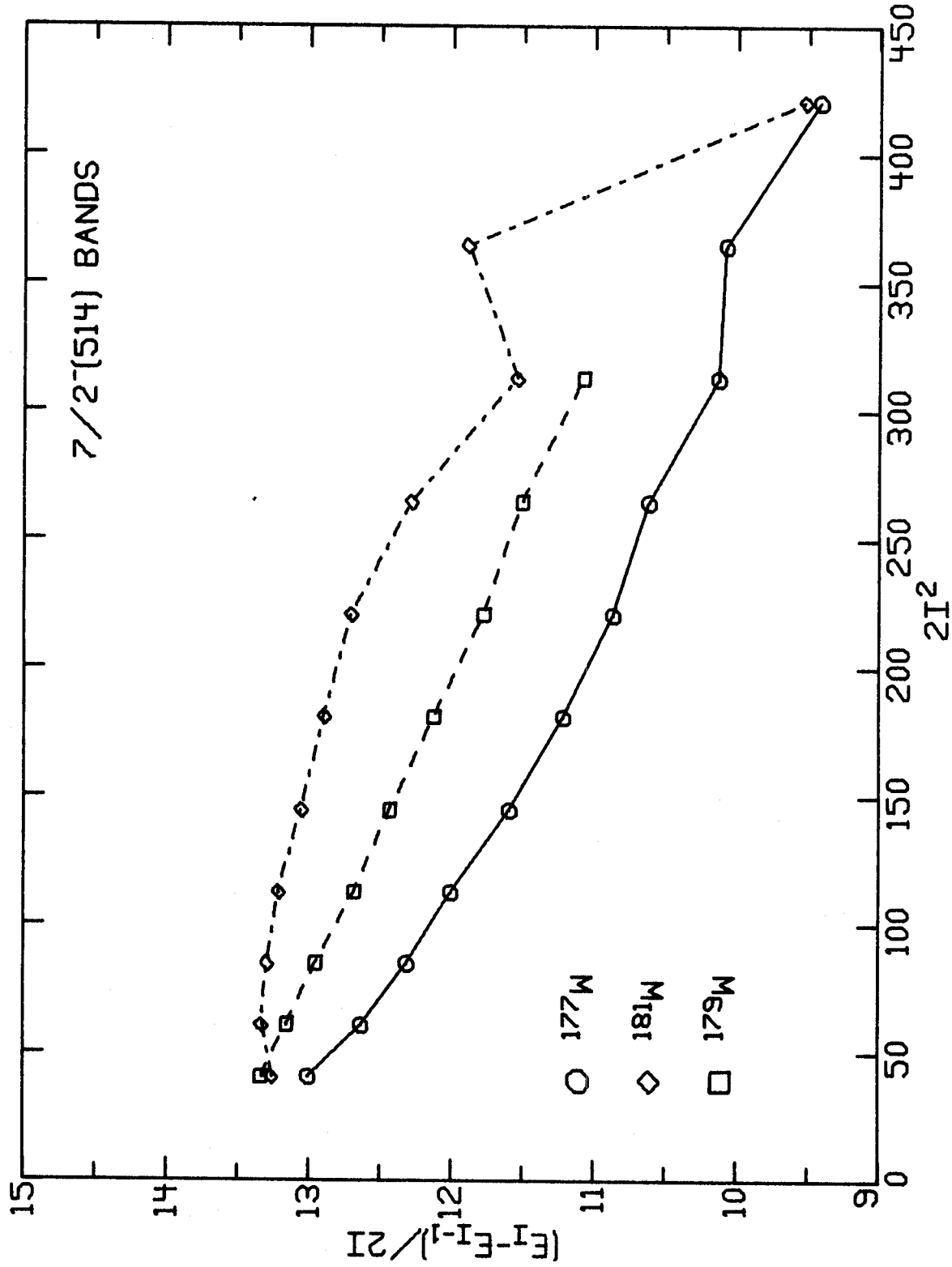

Figure 4-2. A plot of two known $7/2^-[514]$ bands in neighboring odd tungsten nuclei compared with the $7/2^-[514]$ band in ^{177}W.

4.4 The $5/2^-[512]$ Band

Two members of the $5/2^-[512]$ band have been tentatively identified, the 101-keV and 130-keV transitions. The 101-keV line is very strong in the decay of ^{177}Re [Gr75] and its multipolarity, obtained from conversion electron data [Ha75] is $M1+E2$ which suggests that it is an intraband transition from a low spin level. The levels in the $7/2^-[514]$ band are preferentially populated in the $(\alpha,4n)$ reaction and some small amount of feeding into the $5/2^-[512]$ band is seen. The implication of this pattern is that levels with a particular spin value in the 7/2 band are likely to be lower in energy than the same spin members in the 5/2 band. Therefore, it is expected that no levels above the 9/2 member of the $5/2^-[512]$ band will be strongly populated. The $11/2^- \rightarrow 9/2^-$ transition is predicted to have an energy of 160 keV, and a weak 158-keV line seen in the coincidence data is tentatively assigned as this transition.

4.5 Possible 3-Quasiparticle Band

The 144-keV gamma ray is seen strongly in coincidence with many members of the $7/2^+[633]$ band. It appears to feed into the $21/2^+$ level and is possibly an interband transition from a three quasiparticle state. Three band members are proposed to be built on this state with both cascades and crossovers seen. The band follows a smooth rotational behavior with $\frac{\hbar^2}{2\mathfrak{J}}$ of 8.13 keV (for K = 23/2) or 9.86 (for K = 19/2).

The angular distribution of the 144-keV line shown in Figure 4-3 is characteristic of mixed multipolarity with $A_2 = -0.72 \pm 0.05$ and $A_4 = 0.18 \pm 0.05$. Initial spins of 23/2 and 19/2 are both consistent with the angular distribution coefficients, but the A_4 value has the wrong sign to be compatible with a $J_i = 21/2$ assignment.

The lifetime of the 144-keV gamma ray is very short - within the limits measurable in the timing experiments. As shown in Table 4-3, the hindrance per degree of freedom is $\lesssim 5$ which is much smaller than expected for a transition from a three-quasiparticle to a one-quasiparticle band as illustrated by a comparison with data for a $K=23/2 \rightarrow 21/2(K=7/2)$ transition in ^{177}Hf. This low hindrance for the transition in ^{177}W remains unexplained if, in fact, the transition is correctly placed. Recently, a similar puzzling situation was found in ^{181}Os [Ne76] where a gamma-ray cascade was seen feeding promptly into either the 19/2 or 21/2 level of the $9/2^+[624]$ band. No other interpretation of the sequence of levels in ^{177}W is apparent at this time, since the high-spin members ($I \geq 19/2$) of other positive parity bands which are close to the Fermi surface are not expected until about 1.8 MeV excitation.

Table 4-3. Hindrance Factors for Transitions from K = (23/2) Isomers

	E_γ (keV)	$(T_{1/2})_\gamma$(exp)(sec)	$F_w=(T_{1/2})_\gamma(\text{exp})/(T_{1/2})_\gamma(\text{Weiss})$	f_w
^{177}W	144.3	$\lesssim 5\times10^{-9}$ (est)	$\lesssim 7\times10^{4}$	$\lesssim 4.9$
^{177}Hf	55.1	33	5×10^{14}	90

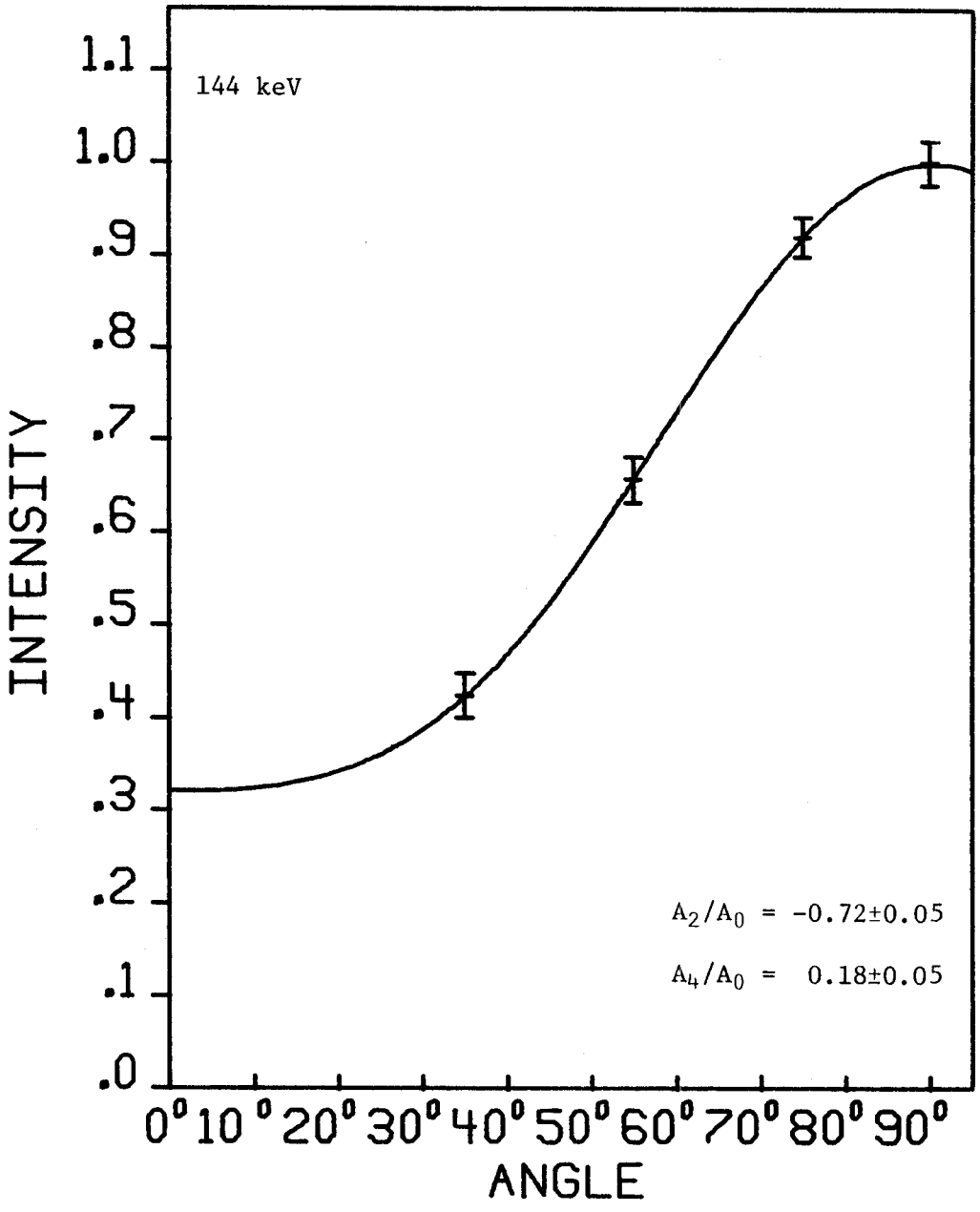

Figure 4-3. Angular distribution data and fitted curve for the 144-keV transition in ^{177}W.

4.6 The Single Particle Level Structure of ^{177}W

Most of the evidence for placement of the single particle orbitals in ^{177}W comes experimentally through either indirect or negative proofs. The rotational bands built on the single particle states all have structures which are characteristic of similar bands in isotonic and isotopic nuclei. The $1/2^-[521]$ band is highly decoupled with intraband transitions proceeding by $E2$ gamma-rays. The $7/2^+[633]$ is also a perturbed structure and can be explained by a mixing of appropriate $i_{13/2}$ bands. The $7/2^-[514]$ band has some small perturbations at high spin values which is typical of the same band in ^{179}W and ^{181}W. Although only weakly populated, the proposed $5/2^-[512]$ band has a rotational constant $\frac{\hbar^2}{2\mathcal{J}}$ similar to that in the ^{179}W $5/2^-[512]$ band.

The relative energies of the bandheads are much more difficult to determine. The $1/2^-[521]$ state was interpreted through the decay pattern [Gr75, Ha75] to be the ground state. From the systematics of the deformations for tungsten nuclei [Ni69], a deformation of $\varepsilon_2 = 0.245$ and $\varepsilon_4 = 0.03$ is predicted for ^{177}W. A calculation of the position of the $1/2^-[521]$ Nilsson orbital places the state about 200 keV above the $5/2^-[512]$ which is the normal ground state in the N=103 isotonic series [Bu71]. This change in the normal ordering of levels in ^{177}W has been interpreted as an implication of a smaller value of ε_2 for ^{177}W [Ha75]. However, in view of the uncertainty in the theoretical calculations, the discrepancy is not unreasonable.

The level which should be seen closest to the ground state is the $5/2^-[512]$. Since each of the two other bands expected to be populated

has K=7/2, both would be likely to feed into the $5/2^-[512]$ state rather than directly into the ground band by K-forbidden transitions. The only strong interband transition which can be seen with the data available is the 84-keV *E*1 gamma-ray which depopulates the $7/2^+[633]$ band, but which is only weakly in coincidence with gamma-rays from the 3/2 and 5/2 members of the ground band. There are no intense gamma-rays seen in the depopulation of the $7/2^-[514]$ or $5/2^-[512]$ bands nor are there any unexplained strong coincidences in the ground band gates. The implication is that the interband transitions must be too low in energy and too highly-converted to be easily seen in the in-beam Ge(Li) spectra. Even assuming that the gamma-rays cannot be detected, certain relationships between the bands can be discerned. The $7/2^-[514]$ band receives a larger percentage of the population than does the $5/2^-[512]$. There are only a few weak transitions connecting the two bands. Therefore, it seems plausible that the levels of the [514] band must be lower in energy than the corresponding members of the [512] band. This would place all the levels with the same spin value lower in energy for the [514] band and would explain why it is populated more strongly.

A consideration of the gamma-ray lifetimes can also be useful in determining the relative bandhead positions. The $7/2^+[633]$ bandhead has a half-life of 10 nsec. A scheme can be constructed with the 84-keV gamma ray feeding into the $5/2^-[512]$ level which may then depopulate into the $1/2^-[521]$ ground band via a relatively long-lived low energy gamma ray. The intensities of the 79-keV and 95-keV ground band transitions were each found to have a delayed component having a 37 nsec half-life. An unidentified 101-keV gamma ray appeared to have the

same lifetime, and it also had enough intensity to account for the ground band components. However, the 101-keV line is assumed not to be the transition from the $5/2^-$ bandhead, because the coincidence data from the decay study of Griffin do not support this assignment. It is possible, though, to place an upper limit of ≈37 nsec on the lifetime of the $5/2^-[512]$ since no appreciable longer-lived delayed components in the ground band intensities can be seen.

The study of ^{177}Re decay by Griffin [Gr76] was prompted initially to supplement the in-beam data which were unable to easily identify the relative locations of single-particle orbitals in ^{177}W. Since the ground state spin of ^{177}Re is 5/2, only low-spin states would be populated in ^{177}W. Griffin performed both singles and gamma-gamma coincidence experiments using a small volume planar detector for characterization of low energy gamma rays. Unfortunately, results of the study were not statistically conclusive. Lack of coincidences between the 95- and 101-keV gamma rays suggested the relative position of the $5/2^-[512]$ at Δ-keV above the $5/2\ 1/2^-[512]$. This assignment has been adopted here, although the in-beam data do not require it.

The energies of calculated Nilsson levels can now be compared with the experimental levels to see if the deformation can be inferred from the relative positions of low-lying states which are populated. At the deformation mentioned at the beginning of this section, not only is the $1/2^-[521]$ state 200 keV too high, but in order to lower the $7/2^-[514]$ single particle energy to reasonable agreement with experiment, the Fermi surface must be placed 200 keV above the $5/2^-[512]$ state, not an altogether unreasonable assumption. If a smaller

deformation for ^{177}W is assumed, however, the orbitals under consideration begin to slowly approach each other in energy and, in fact, at $\varepsilon_2 = 0.210$, there is a crossing of the $1/2^-[521]$ and the $5/2^-[512]$ orbitals.

The fact that the $1/2^-[521]$ appears as the ground state in ^{177}W whereas the $5/2^-[512]$ is the ground state in other N=103 isotones was suggested by Harmatz, *et. al.* [Ha75] to be an indication that perhaps the deformation of this nucleus was smaller than that of the other isotones. Indeed, at a deformation of $\varepsilon_2 = 0.210$ with the Fermi surface placed 150 keV above the $1/2^-[521]$ and with the quasiparticle energies corrected for zero-point rotational energy, the $7/2^-[514]$ and $5/2^-[512]$ states are predicted to be only 48 keV apart, and 86 keV above ground. Since this set of results is roughly consistent with the experimental data, it can be indirectly inferred that ^{177}W may possess a deformation somewhat smaller than other nuclei in the 103 isotonic series, and also somewhat less than expected from the systematics predicted by Nilsson [Ni69].

CHAPTER V

^{178}W EXPERIMENTAL DETERMINATIONS

5.1 Gamma-Ray Singles Spectra

The levels in ^{178}W were populated in an $(\alpha,3n)$ reaction on ^{177}Hf. The Hf foil targets were the same ones that were used in the ^{177}W experiments described in Chapter III. The beam energy used for most of the experiments was chosen to be about 38 MeV. Data were taken between 0 and 1500 keV using the 8% efficient detector. Most of the spectra were accumulated with 8192 conversion gain in the ADC's to improve peak definition while accommodating the large energy range. A singles spectrum taken with the detector at 125° with respect to the beam is shown in Figure 5-1.

The most obvious feature of the spectrum is the prominence of the ground band or *yrast* cascade. The members of this band can be identified by sight up to the $12^+ \rightarrow 10^+$ transition at 579 keV. The $(\alpha,2n)$ and $(\alpha,4n)$ product nuclei are both populated weakly at this alpha energy and since the reaction strength of these odd-nuclei is spread more evenly over many bands, no set of contaminant transitions dominates. ^{178}W decays with a 21.5-day half-life to the ground state of 9.4 m ^{178}Ta which decays to ^{178}Hf. The transitions in ^{178}Hf which constitute the ground band are seen also as weak contaminants.

An efficiency curve for the detector was obtained and relative intensities for the transitions were determined, normalized to the 237-keV $(4^+ \rightarrow 2^+)$ transition. Energies and intensities of peaks that are

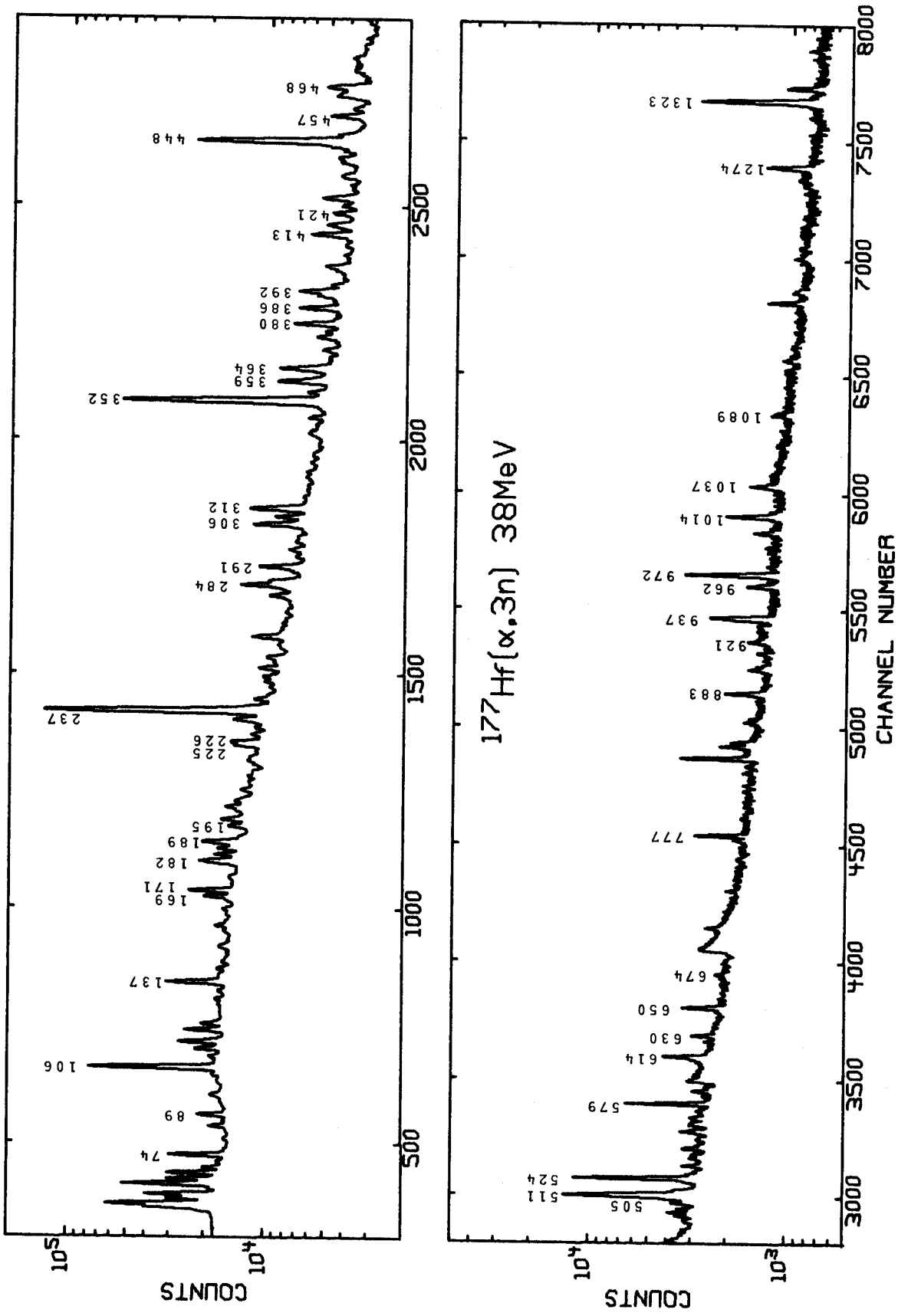

Figure 5-1. Spectrum of ^{177}Hf(α,3n) taken with an 8% efficient detector at 125° with respect to the beam.

believed to belong to ^{178}W are listed in Table 5-1. In general, gamma-rays that have a relative intensity of 0.8 or less which have not been assigned, are not listed in the table unless coincidence information demands that they should be. Since most of the contaminants are known to be ^{179}W, ^{177}W, ^{178}Hf, and ^{177}Ta, the energies of these gamma-rays are not included. The spin assignments for transitions depend on the K-value of the band in which they appear. The bandheads assigned $K^{\pi}=(6)^{+}$ and $K^{\pi}=(6^{-})$ have tentative K-values which are used in the table to assist in identification of the transitions which are associated with each of these bands.

5.2 Angular Distributions

The set of angular distribution data for ^{178}W consists of spectra taken at 90°, 115°, 125°, and 135°. The peak areas were obtained and the curve was fit to $W(\theta) = \sum_{K=0,2,4} A_K P_K(\cos\theta)$. A_2/A_0 and A_4/A_0 were extracted for each transition. In most cases, the errors are large compared to the errors for the ^{177}W transitions of comparable intensity. The chamber used for the $(\alpha,4n)$ experiment has a wider window than the one used for the $(\alpha,3n)$ distribution and the smaller angular range which is obtainable in this case had a significant effect on the precision of the curve-fit. Of course, the detector resolution, which is slightly worse for the 8% detector than for the LEPS also affects the results by making the doublet peaks more difficult to analyze reliably.

Table 5-1. Energies (E_γ), relative intensities (I_γ), angular distribution coefficients, multipolarities, and spin assignments for transitions in ^{178}W. In the cases where no A_4/A_0 is listed, the angular distribution data for those transitions were fit with A_4/A_0 constrained to zero. The transitions labeled with an asterisk are components of closely spaced (<0.5 keV) doublets.

Table 5-1

E_γ (keV)	I_γ (rel. int.)	Angular Distribution Coeff.			Assignment
		A_2/A_0	A_4/A_0		
73.78(5)	16(1)	-0.13±.05		*E*1	$K=6^-\rightarrow K=6^+$
88.59*(5)	4.3(2)	-0.1 ±.1			$K=6^-(7\rightarrow6)$, ^{178}Hf
106.10(5)	32(2)	0.04±.06	0.04±.05	*E*2	$K=0^+(2^+\rightarrow0^+)$
119.89(5)	4.5(3)				^{179}W
131.15(5)	1.00(7)				
137.34(5)	8.4(5)	-0.64±.05	0.06±.05	*M*1, *E*2	$K=6^-(8\rightarrow7)$
150.11(5)	1.00(9)				
157.90(5)	1.6(1)				
163.98(5)	0.97(7)	0.10±.06		*E*2, *M*1	$K=2^-(6^-\rightarrow5^-)$
168.71(5)	3.6(2)	-1.14±.12		*M*1, *E*2	$K=6^-(9\rightarrow8)$
170.82(5)	5.9(3)	-0.69±.08	0.08±.08	*M*1, *E*2	$K=6^+(7\rightarrow6)$
175.95(8)	0.76(9)				
180.90(5)	1.8(1)				$K=2^-(4^-\rightarrow2^-)$

Table 5-1 (cont'd.)

E_γ (keV)	I_γ (rel. int.)	Angular Distribution Coeff.			Assignment
		A_2/A_0	A_4/A_0		
182.30(5)	1.4(1)				3237.4→3055.1
188.09(5)	1.8(1)				$K=6^+(8\rightarrow7)$
194.69(5)	1.8(1)	-0.86±.12		*M*1, *E*2	$K=6^-(10\rightarrow9)$
201.77(5)	2.5(2)	-0.17±.07			
203.73(9)	1.1(2)	-0.4 ±.1		*E*2, *M*1	$K=6^+(9\rightarrow8)$
208.05(5)	1.40(9)				
217.55(6)	0.56(6)				$K=6^+(10\rightarrow9)$
218.86(5)	1.35(9)	-0.2 ±0.1		*E*2, *M*1	$K=6^-(11\rightarrow10)$
224.55(5)	2.8(2)	0.02±.06			$K=2(5\rightarrow3)$
225.83(5)	3.5(2)	0.31±.07	0.04±.06	*E*2	$K=6^-(8\rightarrow6)$
228.54(15)	1.5(1)	-1.1 ±.3			$K=6^+(11\rightarrow10)$
231.17(10)	1.6(3)				
234.16*(6)	4.5(4)				

Table 5-1 (cont'd.)

E_γ (keV)	I_γ (rel. int.)	Angular Distribution Coeff.			Assignment
		A_2/A_0	A_4/A_0		
237.01(5)	100(6)	0.17±.03	0.05±.03	*E*2	$K=0^+(4^+\rightarrow 2^+)$
239.11*(6)	4.1(3)				$K=6^-(12\rightarrow 11)$
241.41(5)	1.8(1)				
260.46(13)	0.27(3)				$K=6^-(13\rightarrow 12)$
264.32*(5)	3.5(2)				^{179}W
269.24(5)	0.8(1)				
283.51(5)	6.2(4)	0.20±.07		*E*2	$K=2^-(6^-\rightarrow 4^-)$
285.09(5)	2.7(2)				$6(K=6^+)\rightarrow 4^+(K=2^+,3^+,4^+)$
290.41(5)	4.6(3)	-0.25±.08			3527.8→3237.4
306.05(5)	5.74(3)	0.21±.05		*E*2	$K=6^-(9\rightarrow 7)$
311.81(5)	5.6(4)				$K=2^-(7^-\rightarrow 5^-)$
345.63(5)	1.3(1)				
348.29(9)	1.3(1)				

Table 5-1 (cont'd.)

E_γ (keV)	I_γ (rel. int.)	Angular Distribution Coeff.			Assignment
		A_2/A_0	A_4/A_0		
351.56(5)	66(4)	0.19±.02	0.02±.02	*E*2	$K=0^+(6^+\rightarrow4^+)$
358.76(5)	5.4(3)	0.2 ±0.1			$K=6^+(8\rightarrow6)$
363.39(6)	4.7(4)	0.20±.04	0.04±.04	*E*2	$K=6^-(10\rightarrow8)$
379.96(5)	4.8(3)	0.27±.06	0.07±.06	*E*2	$K=2^-(8^-\rightarrow6^-)$
385.78(5)	4.0(2)	0.27±.05	0.03±.03	*E*2	$K=2^-(9^-\rightarrow7^-)$
390.34(5)	1.7(1)				$(\alpha,2n)$
392.04(5)	4.4(3)	0.3 ±.1			$K=6^+(9\rightarrow7)$
413.19(5)	3.8(2)	-0.3 ±.2			$K=6^-(11\rightarrow9)$
421.11(5)	2.1(1)				$K=6^+(10\rightarrow8)$
423.94(5)	1.05(8)				
434.63(5)	1.3(1)				
445.52(6)	1.10(9)				$K=6^+(11\rightarrow9)$
447.67*(5)	37(2)	0.21±.02	-0.01±.02	*E*2	$K=0^+(8^+\rightarrow6^+)$; $K=2^-(11^-\rightarrow9^-)$

Table 5-1 (cont'd.)

E_γ (keV)	I_γ (rel. int.)	Angular Distribution Coeff.			Assignment
		A_2/A_0	A_4/A_0		
456.95(5)	3.1(2)				
460.94(22)	0.20(2)				$14^+(K=0^+)\rightarrow 14^+(K=0^+)$
465.36(6)	2.1(1)	0.35±.09	0.06±.08		
467.79*(5)	3.3(3)				$K=2^-(10^-\rightarrow 8^-)$; $K=6^+(13\rightarrow 11)$
496.09(5)	0.98(8)				
498.31(5)	2.3(1)				$K=6^-(13\rightarrow 11)$
505.14(5)	1.5(1)				$K=2^-(13^-\rightarrow 11^-)$
514.75(8)	0.7(1)				$7^-(K=2^-)\rightarrow 8^+(K=0^+)$
523.77(6)	22(1)	0.24±.06	-0.04±.05	*E*2	$K=0^+(10^+\rightarrow 8^+)$
533.03(5)	1.4(1)	0.43±.08	-0.05±.07	*E*2	$K=6^-(14\rightarrow 12)$
545.76(6)	2.0(1)				$K=2^-(12^-\rightarrow 10^-)$
559.68(6)	0.99(9)				$12^+(K=0^+)\rightarrow 12^+(K=0^+)$
568.79(7)	1.1(1)				$K=6^-(15\rightarrow 13)$

Table 5-1 (cont'd.)

E_γ (keV)	I_γ (rel. int.)	Angular Distribution Coeff.			Assignment
		A_2/A_0	A_4/A_0		
579.05(5)	11.3(6)	0.28±.01	0.00±.01	*E*2	$K=0^+(12^+\rightarrow10^+)$
614.17(5)	5.3(3)	0.25±.07		*E*2	$K=0^+(14^+\rightarrow12^+)$
629.77(5)	2.3(1)				$K=0^+(16^+\rightarrow14^+)$
650.40(6)	4.7(3)	-0.17±.03	0.00±.06	*E*1	$5^-(K=2^-)\rightarrow6^+(K=0^+)$
674.55(7)	0.85(7)				$10^+(K=0^+)\rightarrow10^+(K=0^+)$
774.27(8)	0.96(9)	-0.3 ±.1			$8^+(K=0^+)\rightarrow8^+(K=0^+)$
777.53(5)	6.1(4)	-0.15±.05		*E*1	$3^-(K=2^-)\rightarrow4^+(K=0^+)$
824.38(7)	0.9(1)				$11^-(K=2^-)\rightarrow10^+(K=0^+)$
861.8(1)	1.3(1)				$6^+(K=0^+)\rightarrow6^+(K=0^+)$
882.8(1)	4.3(3)	0.14±.06	0.04±.04		$4^-(K=2^-)\rightarrow4^+(K=0^+)$
900.4(1)	1.7(1)	-0.68±.06	0.04±.06	*E*1, *M*2	$9^-(K=2^-)\rightarrow8^+(K=0^+)$
920.9(2)	1.45(8)				$3055.1\rightarrow9(K=6^-)$
938.8(1)	7.4(4)				$2^-(K=2^-)\rightarrow2^+(K=0^+)$

Table 5-1 (cont'd.)

E_γ (keV)	I_γ (rel. int.)	Angular Distribution Coeff. A_2/A_0	Angular Distribution Coeff. A_4/A_0		Assignment
962.4(1)	3.1(2)				$7^-(K=2^-)\rightarrow 6^+(K=0^+)$
970.8(1)	14.7(8)				$6(K=6^+)\rightarrow 6^+(K=0^+)$
1002.1(1)	2.1(1)	-0.17±.08		*E*1	$5^-(K=2^-)\rightarrow 4^+(K=0^+)$
1014.7(1)	7.1(4)				
1037.0(1)	3.1(2)				$4^+(K=2^+,3^+,4^+)\rightarrow 4^+(K=0^+)$
1089.7(1)	1.3(14)				$3055.1\rightarrow 8(K=6^-)$
1206.4(2)	0.8(1)				
1274.5*(1)	5.0(3)				^{22}Na; $4^+(K=2^+,3^+,4^+)\rightarrow 2^+(K=0^+)$
1322.5(1)	20(1)	-0.06±.02			$6(K=6^+)\rightarrow 4^+(K=0^+)$
1332.6(1)	3.4(2)				

The values of A_2/A_0 and A_4/A_0 for the more intense transitions are listed in Table 5-1. For transitions where the data were too poor to determine A_4/A_0, the value of A_4/A_0 was constrained to be zero, and A_2/A_0 was then calculated. For these cases, no A_4/A_0 is listed in the table. Plots of some of the ground band distributions are shown in Figures 5-2 and 5-3 arranged according to increasing energy within the band. The data have been transposed to the 0-90° quadrant. Selected distributions of intense transitions in other rotational bands in ^{178}W are shown in Appendix B. Multipolarities deduced from the distributions are also shown in Table 5-1. The values of A_2/A_0 were, in general, more reliable than the values of A_4/A_0 and could be used to estimate the mixing ratios for the more intense transitions. Assuming alignment of the original target nucleus, the mixing ratios were calculated using the tables found in Ma74. These ratios were used as an independent check of the g_K values found from the branching ratios, and also were used in the determination of the sign of g_K.

5.3 Gamma-Ray Lifetimes

Isomers in ^{178}W were sought in the range 5-500 nsec using the various techniques described in Chapter 2.3. The shortest time range studied was that between consecutive beam bursts which at 38 MeV occur every 54.2 nsec. In this experiment, transitions from the $K^{\pi}=6^+$ bandhead at 1665.7 keV were found to have a half-life of 10.1±0.2 nsec. The isomer decays into the 6^+ and 4^+ members of the ground band and was found to account quite well for the delayed intensity of the first three ground band

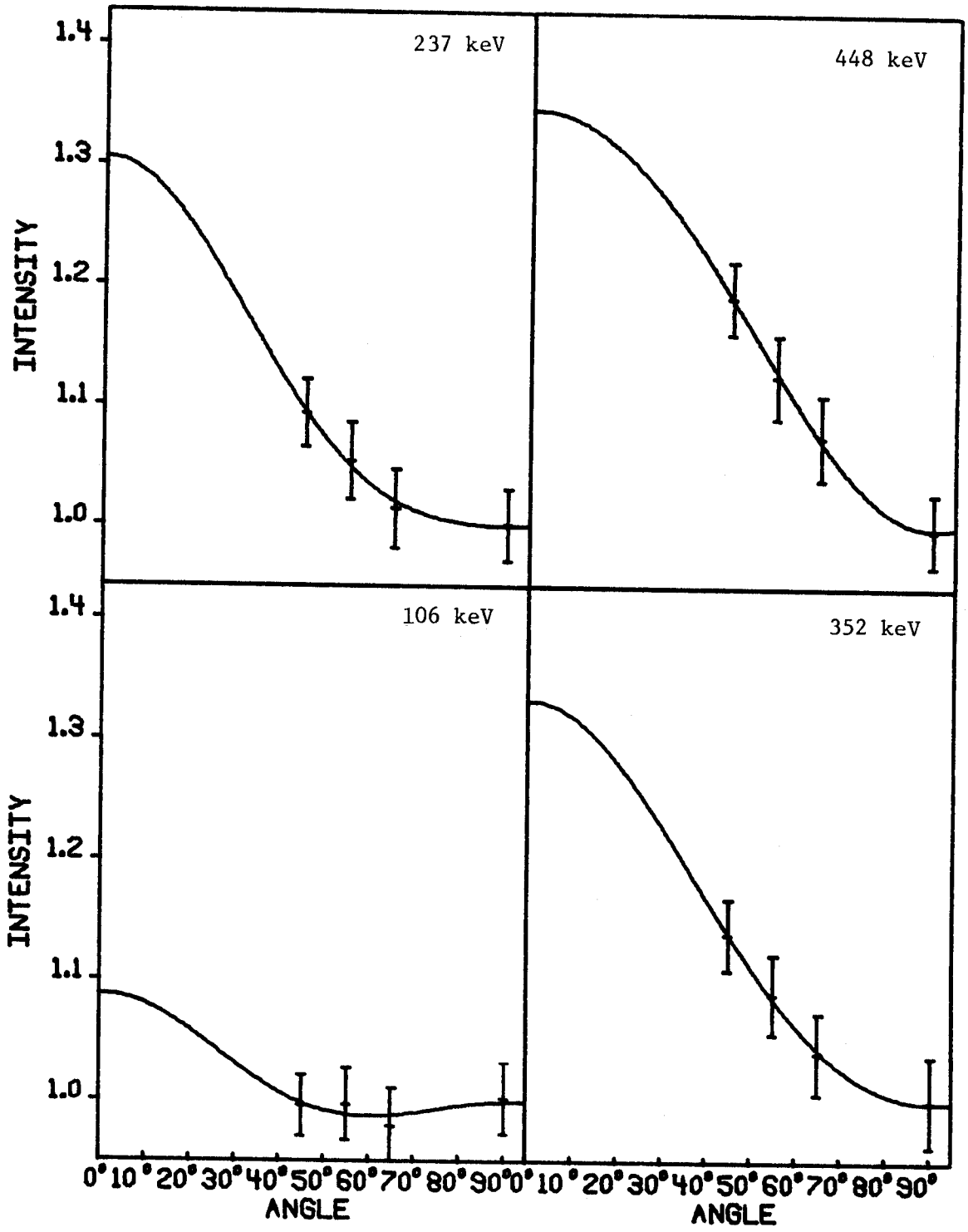

Figure 5-2. Stretched $E2$ K=0 ground band distributions.

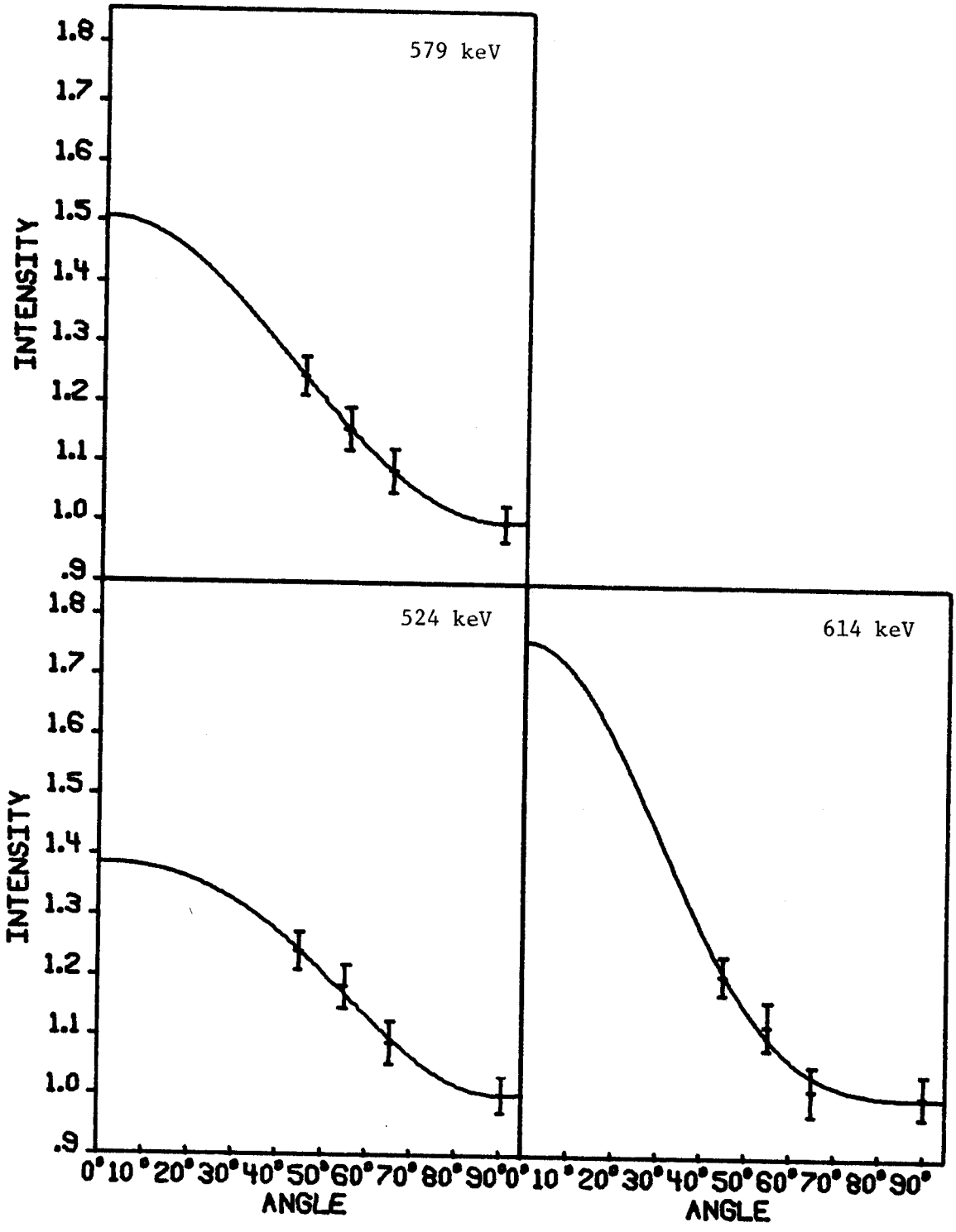

Figure 5-3. Stretched *E*2 K=0 ground band distributions.

transitions. The half-life data for the two delayed gamma rays which deexcite the isomer are plotted in Figure 5-4. The half-life of the 73-keV transition which deexcites the $K^{\pi}=(6^{-})$ band at 1740 keV was not measured in this experiment due to the limitations placed on accurate timing of low energy signals by the detector which was used. There is sufficient information in the $(\alpha,4n)$ timing data, in the delayed gates which were set on the coincidence data, and in the first three time bands of the $(\alpha,3n)$ timing data, however, to corroborate the fact that no prominent isomeric states with half-lives greater than 15 nsec can be identified in ^{178}W. The lifetime of the $K^{\pi}=(6^{-})$ state can be estimated from the $(\alpha,4n)$ data as being less than 10 nsec, but the question of whether or not it is greater than the lifetime of the $K^{\pi}=6^{+}$ state could only be determined by performing a separate experiment at the $(\alpha,3n)$ energy using a planar, small volume detector for good timing accuracy at low energies. Conversion electron measurements indicate that the 73-keV transition is delayed by 8.3 nsec [Ca76].

5.4 Excitation Functions

With the 8% efficient detector at 125° with respect to the beam, the spectra shown in Figures 5-5 to 5-7 were taken at beam energies of 34, 38, 43, and 46 MeV. The counting period was similar for each of the four spectra making it possible to relate the intensities of individual peaks directly to the production of the isotope to which the peaks belong. The transitions in the ground state band of ^{178}W are a good measure of the $(\alpha,3n)$ yield which peaks near 38 MeV. The 84.4-keV

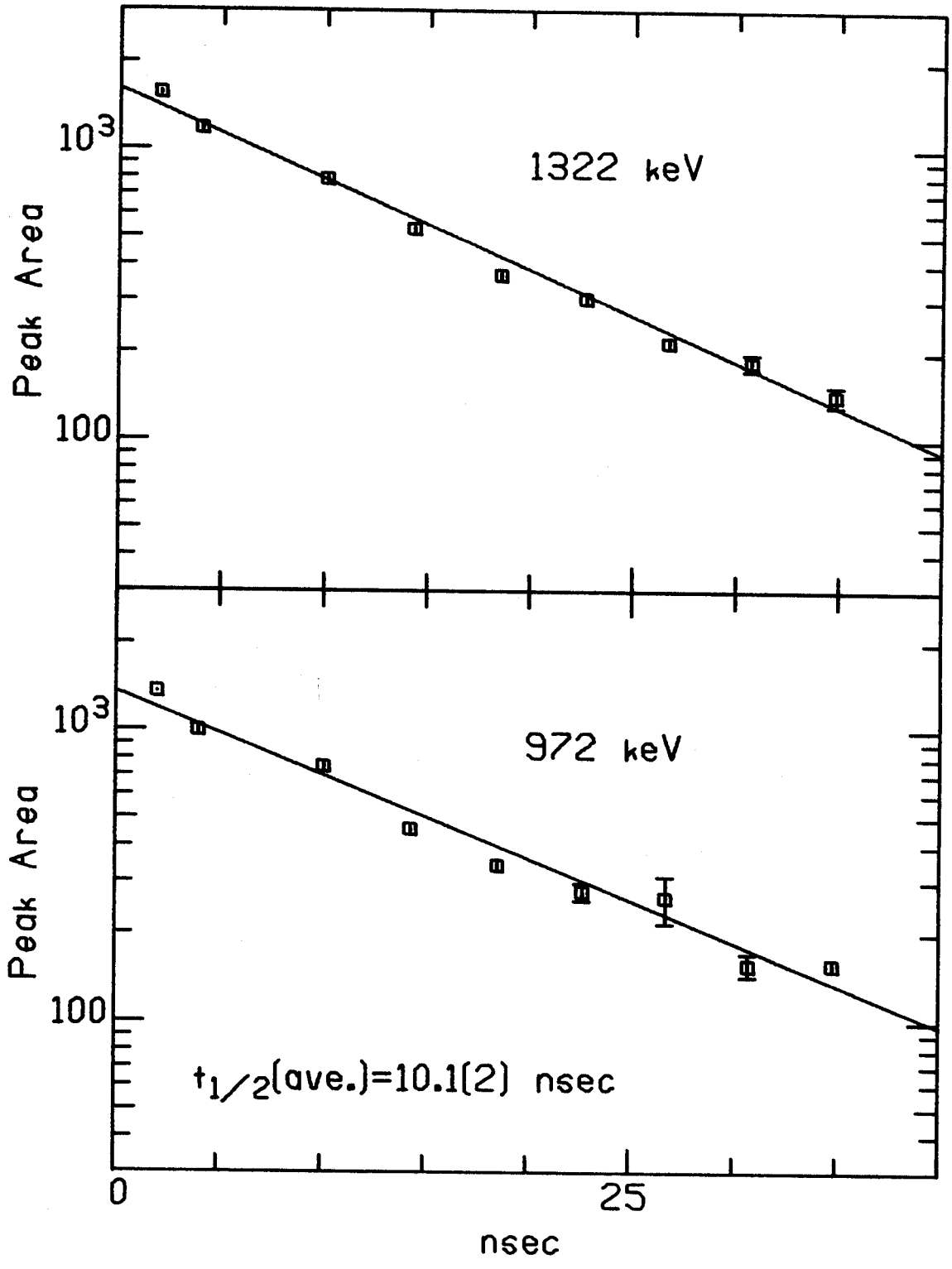

Figure 5-4. Half-life data for the transitions deexciting the 1666-keV isomer in ^{178}W.

Figure 5-5. Excitation function spectra taken at 125° using the alpha particle energies shown. These portions of the 8000-channel spectra display the 50-325 keV gamma-ray energy range.

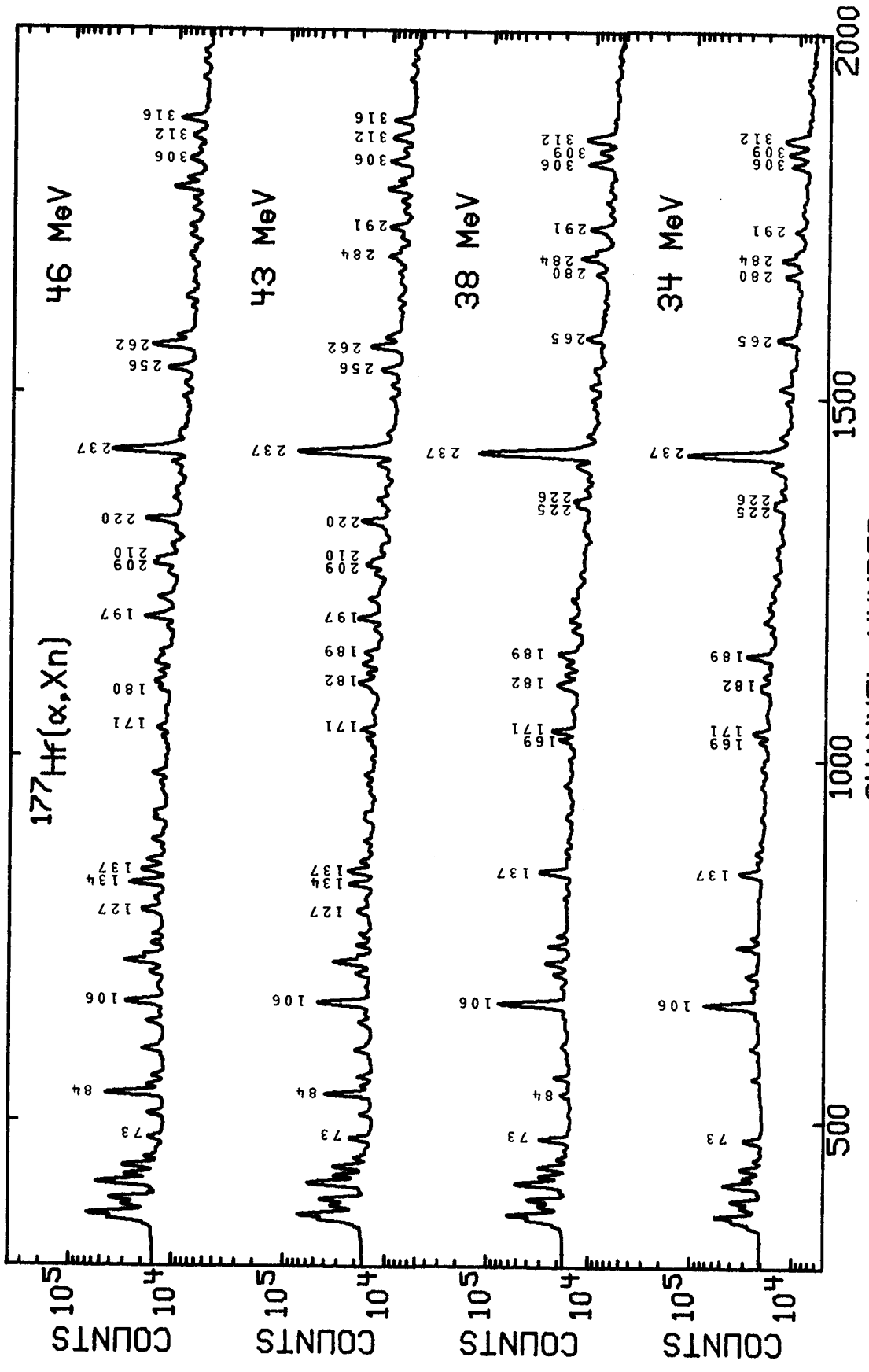
46 MeV
43 MeV
38 MeV
34 MeV
177Hf(α,Xn)
COUNTS
CHANNEL NUMBER
500
1000
1500
2000
10^5
10^4

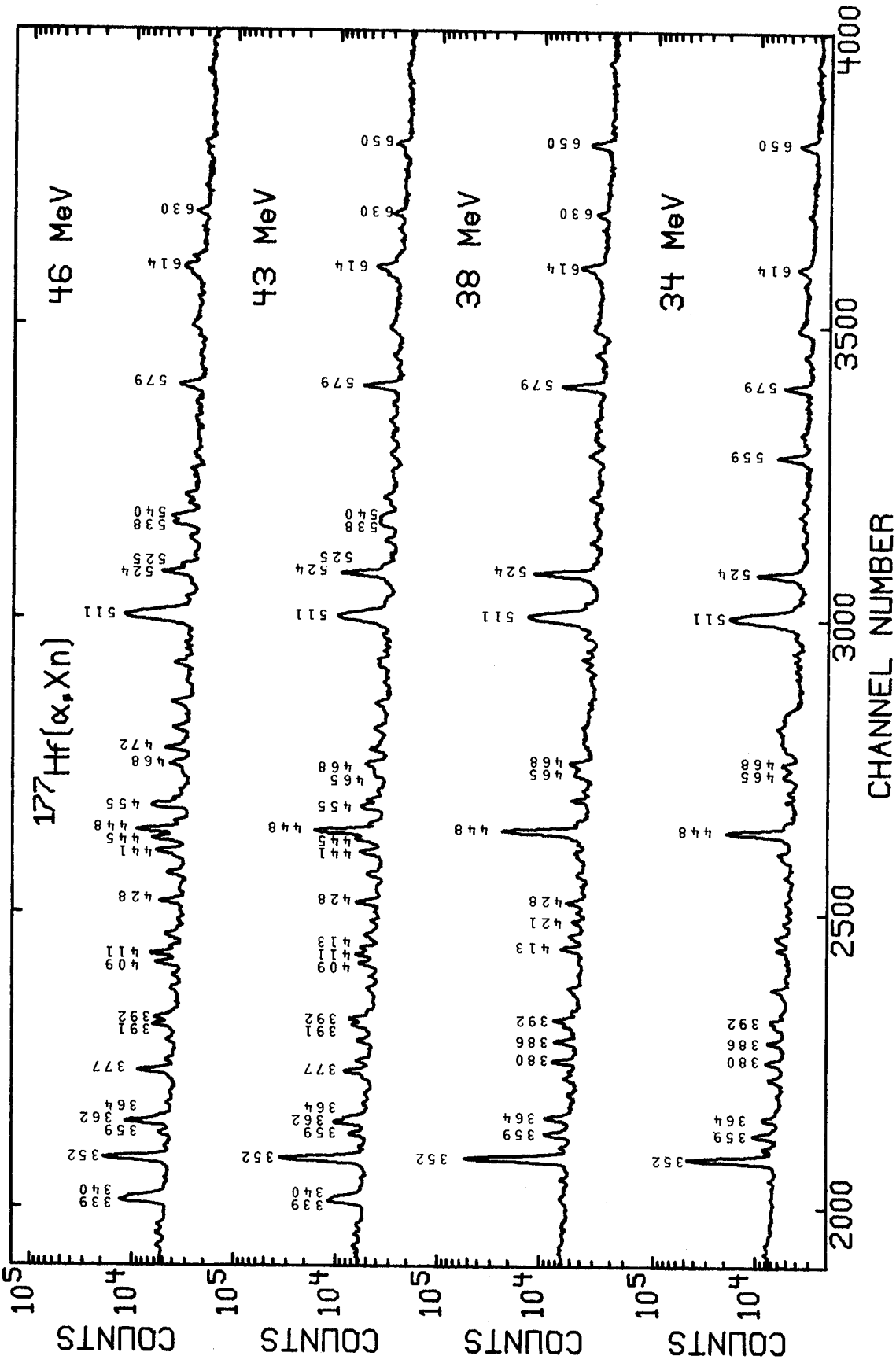

Figure 5-6. Portions of the excitation function spectra displaying the energy range 325-700 keV.

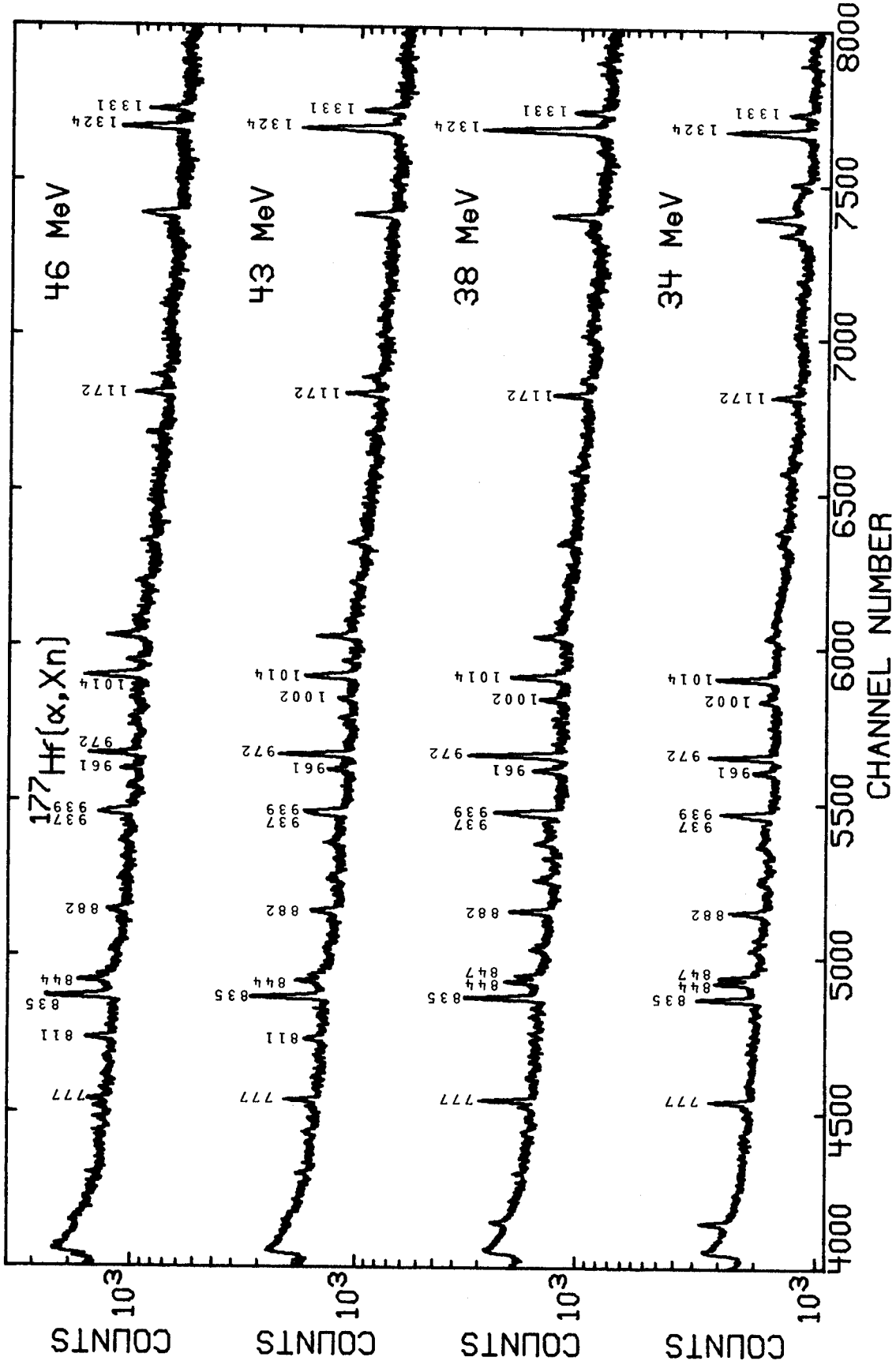

Figure 5-7. Portions of the excitation function spectra displaying the high energy peaks in the range 700-1375 keV.

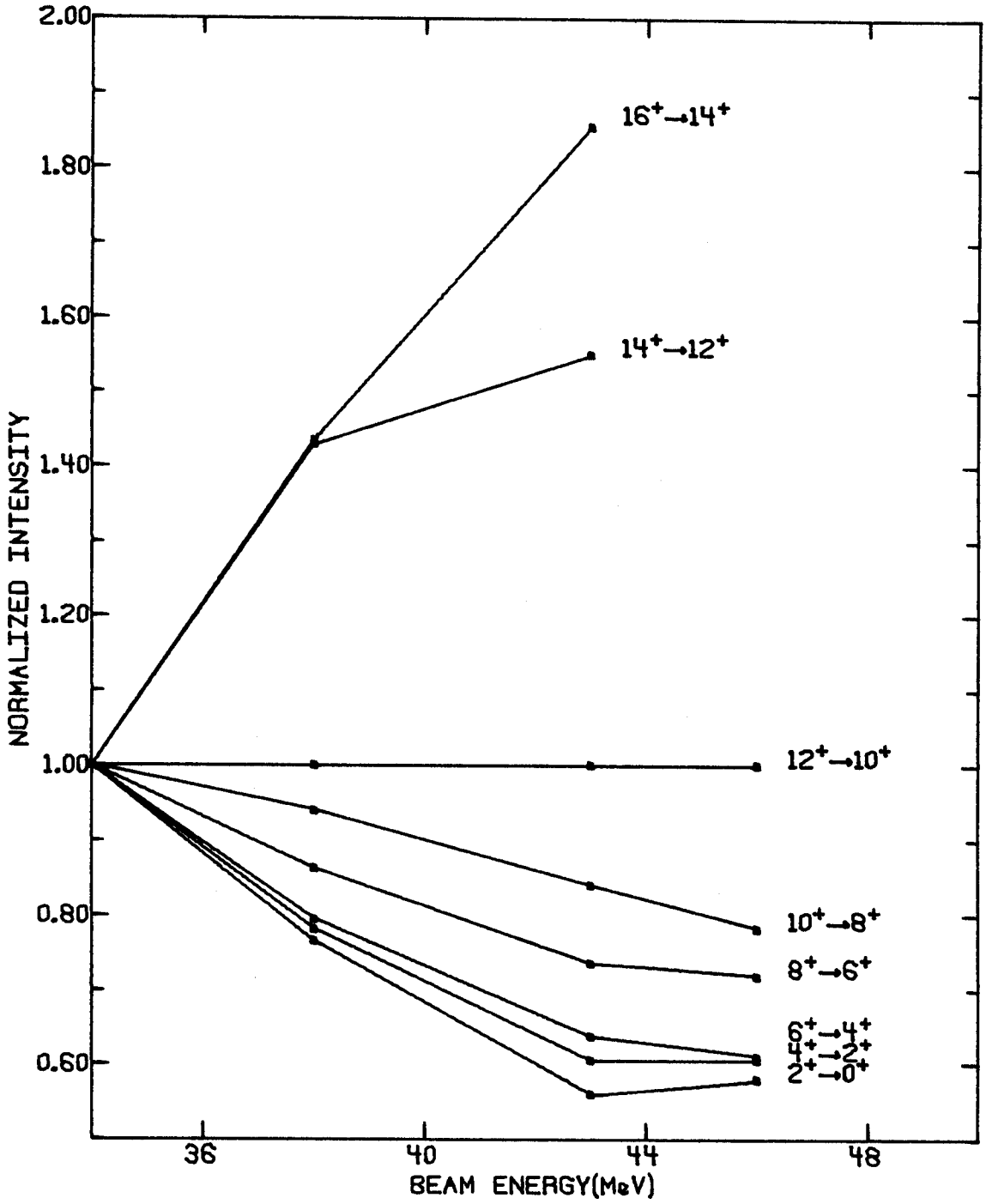

Figure 5-8. Excitation functions of the K=0 ground band of ^{178}W. The peak intensities are normalized to the $12^+ \rightarrow 10^+$ transition intensity, and to the 34-MeV peak intensities.

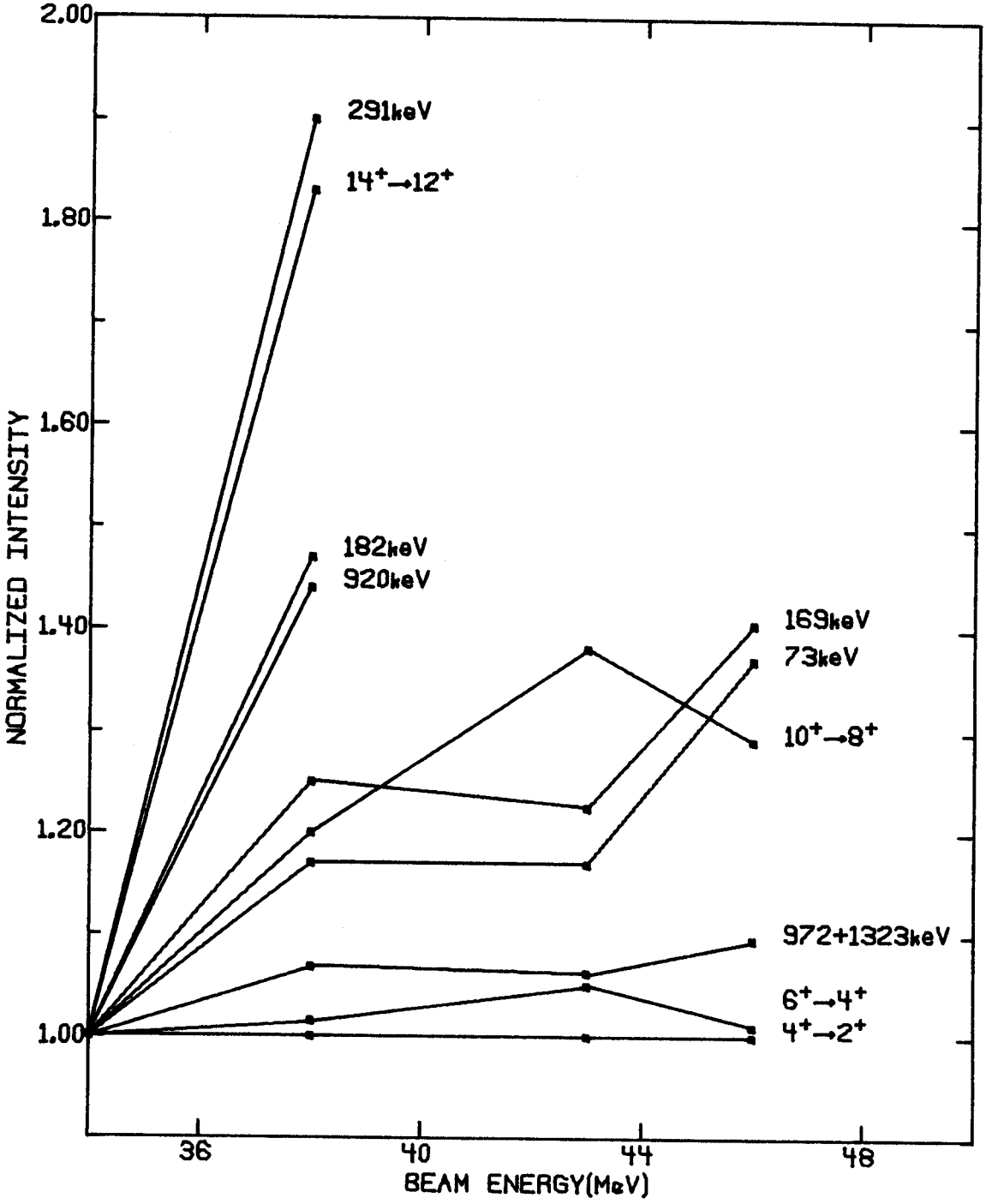

Figure 5-9. Excitation functions of selected transitions compared to the ground band functions. The intensities are normalized to the $4^+ \rightarrow 2^+$ transition intensity, and to the 34-MeV peak intensities.

5.5 Gamma-Gamma-Time Coincidences

Using the same geometry described in Chapter 3.5 for ^{177}W, three-parameter coincidence events were recorded on ten magnetic tapes, each containing 3×10^6 events. The detectors used were both large volume - 8% and 10% efficient - and the TAC resolution was about 24 nsec FWHM. Gating on the tails of the time peak showed no new information, but using the main portion of the TAC with a 300 nsec time acceptance gave gated spectra with the best overall energy efficiencies. The low energy efficiency for the 10% detector was still quite poor, so both sides were gated and the X-side (displaying the 10% spectrum) was used to identify high energy coincidences, while the Y-side showed the low energy coincidences quite well.

The coincidence gates for most of the transitions which have been placed are shown in Appendix A. The gates have been arranged according to rotational bands, with cascade transitions shown first, then cross-over transitions in increasing energy. Samples of both X and Y gates are shown, and are mixed for the sake of displaying important coincidences. Figures A-1 and A-2 are gates for transitions in the K=0 ground band. Only a few of the more important coincidences from members of other bands have been labeled, since the scales are very compressed.

The transitions from even members of the $K=2^-$ octupole band are shown as the gates in Figure A-3 and it should be noticed that very few transitions from odd spin levels can be seen, and then only very weakly. Next the gates on transitions from odd members of this band

are displayed and the most intense feeding to an even level can be measured by the intensity of the 937-keV peak which is the 2^-(K=2) $\rightarrow$ 2^+(K=0) transition. In Figures A-5 and A-6 the interband K=2 $\rightarrow$ K=0 gates are shown with the most obvious transitions being to the ground band levels that are fed. Figures A-7 to A-11 display the gates for the transitions in the $K^\pi=6^-$ and $K^\pi=6^+$ band.

Based on the coincidence information and the gamma ray singles experimental data, the level scheme shown in Figure 5-10 was constructed. All of the transitions except the 1275-keV transition from the 1381-keV level have some coincidence support. The four bands which are shown will each be discussed separately in the next chapter. Several transitions can be placed from the coincidence data as definitely feeding into the ground band. These are the 465-keV and 674-keV gammas which feed into the 10^+ member, the 559-keV which feeds the 12^+ level, and the 460-keV gamma feeding the *yrast* band at 14^+. Several of these lines have been identified as transitions from the β-band and are placed on the level scheme; the origin of the 465-keV line is unknown.

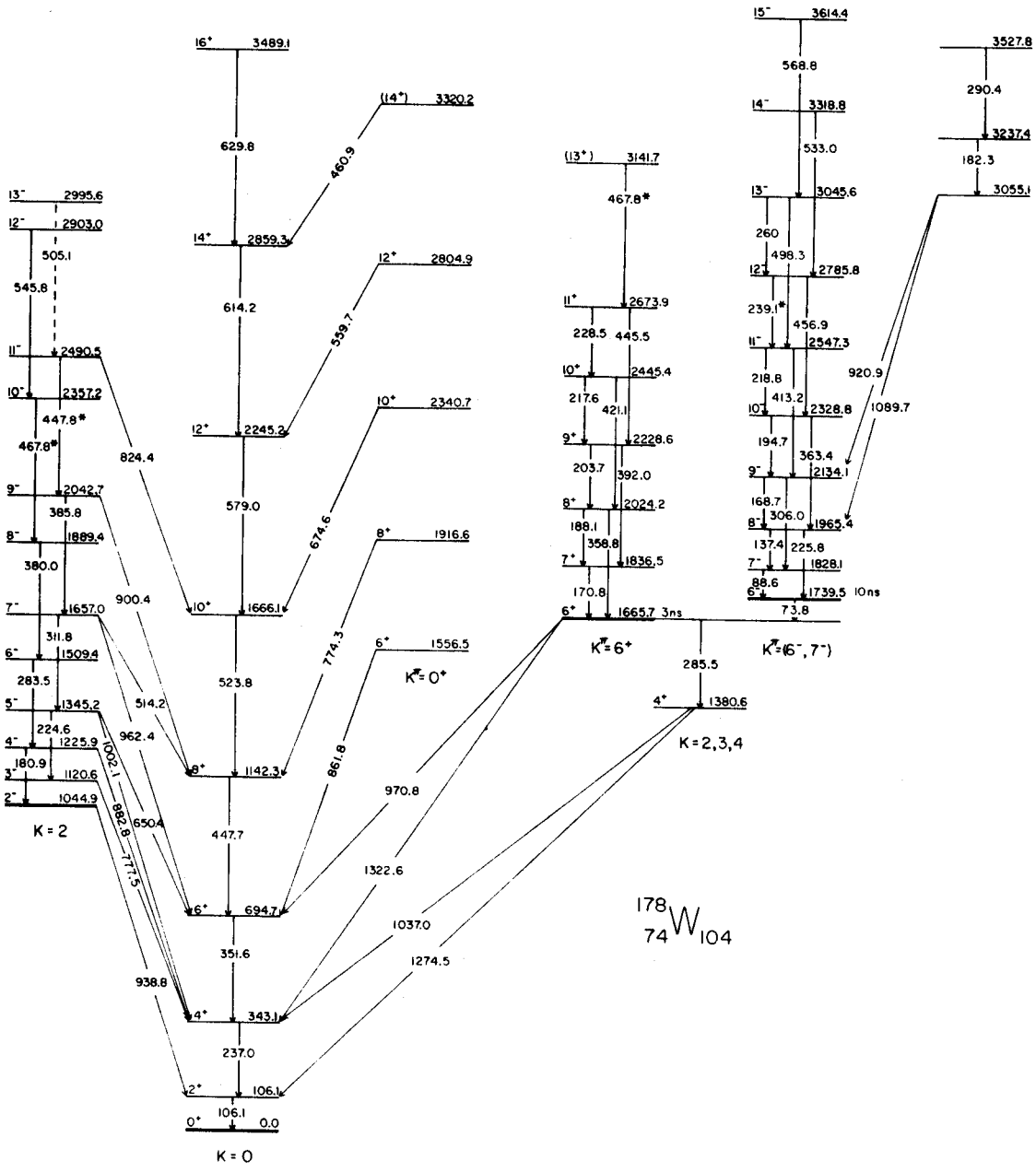
16+ 3489.1
629.8
14+ 2859.3
614.2
12+ 2245.2
579.0
10+ 1666.1
523.8
8+ 1142.3
447.7
6+ 694.7
351.6
4+ 343.1
237.0
2+ 106.1
0+ 106.1 0.0
K = 0
(14+) 3320.2
460.9
12+ 2804.9
559.7
10+ 2340.7
674.6
8+ 1916.6
774.3
6+ 1556.5
861.8
K^π = 0+
13- 2995.6
12- 2903.0
505.1
545.8
11- 2490.5
10- 2357.2
447.8*
467.8*
9- 2042.7
385.8
8- 1889.4
380.0
7- 1657.0
311.8
6- 1509.4
283.5
5- 1345.2
224.6
4- 1225.9
180.9
3- 1120.6
2- 1044.9
K = 2
824.4
900.4
514.2
962.4
1002.1
882.8
650.4
777.5
938.8
(13+) 3141.7
467.8*
11+ 2673.9
228.5
445.5
10+ 2445.4
217.6
421.1
9+ 2228.6
203.7
392.0
8+ 2024.2
188.1
358.8
7+ 1836.5
170.8
6+ 1665.7 3ns
K^π = 6+
285.5
4+ 1380.6
K = 2,3,4
970.8
1322.6
1037.0
1274.5
15- 3614.4
568.8
14- 3318.8
533.0
13- 3045.6
260
498.3
12- 2785.8
239.1*
456.9
11- 2547.3
218.8
413.2
10- 2328.8
194.7
363.4
9- 2134.1
168.7
306.0
8- 1965.4
137.4
225.8
7- 1828.1
88.6
6- 1739.5 10ns
73.8
K^π = (6-, 7-)
3527.8
290.4
3237.4
182.3
3055.1
920.9
1089.7
178 74 W 104

Figure 5-10.

CHAPTER VI

DISCUSSION OF ^{178}W EXPERIMENTAL RESULTS

6.1 The K=0 Ground Band and β-Vibrational Band

The rotational band built on the K=0 ground state is identified here up to spin 16^+. In the decay of ^{178}Re studied in 1970 by Goudsmit, *et. al.* [Go70] the *yrast* cascade could be seen up to spin 6^+. The same transitions, as well as those associated with levels up to spin 10^+ were previously measured in-beam with NaI(Tl) detectors using the ^{181}Ta(p,4n) reaction [Mi65] and up to spin 14^+ via ^{178}Hf(α,4n) reaction [La65]. With the available energy resolution, the latter two experiments showed that the ground band level energies followed the simple I(I+1) energy relation within experimental errors. A plot of the ground band level energies from the current experiment is shown in Figure 6-1. For purposes of comparison, the ground bands of ^{180}W, ^{182}W, and ^{170}Yb are also shown. This type of plot, which is used to emphasize deviations from linearity, displays $(\hbar^2/2\mathcal{J})^{-1}$ on the abscissa versus $(\hbar\omega)^2$. For a constant moment of inertia, a horizontal straight line would be obtained. A "backbending" type nucleus would display an "S-shaped" curve with the backbending phenomena showing up as a sharp increase of the moment of inertia. None of the nuclei on the graph here would be considered strong backbenders. There may be some sort of trend showing up in the ground bands of deformed W-nuclei, so this plot, and the implications of the degree of non-linearity of the plots of ground band energy levels that is involved will be discussed in detail in the next chapter.

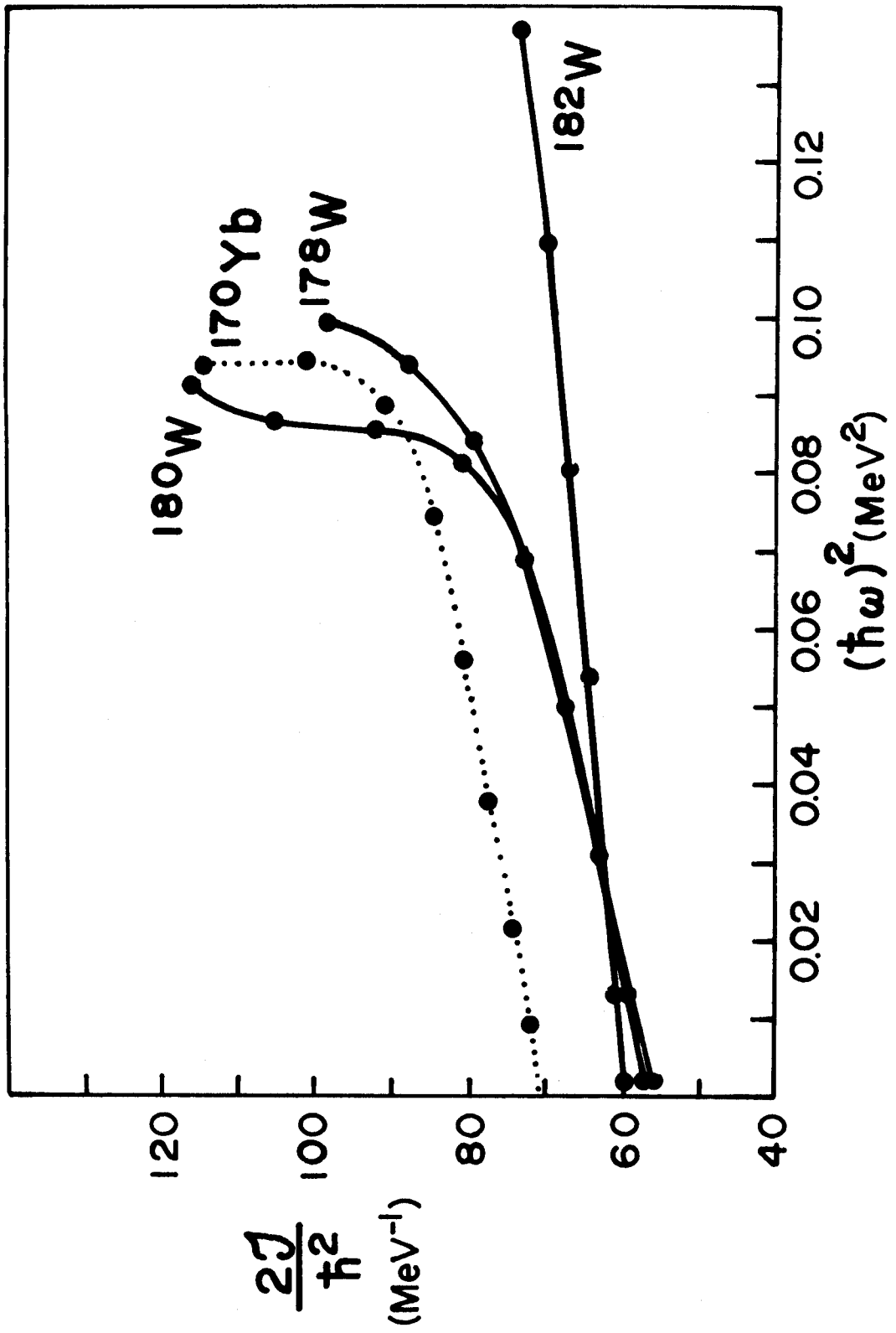

Figure 6-1. Plots of $\frac{2\mathcal{J}}{\hbar^2}$ versus $(\hbar\omega)^2$ for the *yrast* sequences in ^{178,180,182}W and ^{170}Yb.

In the decay of ^{178}Re [Go70], levels at 1083 and 1276 keV were characterized as 2^+ and 4^+ members of a K=0 band. Levels up to spin (10) in this band were identified in the ^{181}Ta(p,4n) in-beam experiments [Ca75] with the bandhead tentatively placed at 1001 keV. A $K^\pi=0^+$ band arising from a collective β-vibration is expected to lie below the pairing gap at about 1 MeV. This band has been located at 1150 keV in ^{176}Hf [Be71] and at 1196 keV in ^{178}Hf [Ga62]. These bands decay primarily by interband transitions to levels in the ground band with the ΔI=0 transitions having large $E0$ components.

In the present ^{177}Hf(α,3n) experiments, several gamma rays which feed promptly into the high spin ground band levels have been identified, and it is found that five of them appear to originate from the spin 6 to (14) members of the β-vibrational band. No intraband feeding is seen, and in fact, only the ΔI=0 interband transitions proceed with measurable intensity. The rotational parameter, $\frac{h^2}{2\mathcal{J}}$, for the β-band is 14.12 keV, and plots of the level energies versus I(I+1) for the ground- and β-bands are shown in Figure 6-2.

6.2 The K=2^- Octupole Band

The bandhead of the K=2^- octupole band is located at 1045 keV and was seen, along with the next two members of the band, in the decay of ^{178}Re [Go70]. In that work, $2^-\rightarrow2^+$ (ground band), $3^-\rightarrow4^+$ (ground band), and the intraband $4^-\rightarrow2^-$ transitions were seen. In-beam, the band is populated up to spin 13, and decays mainly via $E2$ crossovers.

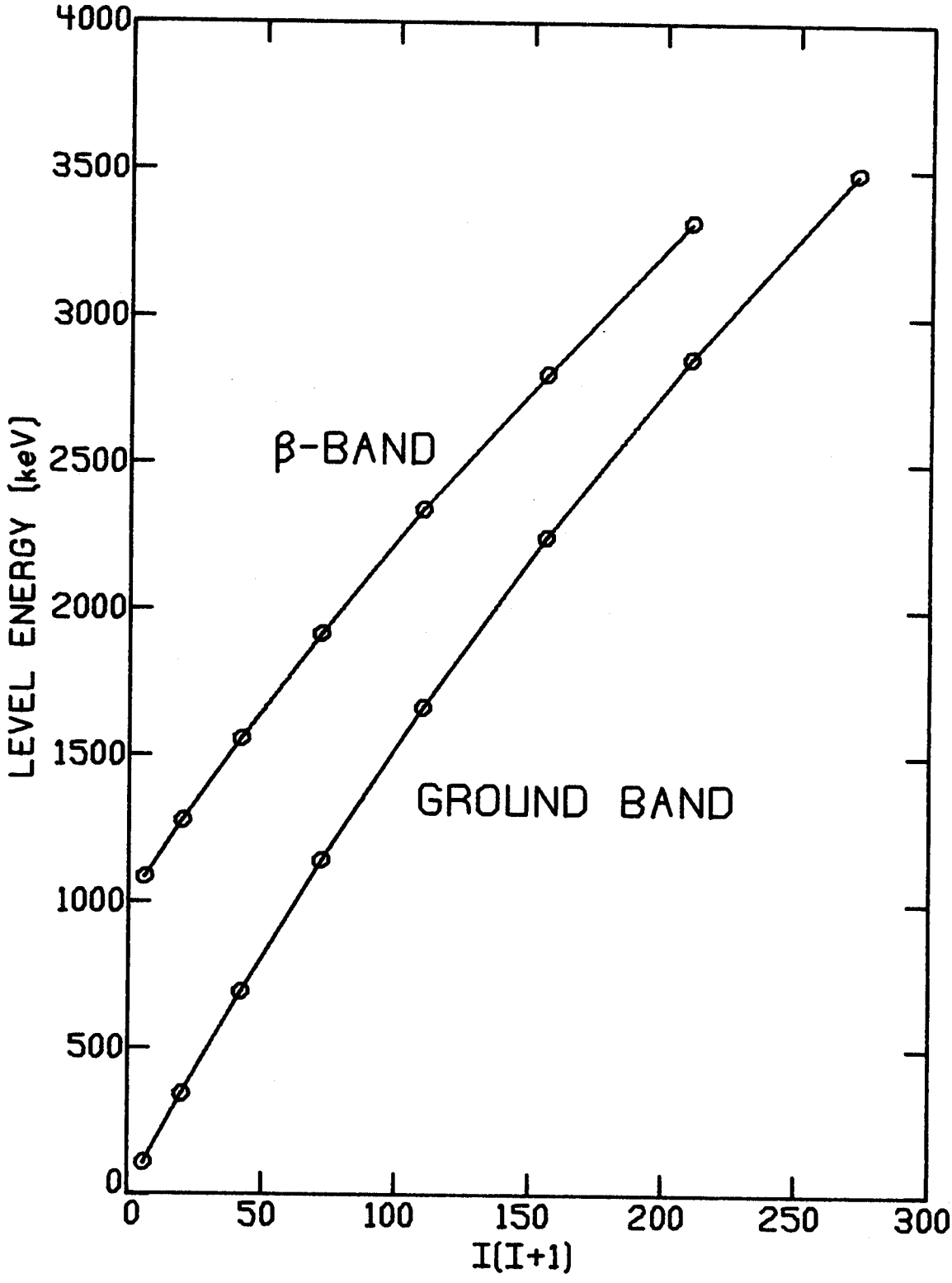

Figure 6-2. Plots of level energy versus I(I+1) for the $K^{\pi}=0^{+}$ ground band and β-vibrational bands in ^{178}W. Data for the 2^{+} and 4^{+} levels of the β-band taken from Go70 and Ca76.

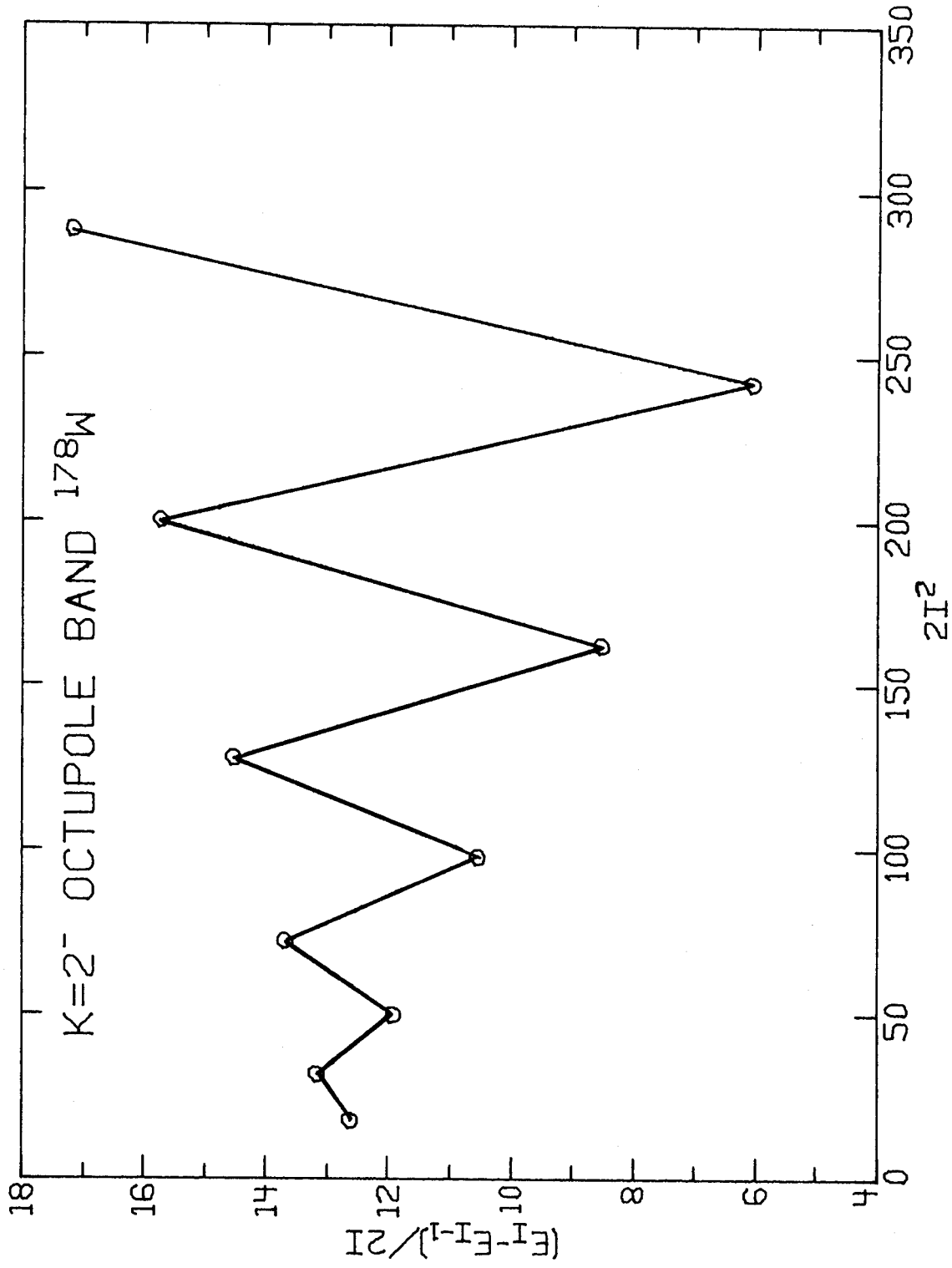

Figure 6-3. Plot of $E_I-E_{I-1}/2I$ versus $2I^2$ for the $K^{\pi}=2^-$ octupole vibrational band in ^{178}W.

This band displays some remarkable characteristics, the most obvious of which is the perturbed structure. By looking at the band on the level diagram (Figure 5-10), it is easily noticed that the energy spacings do not follow a smooth rotational I(I+1) dependence. The feature is more evident on a plot of $E_I-E_{I-1}/2I$ vs. $2I^2$ (Figure 6-3). The odd spin members are all depressed with respect to the even spin members; the odd spin levels are "favored".

The second remarkable feature is the feeding from the members of this K=2 band into the ground band. In general, the even spin members decay through intraband transitions to the bandhead. The 4^- level has a weak branch to the 4^+ ground band member, and the cascade transitions $6^-\rightarrow5^-$, and $4^-\rightarrow3^-$ can be weakly seen. The odd spin levels, on the other hand, have stronger branches to the K=0 ground band, and feed into I±1 members in two cases.

The calculations of Neergaard and Vogel [Nee70] can be at least qualitatively applied to describe the features of this band. Quantitatively, they were successfully used to predict the level energies and B($E3$) values for the octupole bands in several rare earth even-even nuclei, one of which was ^{176}Hf [Kh73a], which should be similar to ^{178}W. The model predicts the relative locations of $K=0^-$, 1^-, 2^-, 3^- octupole states and then mixes these bands through the Coriolis interaction. Mixing of the $K=0^-$ band members only propagates through odd spin members of other bands, since only odd spin members occur for $K=0^-$. This admixture causes the depression of the odd spin levels with respect to the even levels which have mixtures only of K=1, 2, 3 components. In general, it is the K=0 component which enhances the

transitions to the ground band. For ^{176}Hf, Khoo [Kh73a] calculated the transition rates for the interband transitions and showed that the transitions with K=0 components were faster than those without, implying that although (ΔK=0, 1) transitions are both allowed, the *E*1 matrix element is larger for the transitions with ΔK=0 components. Qualitatively, this can be inferred from the deexcitation pattern of the octupole band in ^{178}W, but the mixing calculation was not done since the positions of the lowest $K^{\pi}=0^-$, 1^-, 3^- states are not known, and theoretical calculations are not available for this nucleus.

6.3 The $K^{\pi}=(6^+)$ Band

The level at 1665.7 keV which has a half-life of $\leq$10 nsec is tentatively assigned as a K=6 bandhead. Deexcitation of this band occurs mainly through the 971- and 1323-keV transitions into the 6^+ and 4^+ members of the ground band. No transition to the 2^+ ground band level was found, nor was a transition to the 8^+ member which is difficult to confirm since its energy would be within 1 keV of the $8^+ \rightarrow 6^+$ transition. There is a weak decay branch of 285.5 keV to a level which was seen in the decay study [Go69] and which was assigned tentatively in the (p,4n) study [Ca76] as a 4^+ level. The 1666-keV level was given a K=5 assignment by Canty *et.al.* [Ca76] based on *E*1/*M*2 multipolarities from conversion coefficients for both the 971- and 1323-keV transitions. Angular distribution data of Canty [Ca76] indicate negative signs for the A_4 coefficients for both transitions which are incompatible with ΔI=1; the conversion electron data for the 971-keV peak is consistent with an *M*1/*E*2 mixture, and, in fact, the fit to an *E*1 requires an

unprecedented amount of *M*2 (22%) to be included. The assignment of K=6 is supported by all data except the conversion results of the 1323-keV line. Considerations discussed in section 6.4 of the K-assignment for the 1740-keV state and the 73-keV *E*1 transition which feeds into the K=6 bandhead provide some cross-evidence for the plausibility of a K=6 assignment for the lower band and K=6,7 for the upper band.

The rotational structure of the band built on the 6^+ level is very regular and can be seen up to spin 13. A plot of the levels in this band is shown in Figure 6-4. The rotational parameter $\frac{\hbar^2}{2\mathcal{J}}$ is 12.2 keV which is consistent with the K=6 two-quasiparticle bands in neighboring ^{176}Hf [Kh73b]. The decay of levels in this band proceeds via both cascade and crossover transitions. The branching ratios can be used, then, to calculate a value of $|g_K-g_R|$, with the sign determined by the sign of δ for the cascades in the band. The method used here has been successfully applied to several bands in ^{176}Hf [Kh73b], where supportive charged particle reaction data were available. A thorough consideration of the calculation of g_K from branching ratios is contained in the reference cited above. In general, for a singlet two-quasiparticle state, in the asympototic limit

$$g_K = 0 \quad \text{for neutrons}$$

$$g_K = 1 \quad \text{for protons.}$$

The quantity $\frac{|g_K-g_R|^2}{Q_o}$ is calculated from the expressions [A164]:

$$\frac{|g_K-g_R|^2}{Q_o} = [0.87\{E(I\rightarrow I-1)\}^2/(I^2-1)] \cdot (\frac{1}{\delta^2})$$

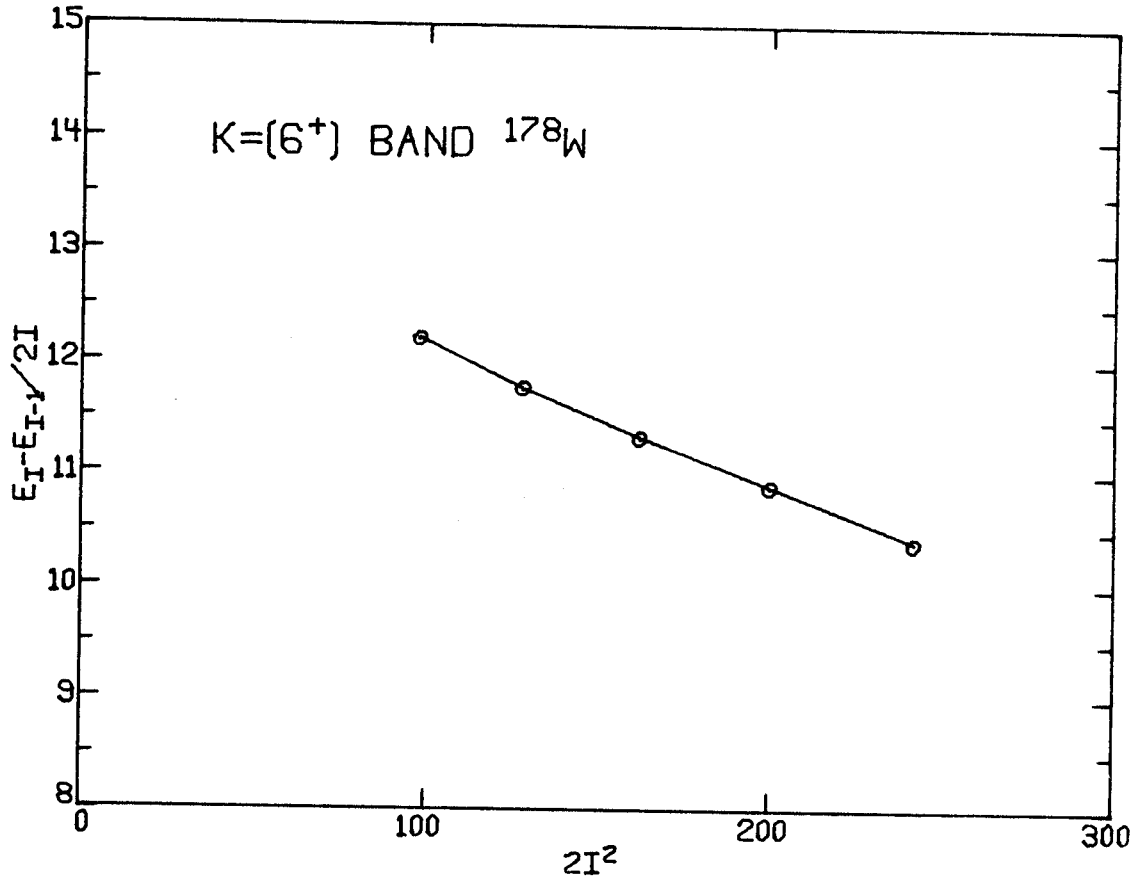

Figure 6-4. A plot of $E_I-E_{I-1}/2I$ versus $2I^2$ for the $K^{\pi}=(6^+)$ band in ^{178}W.

where δ, the mixing ratio, is the $E2/M1$ amplitude ratio in the cascade transition, and

$$1 + \frac{1}{\delta^2} = [(I+1)(I-1+K)(I-1-K)/2\lambda K^2(2I-1)] \cdot \{E(I\rightarrow I-2)/E(I\rightarrow I-1)\}^5$$

where $\lambda = I_\gamma(I\rightarrow I-2)/I_\gamma(I\rightarrow I-1)$, the crossover/cascade branching ratio.

A value for $Q_o \simeq 6.6$ barns is approximated from the measured values for ^{180}W and ^{182}W [Lö70] and the value for $g_R = 0.246$ taken from a calculation in Kr68.

A large number of transitions in this band are components of multiplets, which makes an accurate determination of the branching ratios a difficult task. Since the branching ratios are constant, independently of how the level was populated, intensities from the excitation function data taken at beam energies of 34, 38, and 43 MeV were all compared. A value for g_K was then calculated using the most consistent set of branching ratios; and included also was an independent determination using the mixing ratio, δ, of the 171-keV gamma ray which was obtained from the angular distribution shown in Figure 6-5 using the extracted A_2 and A_4 in conjunction with the tables in Ma74. The value of g_K which was obtained is +0.06(14) implying that this band is predominantly a two-quasi-neutron structure. A $K^\pi=6^+$ level consisting of the neutron configuration $\{7/2^-[514], 5/2^-[512]\}$ is expected to lie in the vicinity of 1.6 MeV using the quasiparticle energies shown in Figure 2-2. Due to the error limits on the value of g_K, an undetermined amount of proton admixture up to 20% maximum could not be ruled out in this band.

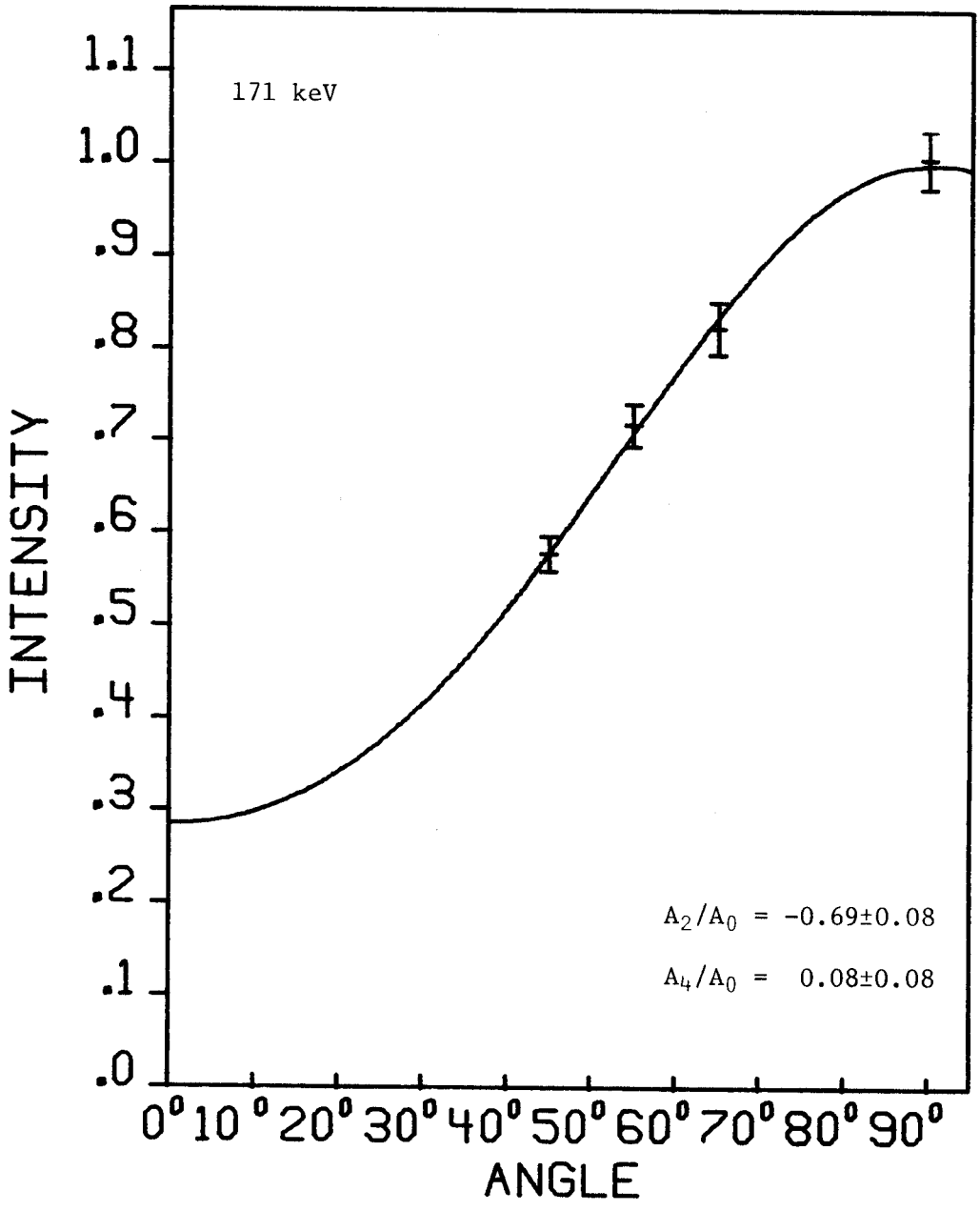

Figure 6-5. Angular distribution data and fitted curve for the 171-keV gamma ray.

6.4 The $K^{\pi}=(6,7)^{-}$ Band

The level at 1739.5 keV which feeds into the K=6 bandhead at 1665.7 keV via a strong 73-keV transition (whose lifetime is not easily extracted from the available timing measurements) is assigned as the bandhead of a K-5,6, or 7 band. Balancing the intensities of all known transitions feeding into the level with the intensities of transitions depopulating the level gives an upper limit on the conversion coefficient of the 73-keV transition of $\alpha_{tot} \leq 1$. Only an E1 conversion coefficient ($\alpha_{tot}=0.87$) is consistent with this result. The angular distribution of the 73-keV transition is also consistent with the assignment of an *E*1 multipolarity. From this conclusion, an assignment of $K^{\pi}=5^{-},6^{-}$ or 7^{-} can be inferred.

Levels in this band are populated more strongly than levels in the $K^{\pi}=6^{+}$ band, so the branching ratios can be determined with greater accuracy. A calculation of g_K using the expressions given in Section 3 of this chapter yields the following values:

K=5	$g_K=+0.034(2)$
K=6	$g_K=+0.093(5)$
K=7	$g_K=+0.14(5)$

In this band, g_K remains constant within the calculated errors throughout the band. The mixing ratios calculated from the A_2/A_0's of the cascade transitions are consistent with the mixing ratios calculated from the branching ratios. The sign of δ was obtained in the former calculation and is negative for the cascades in this band.

In order to compare the calculated g_K values for K=6,7 with theoretical values, the expression for a triplet spin configuration in

the limit of large deformation [Kh73b]

$$g_K = 1/K(g_s + (K-1)g_\ell)$$

must be evaluated. Using the free nucleon values

$$g_s = \begin{cases} 5.585 \\ -3.826 \end{cases} \qquad g_\ell = \begin{cases} 1 \text{ protons} \\ 0 \text{ neutrons} \end{cases}$$

and g_s(effective) = 0.6 g_s(free), the above expression yields:

	neutrons	protons
K=6	-0.38	+1.39
K=7	-0.33	+1.34

The possible combinations of low-lying neutron and proton orbitals which can form bands having appropriate k-values are:

			E_{ex}	g_K
Neutrons				
$K^\pi=5^-$	$\{1/2^-[521], 9/2^+[624]\}$	singlet	1.83 MeV	0
$K^\pi=6^-$	$\{5/2^-[512], 7/2^+[633]\}$	triplet	1.55 MeV	-0.38
$K^\pi=6^+$	$\{5/2^-[512], 7/2^-[514]\}$	singlet	1.63 MeV	0
$K^\pi=7^-$	$\{7/2^+[633], 7/2^-[514]\}$	singlet	1.70 MeV	0
Protons				
$K^\pi=6^+$	$\{5/2^+[402], 7/2^+[404]\}$	singlet	1.89 MeV	1
$K^\pi=7^-$	$\{5/2^+[402], 9/2^-[514]\}$	triplet	1.83 MeV	+1.34

Since the band built on the 1740-keV level is more strongly populated than the lower band, this suggests that it is more yrast in character than the lower K=6 band, and a K=5 assignment would give an energy for a level having a particular spin in the upper band which was higher in energy than the level with corresponding spin in the lower band. A K=6 or 7 assignment is thus preferred over K=5.

A comparison of the values of g_K deduced from mixing and branching ratios, with the theoretical g_K's for triplet and singlet spin configurations shows that only a two-quasineutron singlet configuration is compatible with the data. The neutron configuration $\{7/2^+[633],7/2^-[514]\}$ is tentatively assigned, then, as the major component of this band, with the amount of two proton admixture estimated as 10%.

The energy levels in this band are plotted in Figure 6-6 assuming a K=6 (for reasons explained below) for the bandhead. One noticeable feature of this curve is the compression of the low spin levels. The phenomenon could be understood if the levels did not constitute a single band, and if the 7^- level were instead the bandhead of the $K=7^-$ two quasineutron band, and the 6^- level assigned as the two-quasineutron triplet spin configuration $\{5/2^-[512], 7/2^+[633]\}$. This combination of Nilsson states may be expected to be populated at a relatively low excitation since both orbitals are seen low in excitation, and within 100 keV of each other in ^{177}W. (The $7/2^-[514]$ is level also seen low in excitation in ^{177}W which lends plausibility to the K=6 assignment for the 1665-keV bandhead.)

The other noticeable feature of the curve plotted in Figure 6-6 is the presence at low spins of an apparent positive β-term in the

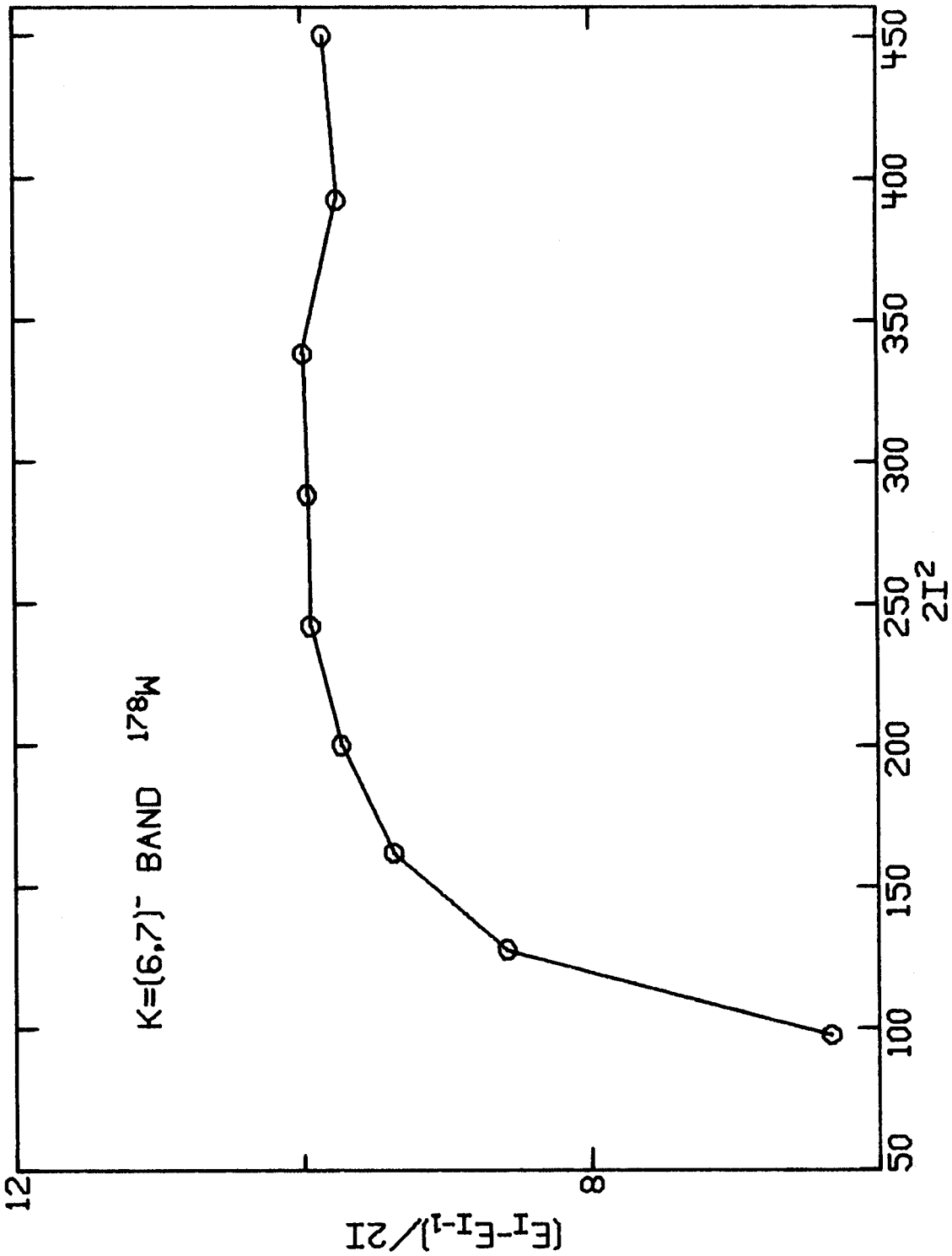

Figure 6-6. A plot of $E_I-E_{I-1}/2I$ versus $2I^2$ for the levels in the $K^{\pi}=(6,7)^-$ band.

expansion

$$E = E_0 + A[I(I+1)-K^2] + B[I(I+1)-K^2]^2$$

This effect has been experimentally seen [Kh73b] for other bands in this region containing $i_{13/2}$ neutron components.

In summary, the 1740-keV level may be tentatively assigned as a two-quasineutron $K^{\pi}=6^-$ triplet spin state with another band at 1828-keV feeding into it. Alternately, it may be assigned as the bandhead of the low-lying two neutron singlet spin $K^{\pi}=7^-$ band, with low-spin compression in the band caused by a band-mixing effect with a higher-lying K=8 band. Since this perturbing K=8 band does not have a spin 7 level, the 8-7 spacing in the lower band would be anomalously small, which would explain the abnormally low point in Figure 6-6. Available data do not allow a clear distinction between these two possibilities.

CHAPTER VII

CONCLUDING REMARKS: BACKBENDING AND THE $i_{13/2}$ ORBITAL

Both in ^{177}W and in ^{183}Os (Appendix E), the odd neutron may occupy an $i_{13/2}$ orbital. In ^{177}W, the $7/2^+[633]$ orbital is close to the Fermi surface, in ^{183}Os the $9/2^+[624]$ is low-lying. The bands which are built on both of these deformed single particle states are highly perturbed structures. In each case, the perturbations may be theoretically reproduced by a mixing with higher energy $i_{13/2}$ positive parity bands via the Coriolis interaction. It has been proposed by Stephens and Simon [St72] that the "backbending" effect in even-even *yrast* sequences is a rotation-alignment effect caused by a pair of neutrons in the $i_{13/2}$ orbital. This high-j pair will be the most affected by the Coriolis force with the result that their momenta become unpaired, and instead align separately with the core rotational momentum. A test of this theory may be indirectly obtained from a study of the odd neutron cases such as ^{177,179}W and ^{183}Os where $i_{13/2}$ bands are observed to very high spin values.

The type of behavior that one would like to predict is shown in the inset in Figure 7-1. In this plot, the *yrast* sequences of the even tungstens 178, 180, and 182 are displayed in the usual manner. The band in ^{182}W follows a nearly ideal rotational pattern, while in ^{180}W the *yrast* levels take a sharp upbend which is not as striking as e.g. ^{182}Os [Wa72] but is comparable to ^{170}Yb (see Figure 6-1). The question of

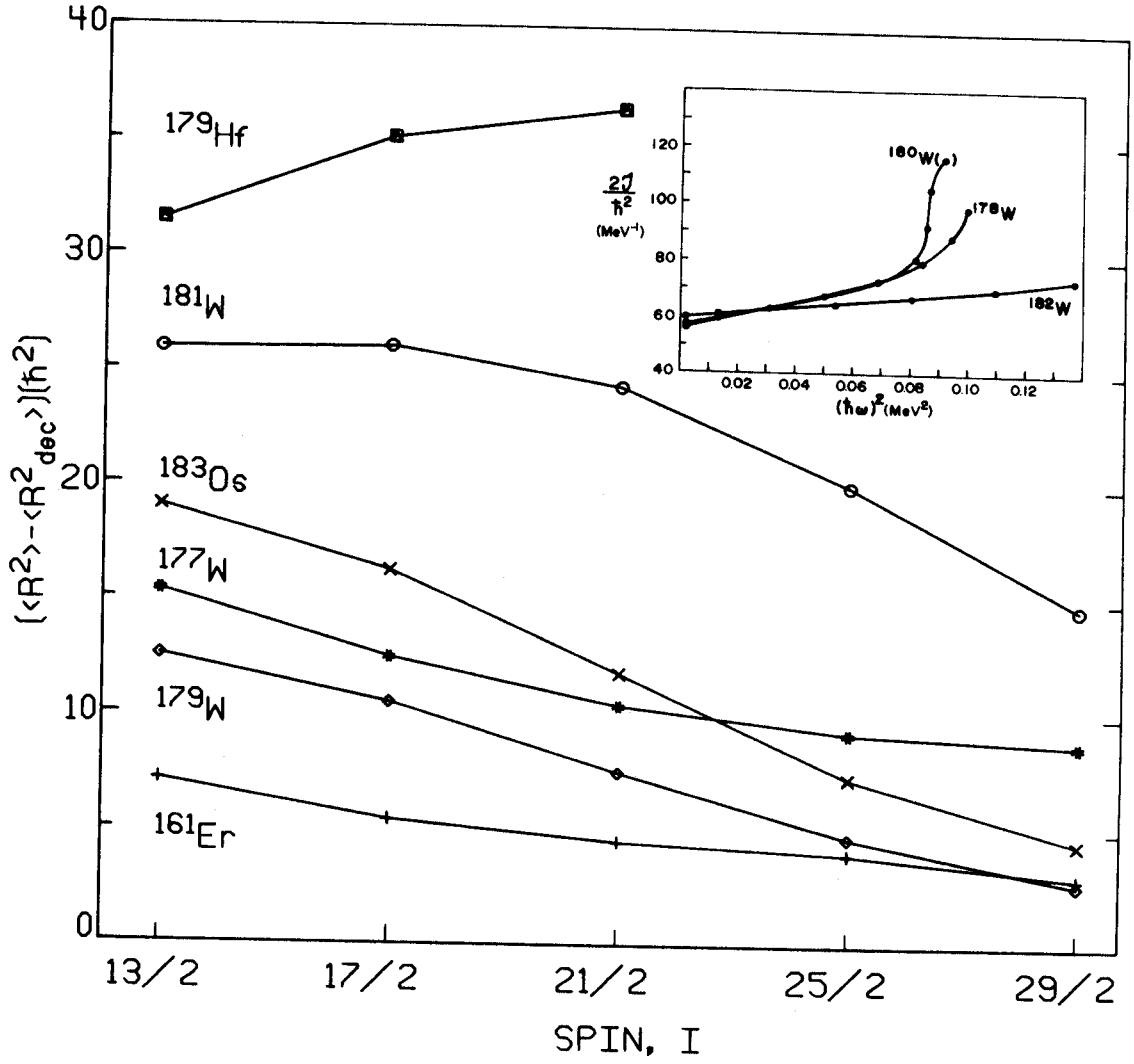

Figure 7-1. A plot of the value of $[\langle \vec{R}^2 \rangle - \langle \vec{R}^2_{dec} \rangle]$ as a function of spin for several rare earth nuclei. Data are taken from Hj70 (^{161}Er), Be75 (^{179}W), Li73 (^{181}W), and Hü70 (^{179}Hf). Inset shows even-even tungsten *yrast* bands taken from Wa72 (^{180}W) and Je74 (^{182}W).

whether the tungsten behavior is attributable to the $i_{13/2}$ neutrons or if the $h_{9/2}$ protons are contributing to the perturbation in a significant manner becomes relevant here, since it has recently been argued [Ne76] that it is the $h_{9/2}$ protons which are inducing the strong backbending seen in the osmium isotopes. In the osmium region of interest, the Fermi surface is located near higher-Ω $i_{13/2}$ orbitals than in the tungstens, so the decoupling effect of the Coriolis interaction is expected to be more effective for the tungsten $i_{13/2}$ neutrons (c.f. equation 2-9).

To calculate the amount of decoupling of the $i_{13/2}$ neutrons in the odd-A nuclei, first, the energy levels associated with $i_{13/2}$ bands are fit using the procedure described in Chapter 4.2. Since states having K±1 are mixed by the Coriolis interaction, the wavefunctions which are determined for each level are constructed of a linear combination in Ω of the $i_{13/2}$ orbitals. These eigenstates, which are written as $\Sigma f^{I} |I\Omega\rangle$, are then transformed according to the weak coupling scheme of Vogel [Vo70] to the $|IRj\rangle$ basis. Then, using a procedure described by Bernthal in Be74, the expectation value of the rotational angular momentum is calculated for each spin state using the overlap of the two wavefunctions [Vo70],

$$\langle IRj | I\Omega\rangle = \sqrt{2} \sum_{\Omega=1/2}^{j} (I\Omega j-\Omega | R0)(-1)^{j-\Omega} f_{\Omega}^{I} C_{j\ell}^{\Omega},$$

where the $C_{j\ell}^{\Omega}$ are the Nilsson coefficients, to give [Be74]:

$$\langle \vec{R}^2 \rangle = \sum_{R,j} \langle IRj | I\Omega\rangle^2 R(R+1).$$

The values for $\langle R^2 \rangle$ thus calculated are compared with the minimum (decoupled) value possible for $\vec{R} = \vec{I} - \vec{j}$. A plot of $[\langle \vec{R}^2 \rangle - \langle \vec{R}^2_{dec} \rangle]$ vs. spin is shown in Figure 7-1 for some rare earth nuclei including ^{183}Os and ^{177}W. In a completely decoupled $i_{13/2}$ band (the particle angular momentum aligned with the core angular momentum), the quantity on the abscissa should tend to zero. For higher spin values, the aligning (Coriolis) force becomes very strong and the values approach the decoupled value. If the amount of decoupling in the band built on a single $i_{13/2}$ particle is to be a harbinger of "backbending" then a trend between odd and even-even systems should be evident on this plot.

On examination of some of the nuclei represented on this plot, it can be noted that the band in ^{179}Hf, which is not in a region of backbenders, displays the behavior expected of a strongly-coupled system i.e. the total spin reflects only an average increase in the angular momentum of the core. At the other extreme, ^{161}Er shows the most decoupled positive parity band plotted in Figure 7-1 and is indeed in a region of well-known backbenders. The case of ^{183}Os is not quite as simple. Neighboring ^{182}Os and ^{184}Os both have anomalous *yrast* sequences, and one would expect that the odd neutron in ^{183}Os would be highly decoupled. At very high spins, this seems to be the case, but at lower spins it shows behavior intermediate between strong and weak coupling. At very high spins - 25/2 and greater - the wavefunctions may not be as reliable as they are for lower spin states due to effects which the normal model does not take into explicit account i.e. there may be shape variations, moment of inertia changes, and changes

in the single particle spectrum. For this reason, the ^{183}Os case may not be easily explained by the $i_{13/2}$-neutron decoupling picture shown here.

The ordering of the odd tungsten nuclei proceeding toward a greater degree of decoupling is ^{181}W, ^{177}W, ^{179}W; the amount of backbending in the neighboring even-evens increases in the order ^{182}W, ^{178}W, ^{180}W consistent with the A-1 trend. In Figure 7-2, the *yrast* levels in mass 177-182 tungsten are shown. The trend in compression of the positive parity bands in the odd-*A* sequence reflects qualitatively the A-1 trend which is also found in the decoupling picture. It is expected that the even nuclei should follow the A-1 trend more closely than the A+1 behavior since the addition of a nucleon into a partly occupied orbital will induce less change in the position of the Fermi surface than the addition of an odd nucleon into a paired system. Only one exception to the observation that the even-even behavior can be predicted by the decoupling seen in the A-1 neighbor has been noted, that of ^{170}Yb.

For the tungsten nuclei, then, it appears to be meaningful to discuss the even-even *yrast* behavior in terms of the $i_{13/2}$ neutron decoupling trend. The amount of $h_{9/2}$ proton involvement has not yet been determined. For the case of ^{183}Os, an experiment was performed which populated the positive parity band to spin (45/2) [Ne76]. Backbending was detected in this band, clearly indicating the $h_{9/2}$ proton involvement. Such an experiment for ^{179}W would be an important test of the proton behavior in ^{180}W.

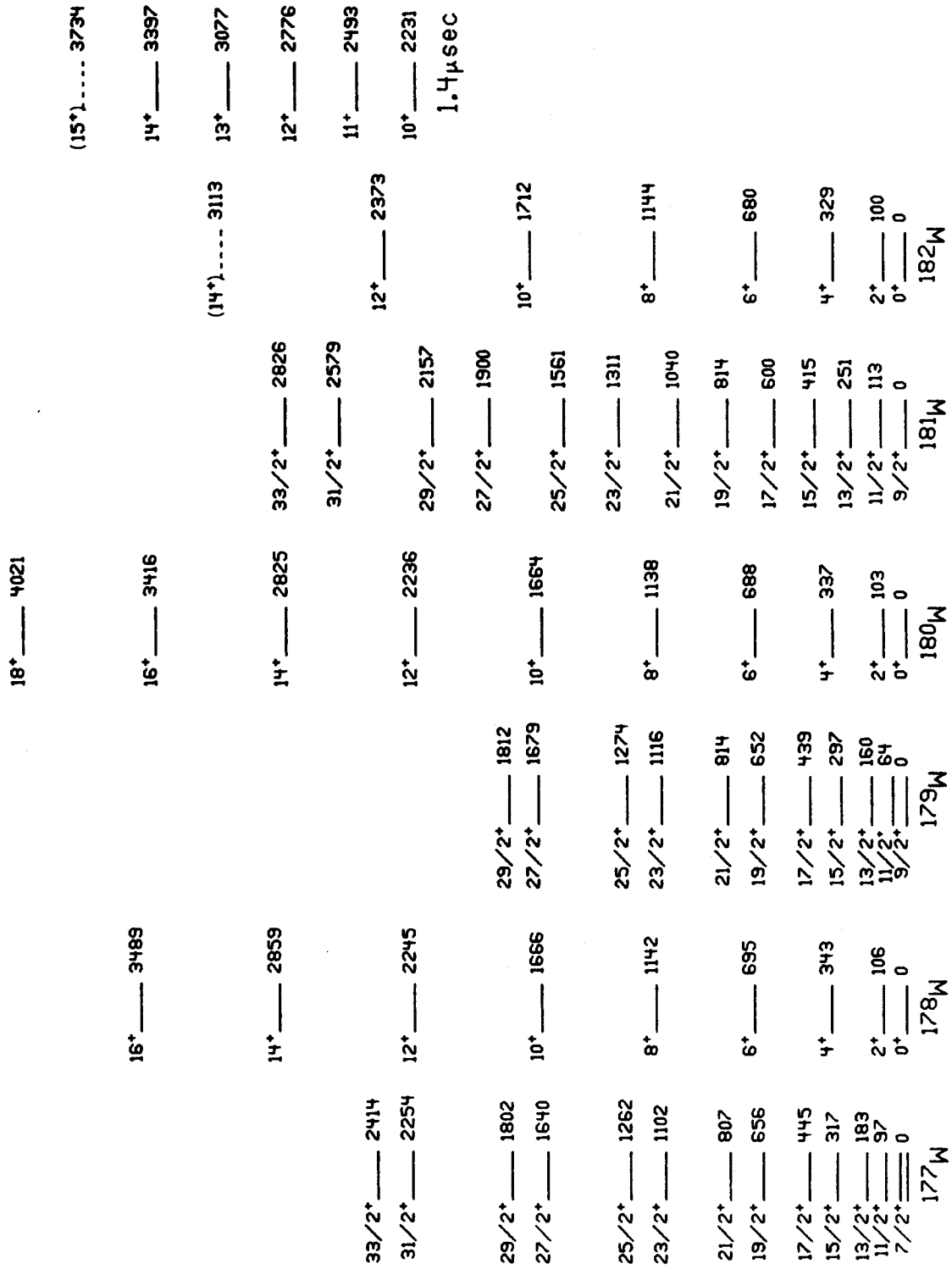

Figure 7-2. A plot of the *yrast* levels in tungsten nuclei mass 177-182.

Since the effects of Coriolis decoupling of a high-j particle are expected to be greatest for the low-Ω orbitals, the location of the Fermi surface with respect to these orbitals is needed for an accurate determination of the matrix elements, and hence, of the Ω-composition of the wavefunctions. The degree of backbending, then, is sensitive to the exact position of the Fermi surface with respect to the $i_{13/2}$ orbitals [Ha73, Fa74] and in particular its nearness to the low-Ω orbitals [St74] both of which depend on the hexadecapole deformation which may be increasing in this region [Ni69]. Thus, there remain questions on the detailed role of the $i_{13/2}$ neutrons in the tungsten backbending-type behavior, although the prediction of the ^{180}W *yrast* anomaly [Be76] is strongly suggested by the general trends observed in the odd-*N* positive parity bands.

REFERENCES

REFERENCES

A

[A164] P. Alexander, F. Boehm, and E. Kankeleit, Phys. Rev. B133, 284 (1964).

[A172] B. L. Alder and N. N. Perrin, Nucl. Phys. A197, 593 (1972).

B

[Ba57] J. Bardeen, L. N. Cooper, and J. R. Schreiffer, Phys. Rev. 108, 162 (1957).

[Be71] F. M. Bernthal, J. O. Rasmussen, and J. M. Hollander, Phys. Rev. C3, 1294 (1971).

[Be74] F. M. Bernthal, J. S. Boyno, T. L. Khoo, and R. A. Warner, Phys. Rev. Letters 33, 1313 (1974).

[Be75] F. M. Bernthal and R. A. Warner, Phys. Rev. C11, 188 (1975).

[Be76] F. M. Bernthal, C. L. Dors, B. D. Jeltema, T. L. Khoo, and R. A. Warner, submitted to Phys. Letters.

[Bo52] A. Bohr, Dan. Mat. Fys. Medd. 26, No. 14 (1972).

[Bo58] A. Bohr, B. R. Mottelson, and D. Pines, Phys. Rev. 110, 936 (1958).

[BETA] Program BETABLE written by T. C. Clements at Lawrence Berkeley Lab (1966).

[Bu71] M. E. Bunker and C. W. Reich, Rev. Mod. Phys. 43, 348 (1971).

C

[Ca76] M. J. Canty, N. E. Davison, D. A. Bohan, and P. Yuen, to be published.

[CS8N] Program CS8N written by T. Sikkeland and D. Lebeck, University of California, Berkeley.

F

[Fa74] A. Faessler, F. Grümmer, L. Lin, and J. Urbano, Phys. Letters 48B, 87 (1974).

G

[Ga62] C. J. Gallagher and V. G. Soloviev, Mat. Fys. Skr. Dan. Selsk. 2, No. 2 (1962).

[Go70] P. F. A. Goudsmit, J. Konijn, and F. W. N. deBoer, Nucl. Phys. A151, 513 (1970).

[Gr75] H. C. Griffin, private communication.

H

[Ha73] A. J. Hartley, R. Chapman, G. D. Dracoulis, S. Flanagan, W. Gelletly, and J. N. Mo, J. Phys. A6, L60 (1973).

[Ha75] B. Harmatz, D. J. Horen, and Y. A. Ellis, Phys. Rev. C12, 1083 (1975).

[Hj70] S. A. Hjorth, H. Ryde, K. A. Hagemann, G. Lovhoiden, and J. C. Waddington, Nucl. Phys. A144, 513 (1970).

[Hü70] H. Hübel, R. A. Naumann, M. L. Anderson, J. S. Larsen, O. B. Nielsen, and N. O. Roy Poulson, Phys. Rev. C1, 1845 (1970).

[Hu73] S. Hultzberg, I. Rezanka, and H. Ryde, Nucl. Phys. A205, 321 (1973).

J

[Je74] B. D. Jeltema, M.S. Thesis, Michigan State University, 1974.

[Jo73] A. Johnson and Z. Szymański, Phys. Lett. C 7, 181 (1973).

K

[Kh72] T. L. Khoo, L. A. Finlayson, and P. Sigg, Michigan State University Cyclotron Laboratory Annual Report (1972-73).

[Kh73a] T. L. Khoo, J. C. Waddington, Z. Preibisz, and M. W. Johns, Nucl. Phys. A202, 289 (1973).

[Kh73b] T. L. Khoo, J. C. Waddington, and M. W. Johns, Can. J. Physics 51, 2307 (1973).

[KKREC] Program KKRECOVERY. Three-parameter sorting routine written by C. B. Morgan for the Σ-7 computer. Unpublished.

[Kr68] J. Krumlinde, Nucl. Phys. A121, 306 (1968).

L

[La65] N. L. Lark and H. Morinaga, Nucl. Phys. 63, 466 (1965).

[Li72] Th. Lindblad and H. Ryde, Nucl. Phys. A193, 155 (1972).

[Li73] Th. Lindblad, H. Ryde, and P. Kleinheinz, Nucl. Phys. A210, 253 (1973).

[Lö70] K. Löbner, M. Vetter, and V. Hönig, Nucl. Data Tables A7, 495 (1970).

M

[Ma74] E. Der Mateosian and A. W. Sunyar, Atomic Data and Nuclear Data Tables 13, 391 (1974).

[Mi65] K. Miyamo, M. Ishihara, Y. Shida, H. Morinaga, T. Kuroyanagi, and T. Tamura, Nucl. Phys. 61, 25 (1965).

[Mo59] B. R. Mottelson and S. G. Nilsson, Mat. Fys. Skr. Dan. Vid. Selsk. 1, No. 8 (1959).

N

[Nee70] K. Neergård and P. Vogel, Nucl. Phys. A145, 33 (1970).

[New70] J. O. Newton, F. S. Stephens, R. M. Diamond, W. H. Kelly, and D. Ward, Nucl. Phys. A141, 631 (1970).

[Ne76] A. Neskakis, R. M. Lieder, M. Müller-Veggian, H. Beuscher, W. F. Davidson, and C. Mayer-Böricke, Nucl. Phys. A261, 189 (1976).

[Ni55] S. G. Nilsson, Mat. Fys. Medd. Dan. Vid. Selsk. 29, No. 16 (1955).

[Ni69] S. G. Nilsson, C. F. Tsang, A. Sobiczewski, Z. Szymanski, S. Wycech, C. Gustafson, I. Lamm, P. Möller, and B. Nilsson, Nucl. Phys. A131, 1 (1969).

[NILS] Nilsson Rochester Code. Program written by B. Nilsson, adapted for the Rochester IBM-360 by Th. Elze, 1970.

O

[Og71] W. Ogle, S. Wahlborn, R. Piepenbring, and J. Fredriksson, Rev. Mod. Phys. 43, 424 (1971).

[Os75] E. Osnes, J. Rekstad, and O. K. Gjotterad, Nucl. Phys. A253, 45 (1975).

P

[Pr62] M. A. Preston, *Physics of the Nucleus* (Addison-Wesley, 1962).

[Pr75] M. A. Preston and R. K. Bhaduri, *Structure of the Nucleus* (Addison-Wesley, 1975).

R

[Re76] J. Rekstad, E. Osnes, and G. Løvhøiden, Phys. Letters 62B, 15 (1976).

[Ri74] P. Ring, H. J. Mang, and B. Banerjee, Nucl. Phys. A225, 141 (1974).

[Ro69] J. T. Routti and S. G. Prussin, Nucl. Instr. Meth. 72, 125 (1969).

S

[Sl72] G. Sletten and P. Knudsen, Nucl. Instr. Meth. 102, 459 (1972). Technique used for making targets is outlined in this paper.

[St72] F. S. Stephens and R. S. Simon, Nucl. Phys. A183, 257 (1972).

[St74] F. S. Stephens, P. Kleinheinz, R. K. Sheline, and R. S. Simon, Nucl. Phys. A222, 235 (1974).

T

[TOOTS] Program TOOTSIE written for the Sigma-7 computer by D. Bayer (1971).

V

[Vo70] P. Vogel, Phys. Lett. 33B, 400 (1970).

W

[Wa72] R. A. Warner and F. M. Bernthal, Michigan State University Cyclotron Laboratory Annual Report (1971-72).

APPENDICES

APPENDIX A

Gated Coincidence Spectra of Transitions in ^{178}W

The following background subtracted gated spectra were obtained from a coincidence experiment which was performed with two large volume - 8% and 10% - efficient detectors. The X-gates display spectra taken with low gain, and are used to show high energy coincidences. The Y-gates display the high-gain spectra, used for better identification of low energy coincidences.

In general, the peaks which are not labeled in a gate belong to another rotational band, and are then labeled in the same gate shown in that band. The peaks which originate in contaminant nuclei, mainly ^{179}W and ^{178}Hf, are labeled with a †.

The top of each Y-axis is used as a limit, and overflows are not shown. Note that the X-scales are highly compressed so that in some cases statistical fluctuations in the background may appear as peaks. In the expanded gates, the distinction is easily made between peaks and background.

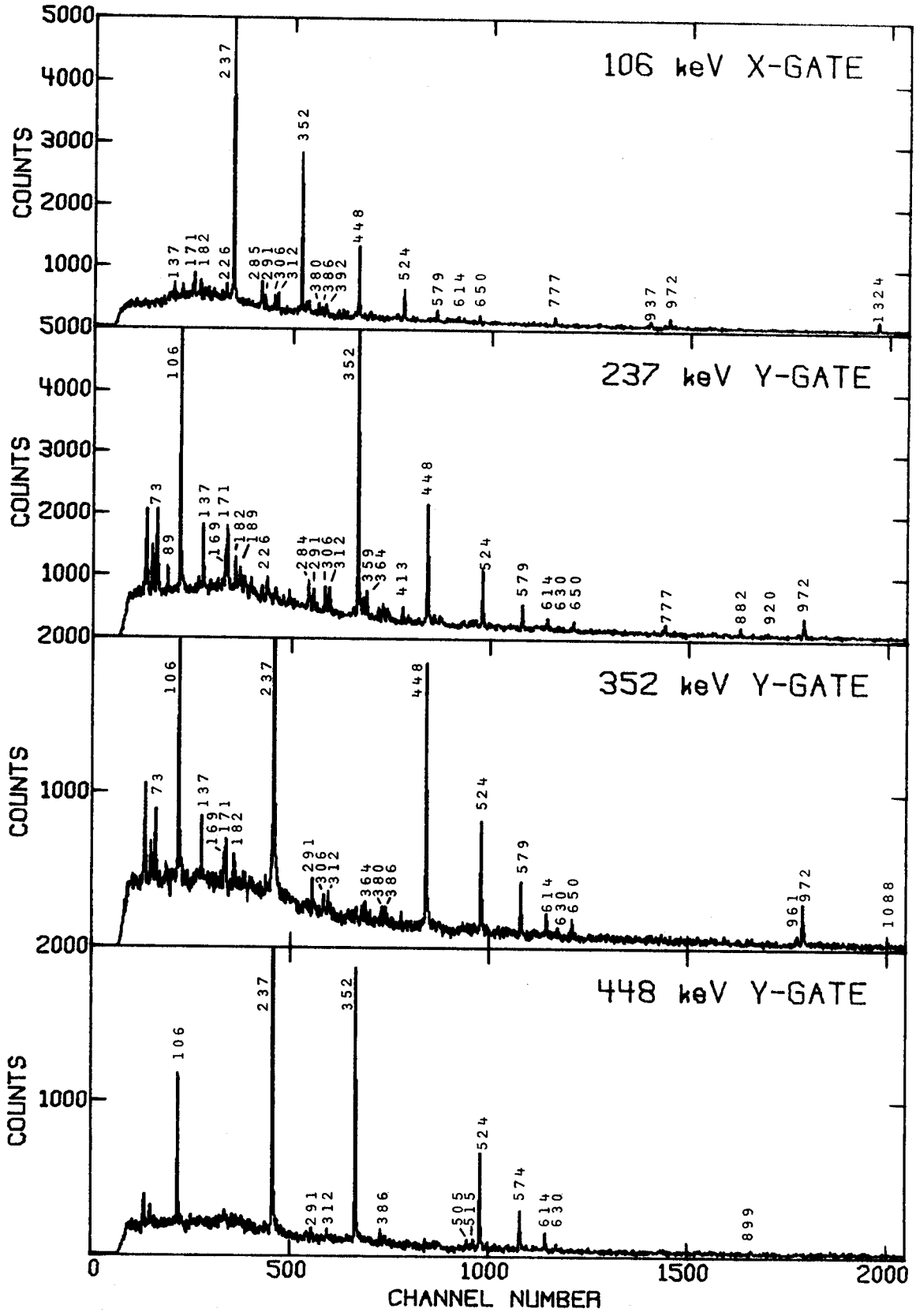

Figure A-1. Gated spectra of the first four ground band transitions.

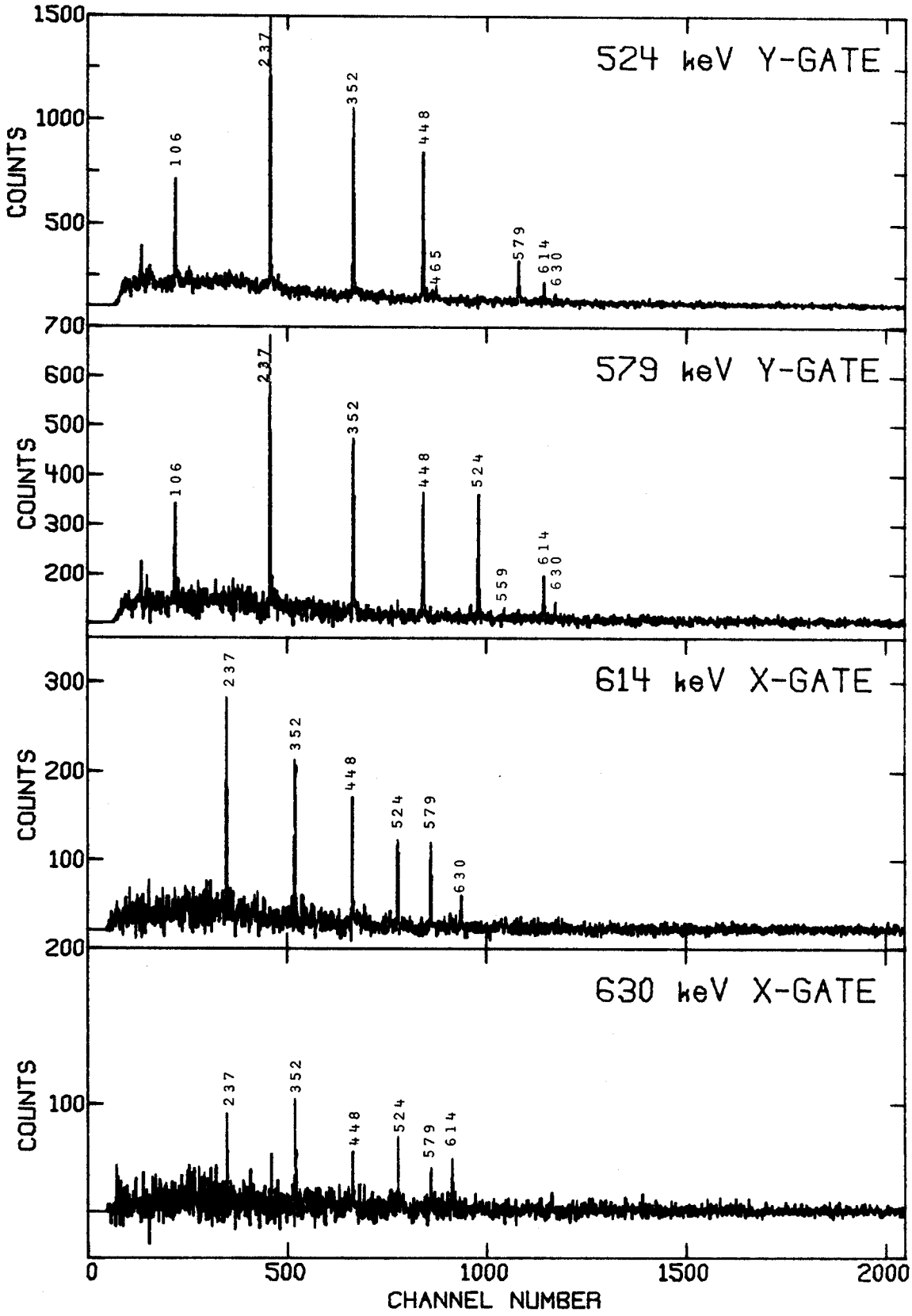

Figure A-2. Gates on the high energy ground band transitions.

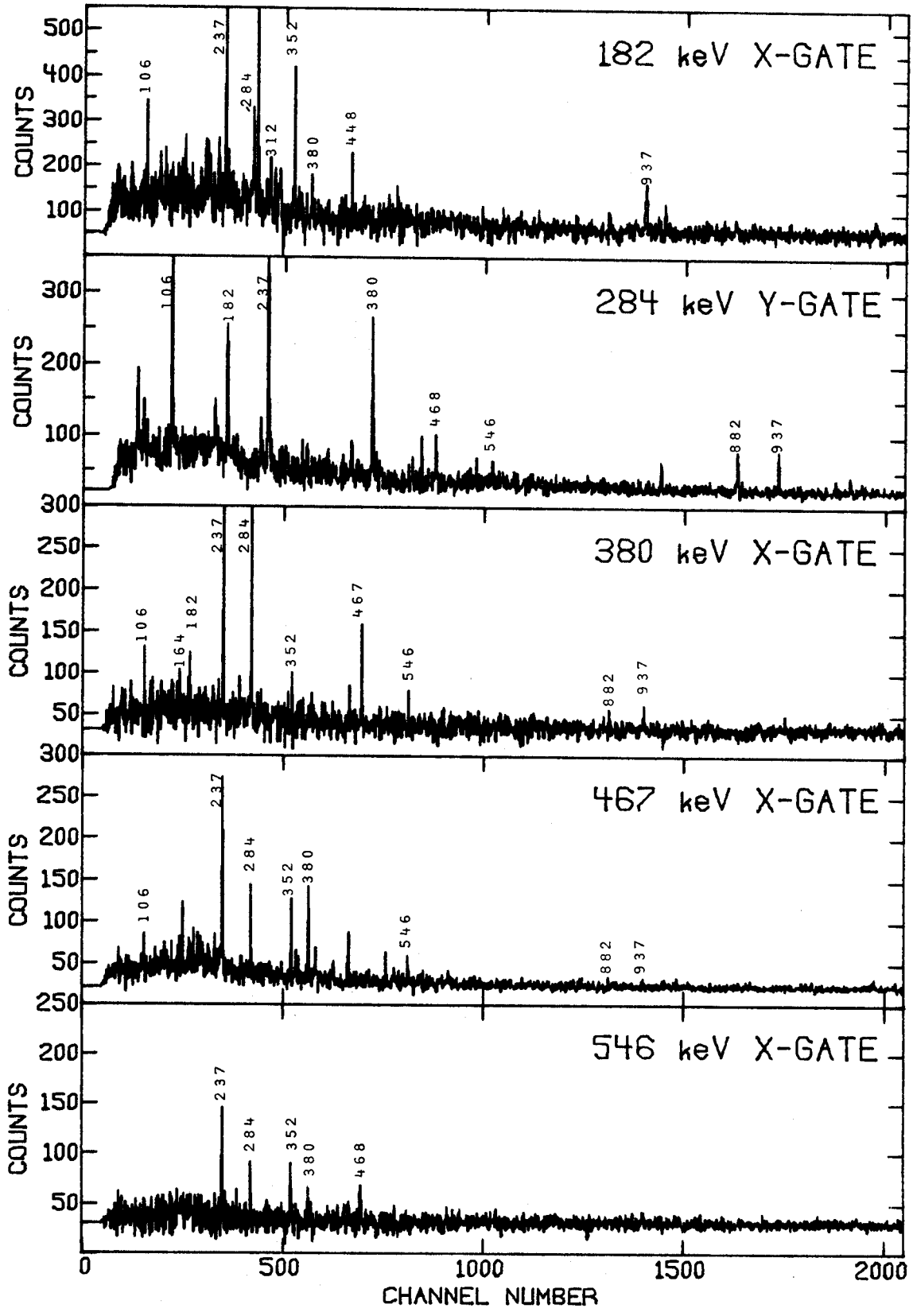

Figure A-3. Gated spectra of crossover transitions from even-spin members of the $K^{\pi}=2^{-}$ octupole band.

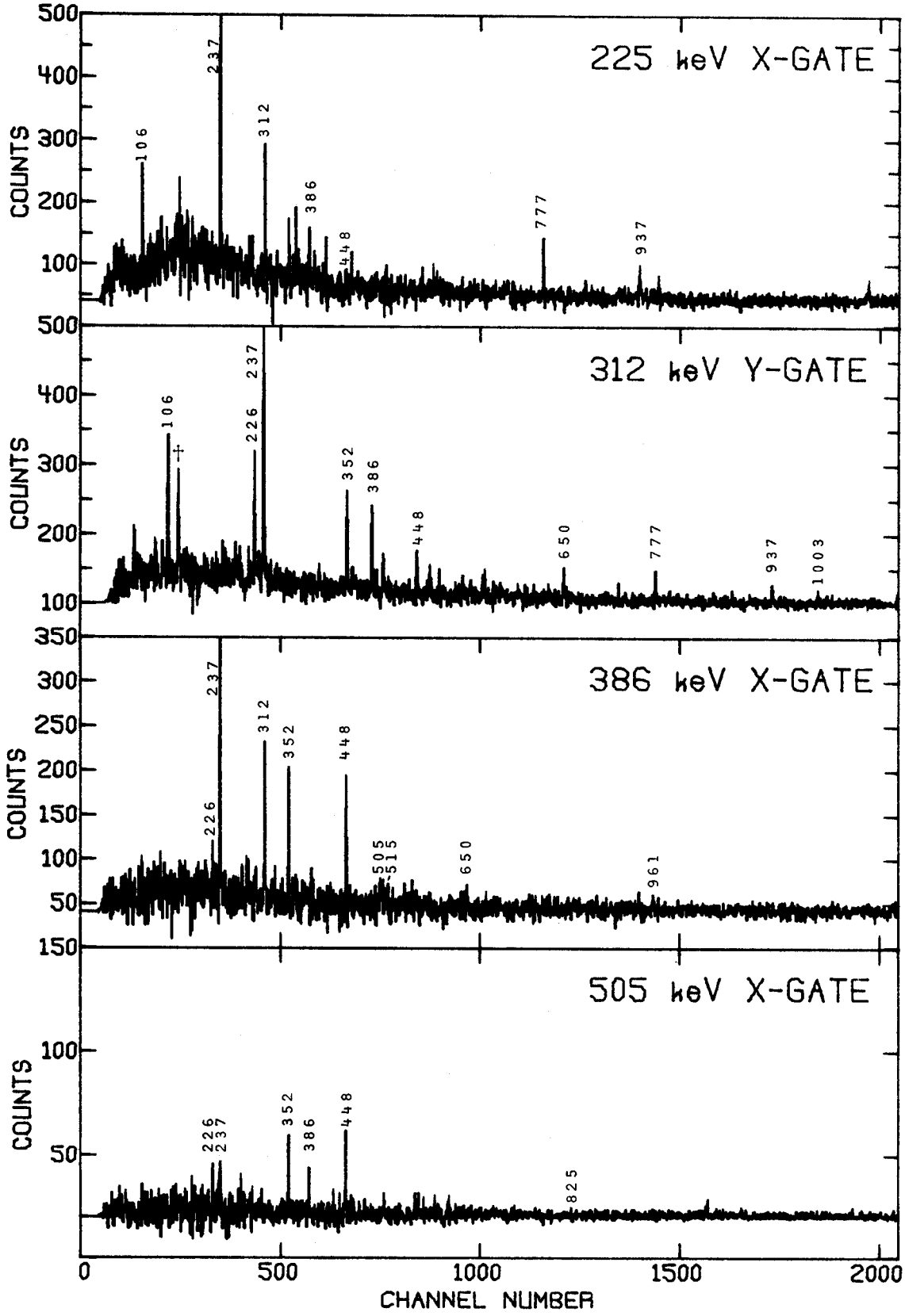

Figure A-4. Gated spectra of crossover transitions from odd-spin members of the $K^{\pi}=2^{-}$ octupole band.

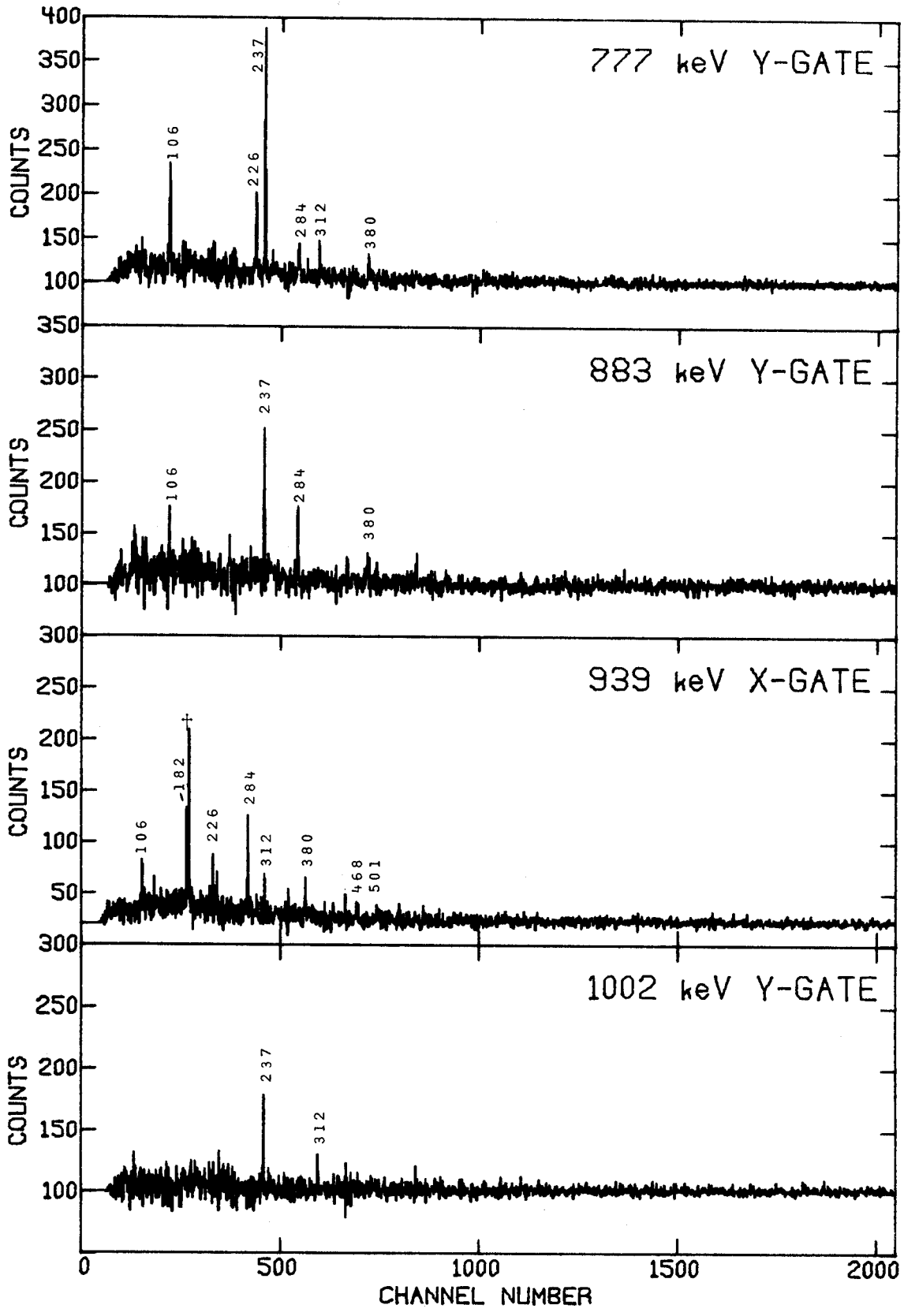

Figure A-5. Gates on some interband transitions between the $K^{\pi}=2^{-}$ octupole band and the $K^{\pi}=0^{+}$ ground band.

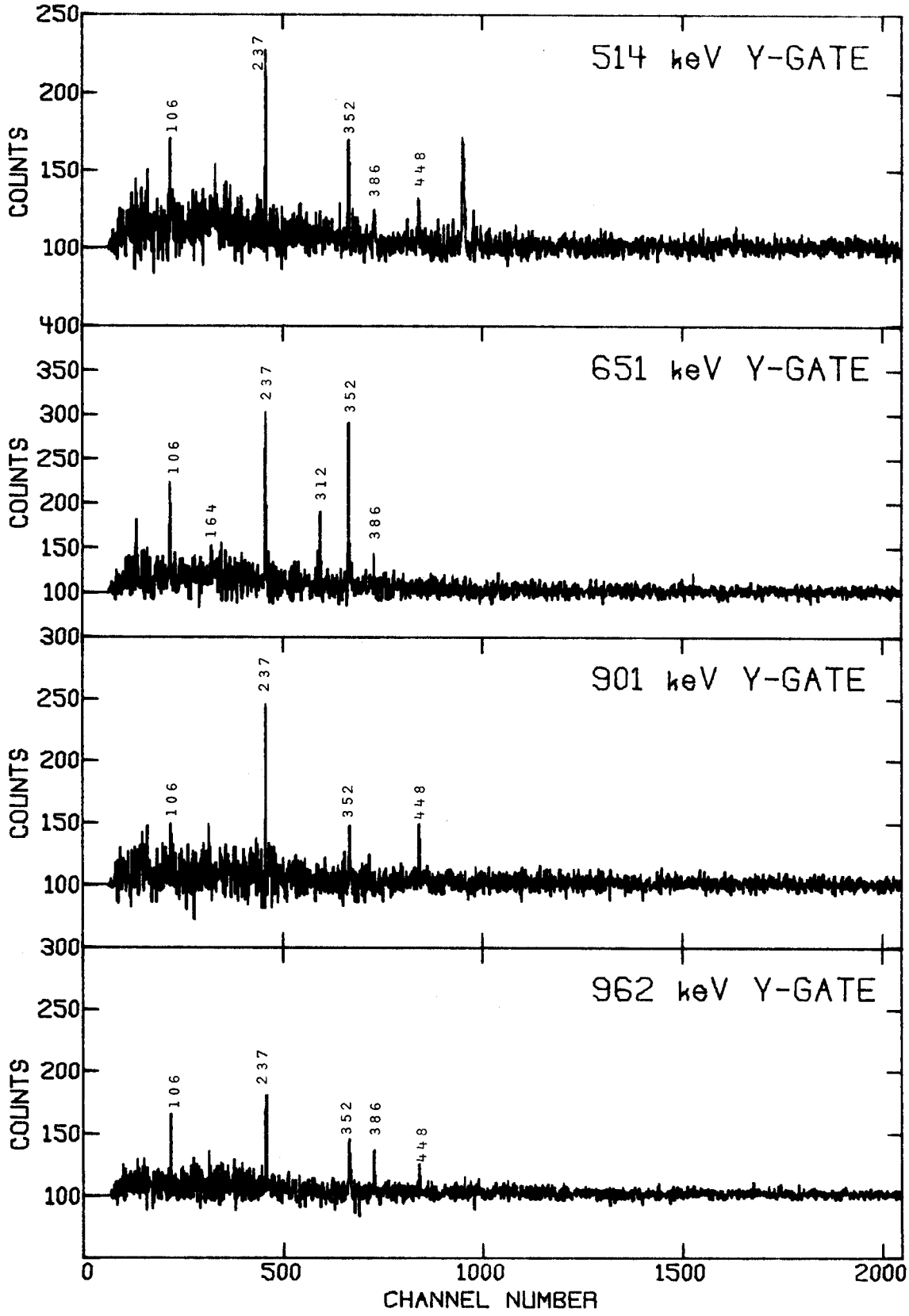

Figure A-6. Gates on the interband transitions from the higher energy levels of the octupole band to ground band levels.

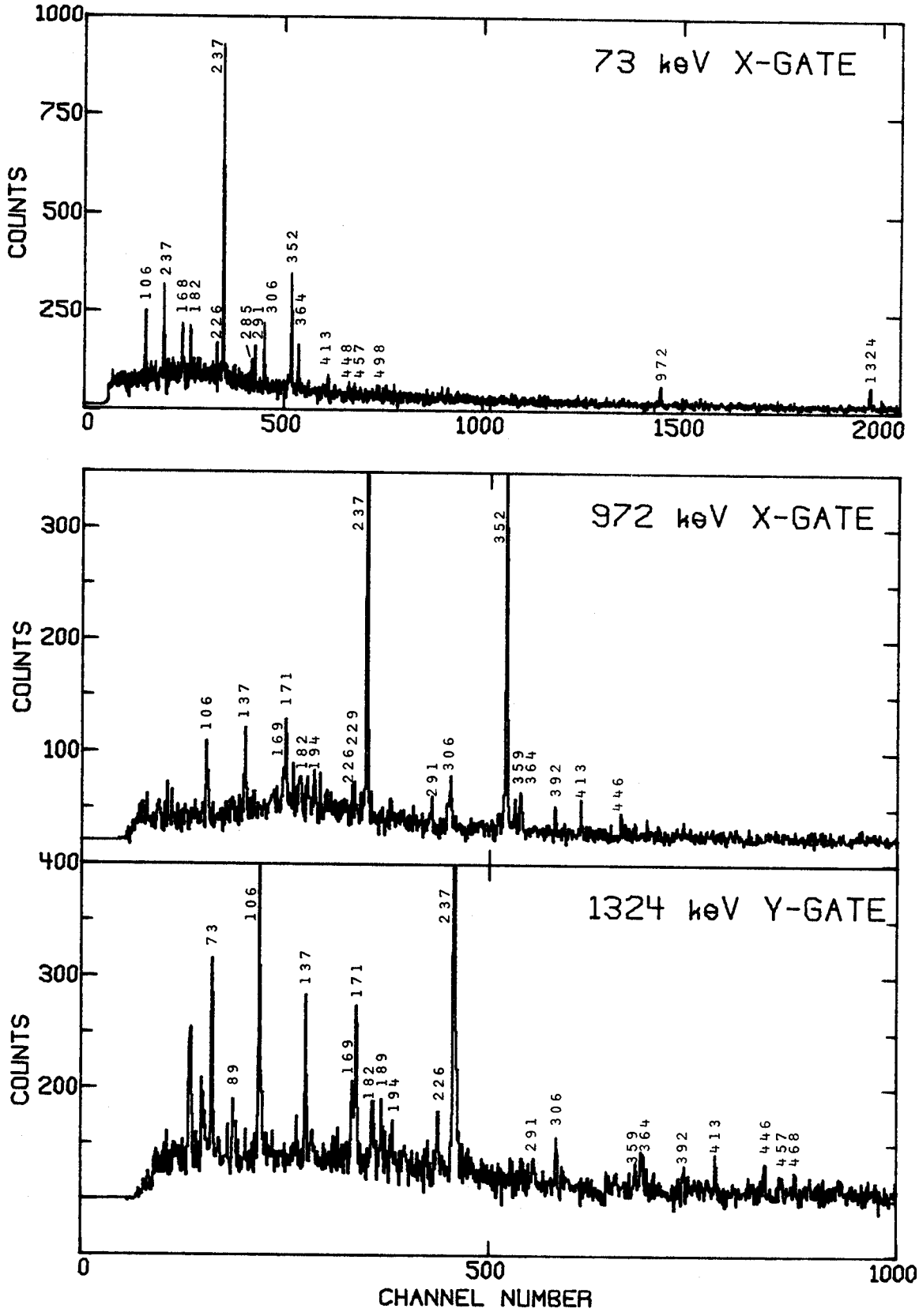

Figure A-7. Gates on the interband transitions from the $K^{\pi}=6^{+}$ to ground band, and on the transition between the $K^{\pi}=(6,7)^{-}$ and $K^{\pi}=6^{+}$ bands.

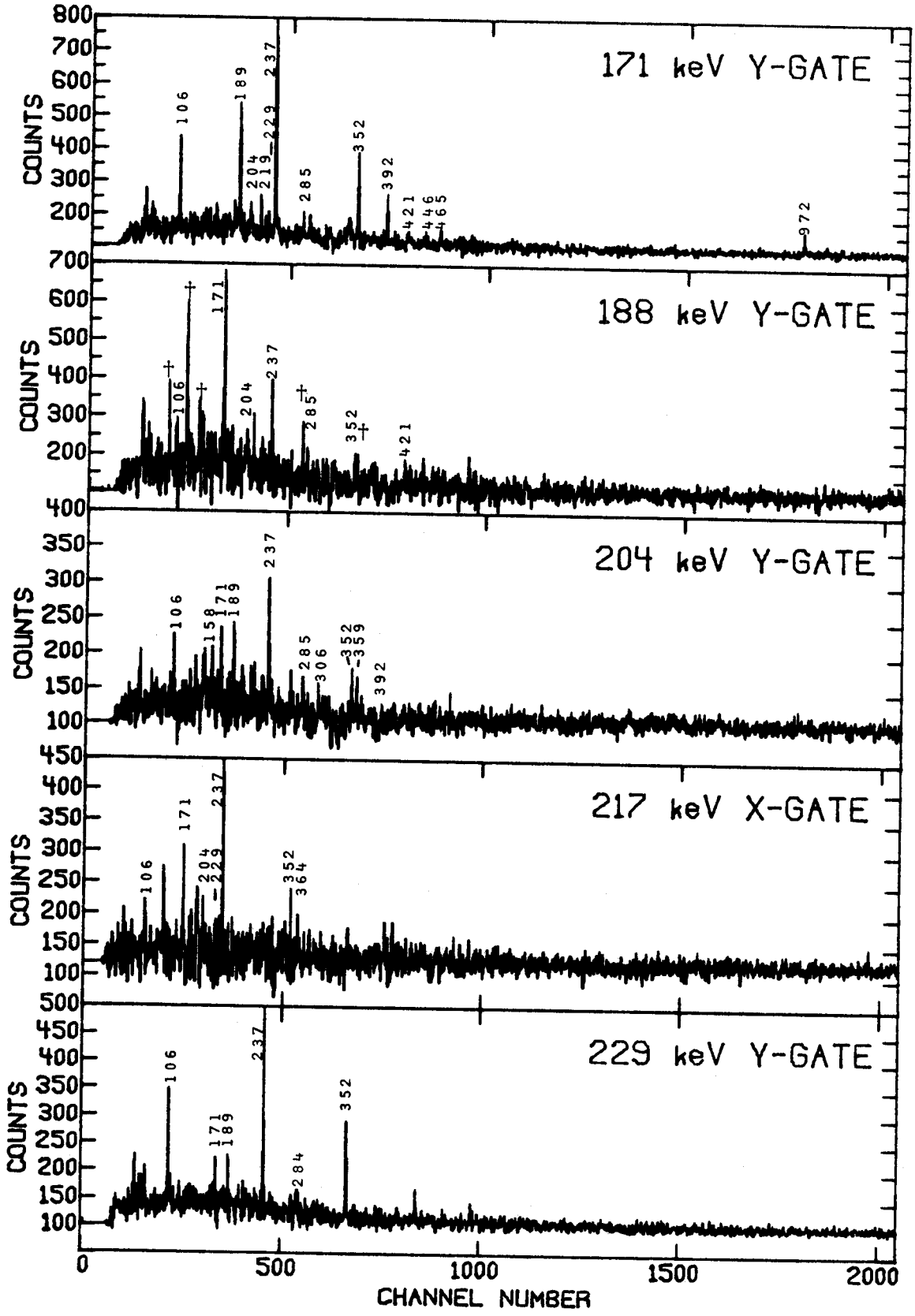

Figure A-8. Gated spectra of cascade transitions in the $K^{\pi}=6^{+}$ band.

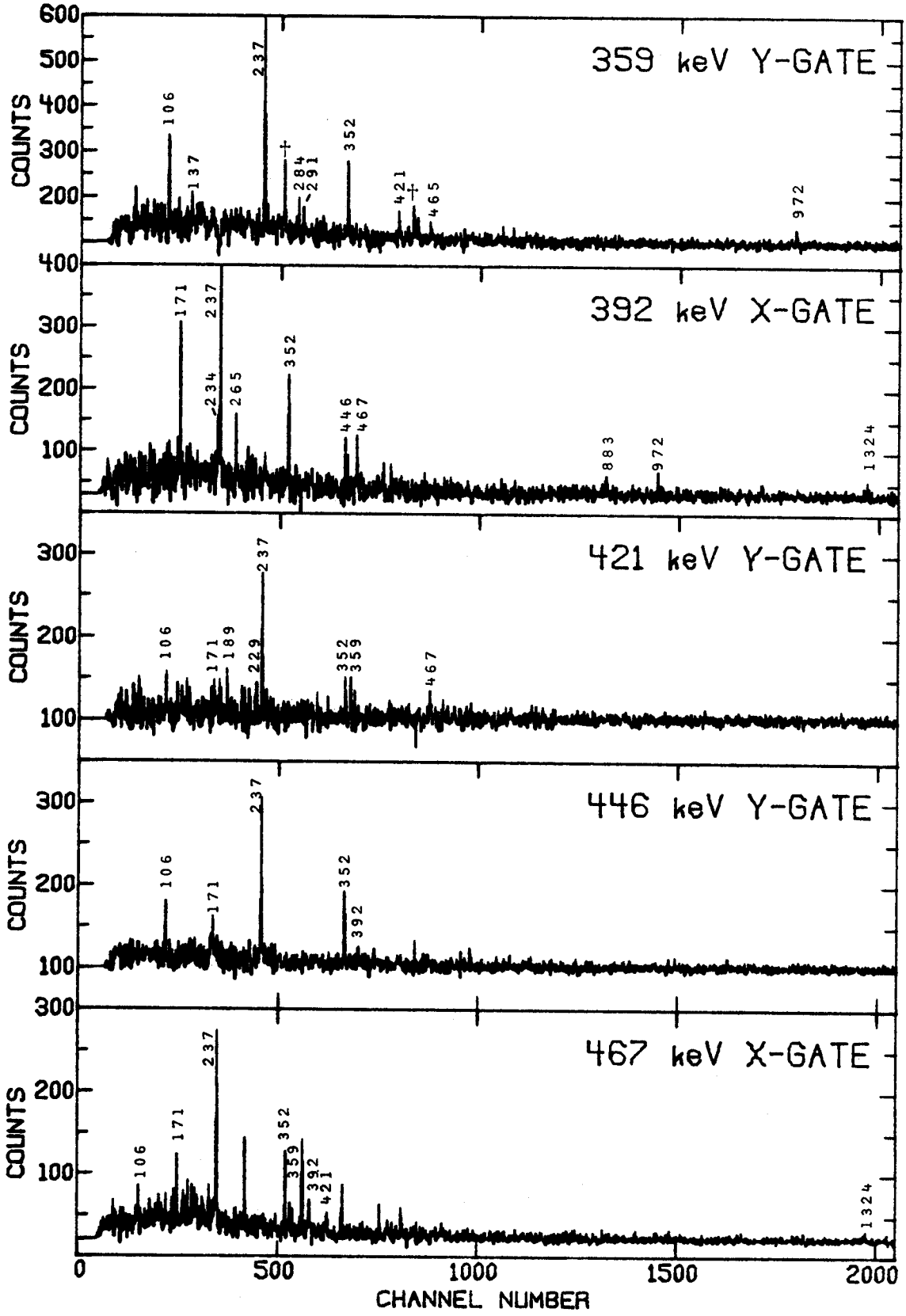

Figure A-9. Gated spectra of crossover transitions in the $K^{\pi}=6^{+}$ band.

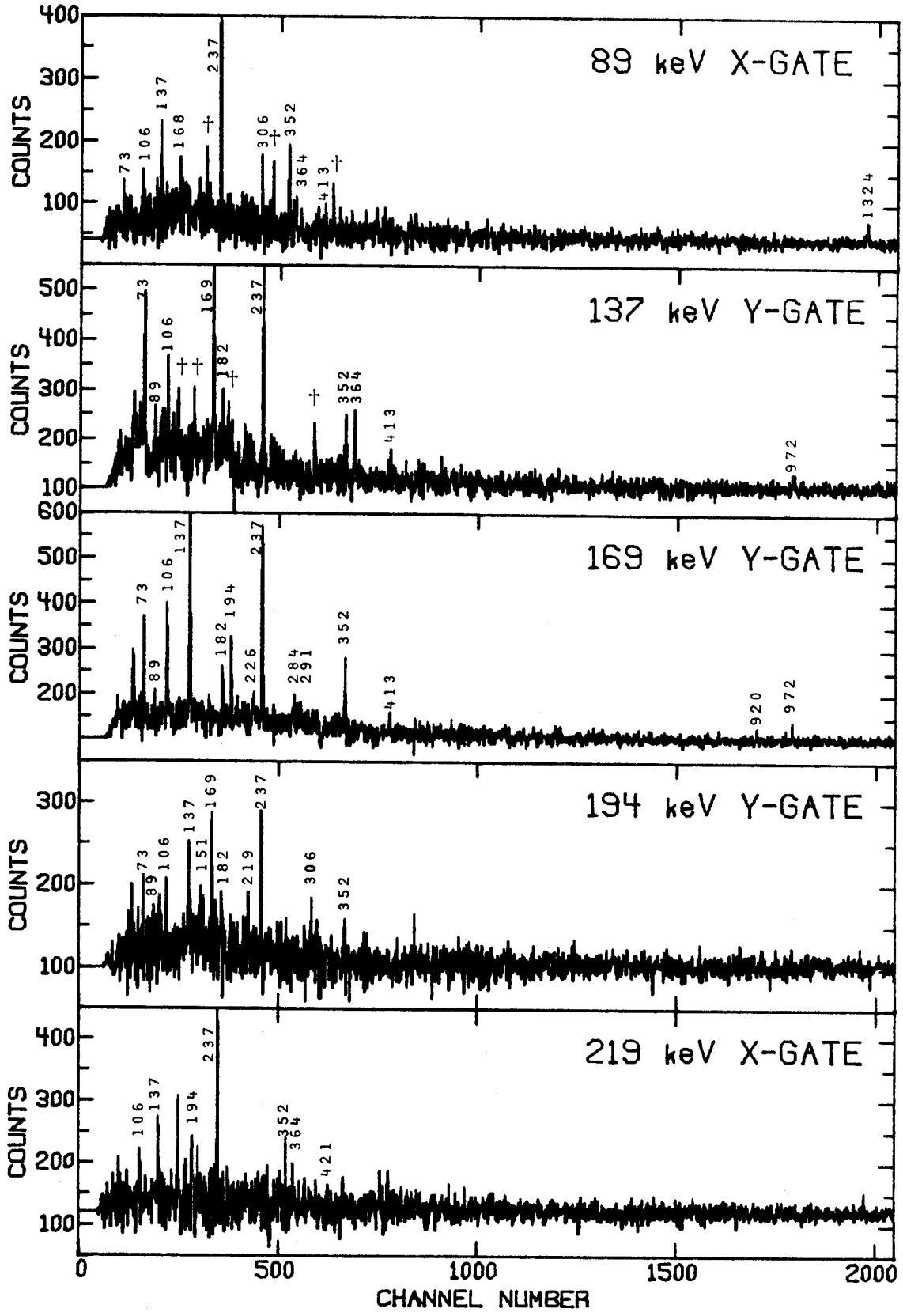

Figure A-10. Gates on the cascade transitions in the $K^{\pi}=(6,7)^{-}$ band.

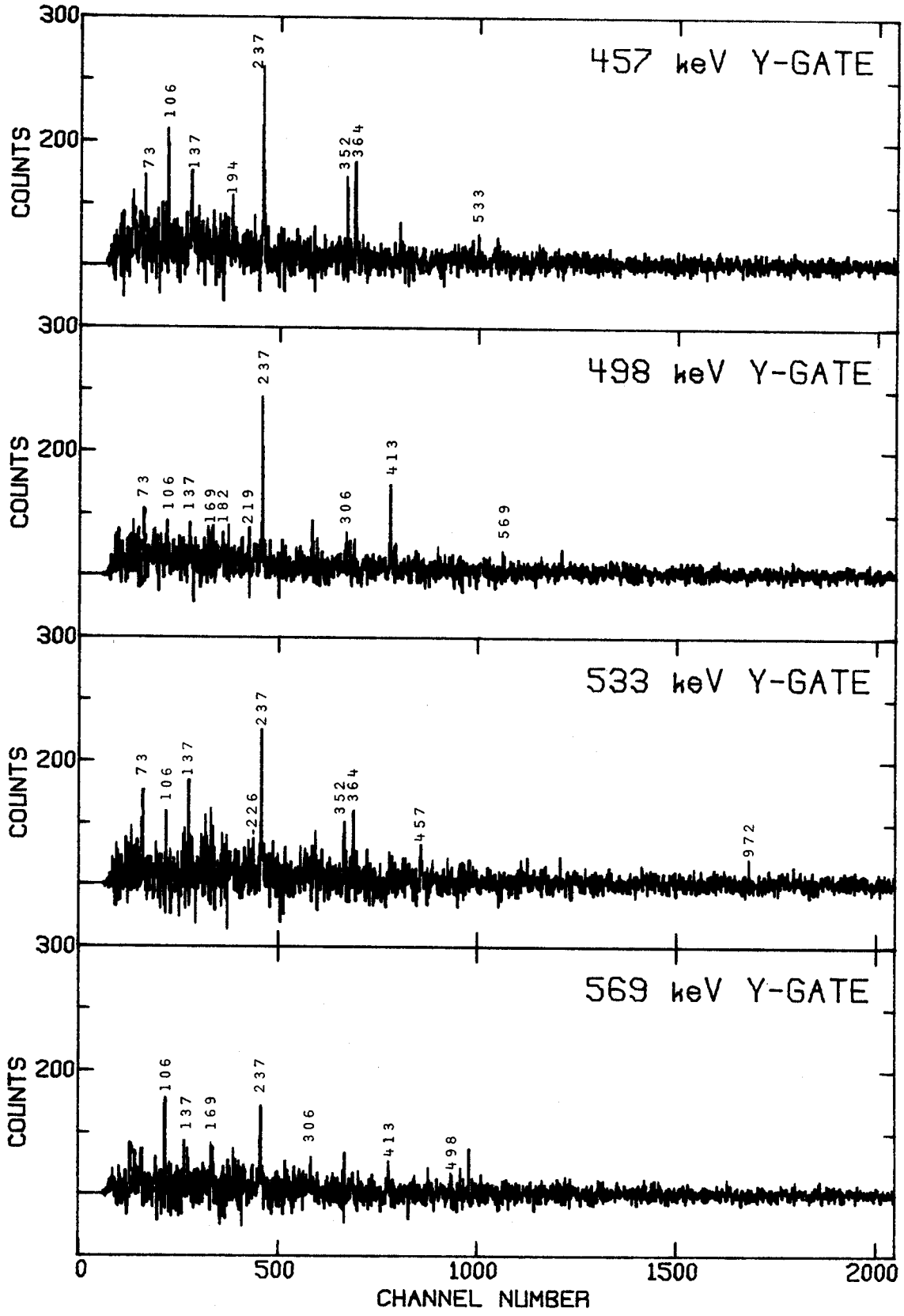

Figure A-11. Gates on the crossover transitions in the $K^{\pi}=(6,7)^{-}$ band.

APPENDIX B

Angular Distribution Plots of ^{178}W Transitions

The angular distribution data shown here have been transposed to the 0-90° quadrant for plotting purposes. The data are fitted to the equation:

$$W(\theta) = \sum_{K=0,2,4} A_K P_K(\cos\theta)$$

using the program GADFIT (written by R. A. Warner). The values of A_2/A_0 and A_4/A_0 obtained from these fits are listed in Table 5-1.

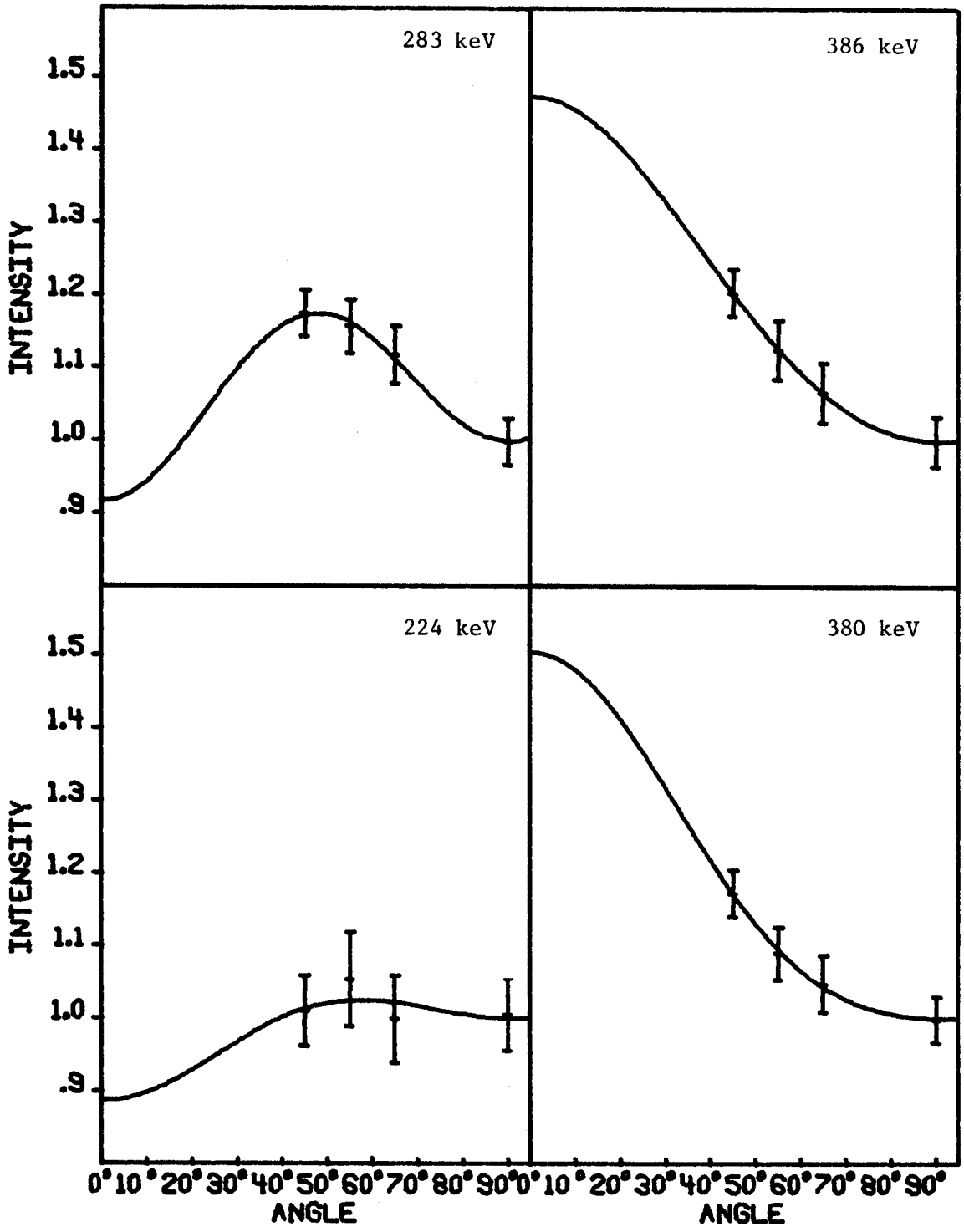

Figure B-1. Angular distributions of some crossover transitions in the K=2 octupole band.

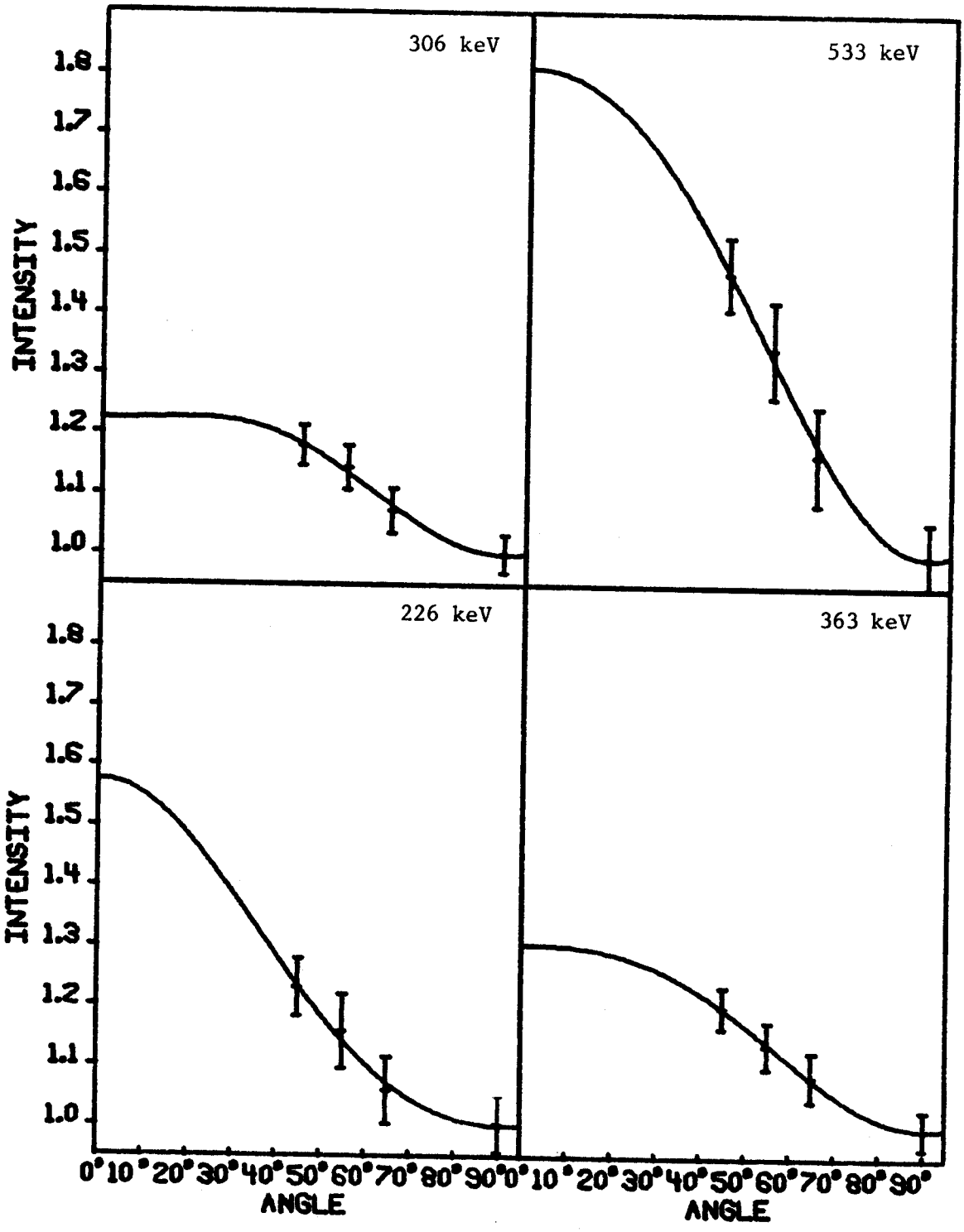

Figure B-2. Angular distributions of some crossover transitions in the K=2 octupole band.

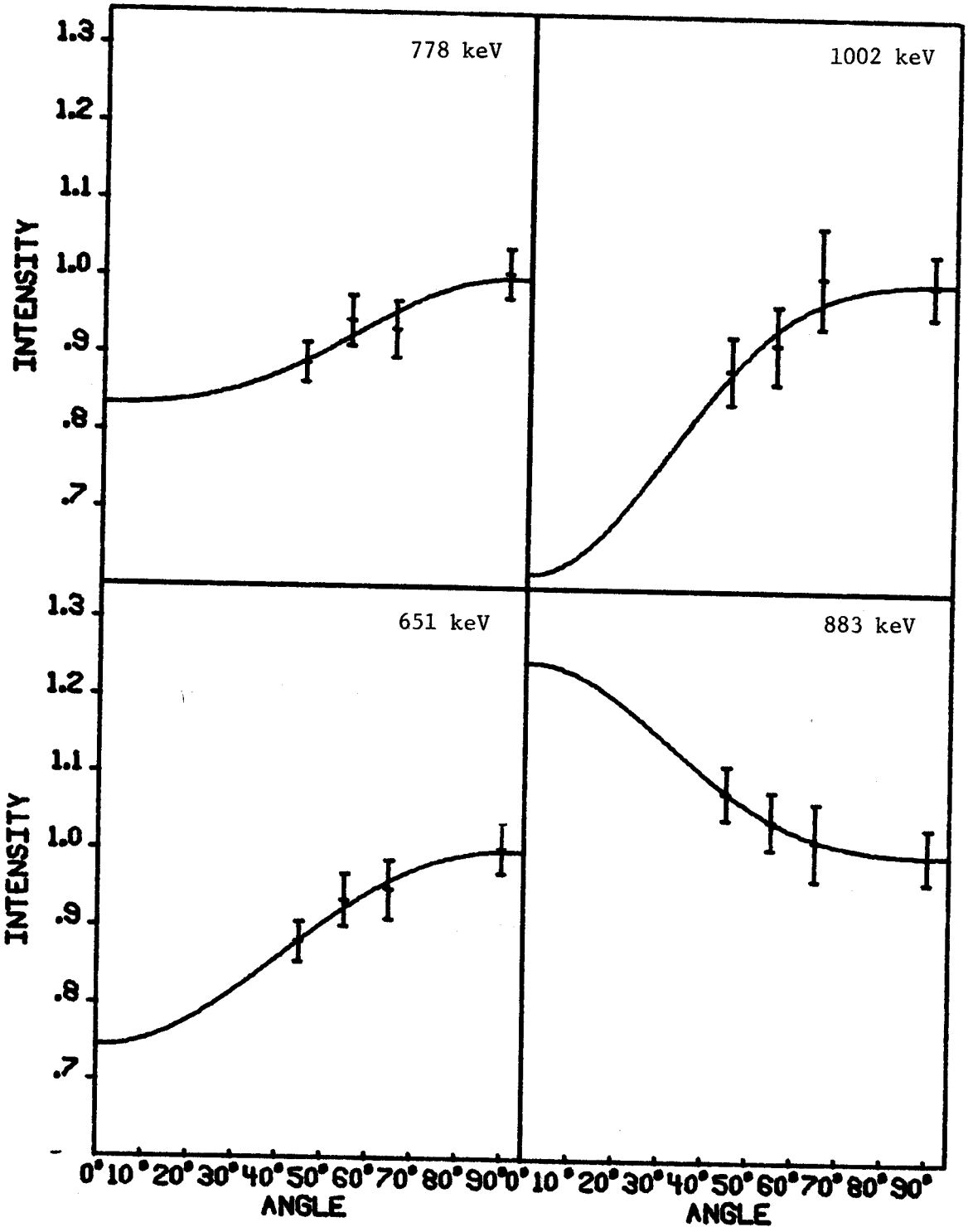

Figure B-3. Angular distributions of some interband transitions between the K=2 octupole band and the ground band.

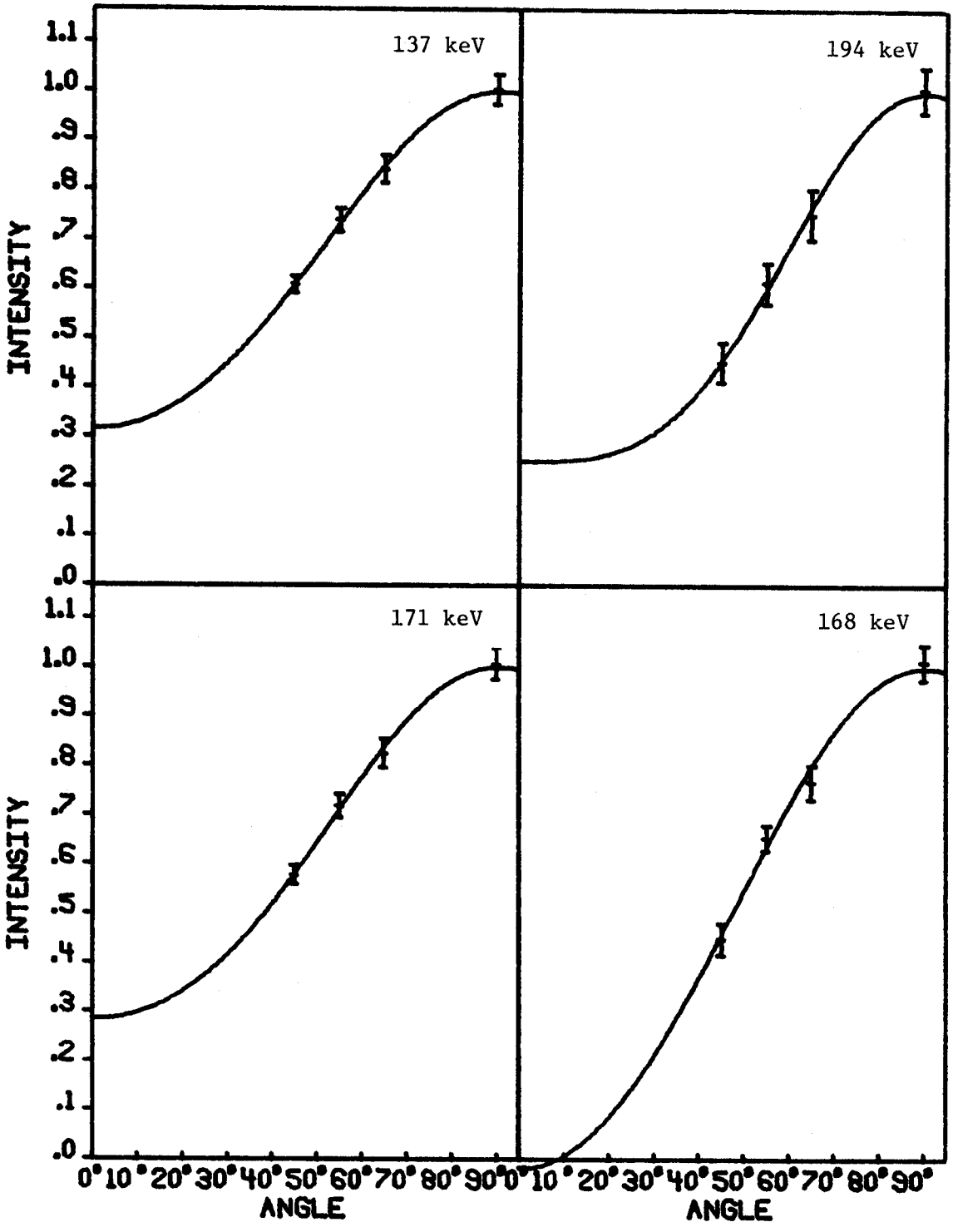

Figure B-4. Angular distributions of cascade transitions in the $K^{\pi}=(6,7)^{-}$ band.

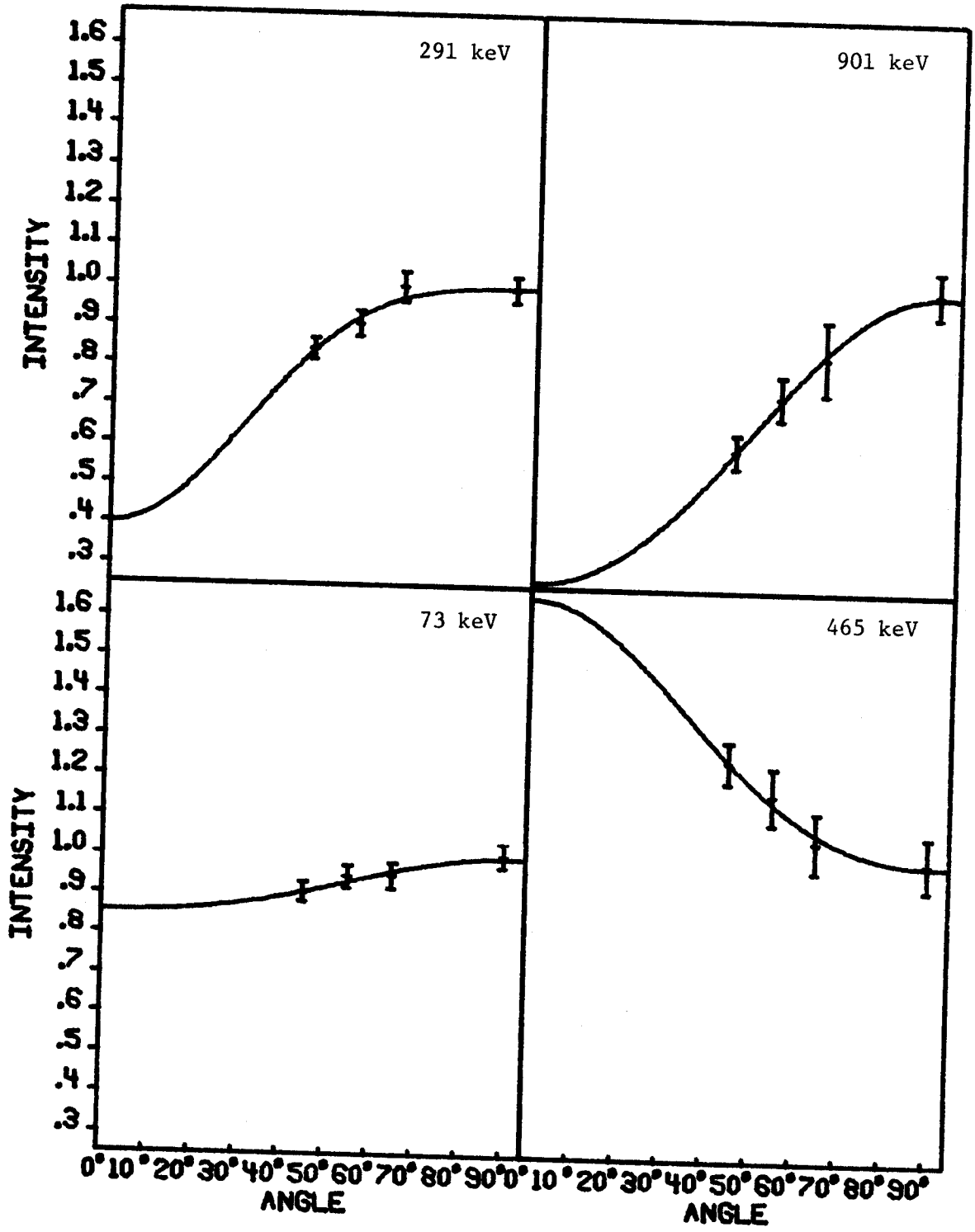

Figure B-5. Angular distributions of various interband transitions and of the unassigned 291-keV transition.

APPENDIX C

Gated Coincidence Spectra of Transitions in ^{177}W

The background subtracted gated coincidence spectra in this section were obtained in one of two coincidence experiments, the first performed with two large volume - 7 and 10% - efficient detectors, the second performed with the planar LEPS and the 8% detector. Gates labeled X' and Y' display the LEPS and 8% gated spectra respectively. Peaks which have a † above them are associated with contaminants. X-rays are not labeled nor are peaks which belong to another rotational band. The top of each Y-scale is used as a cutoff, with overflows not shown.

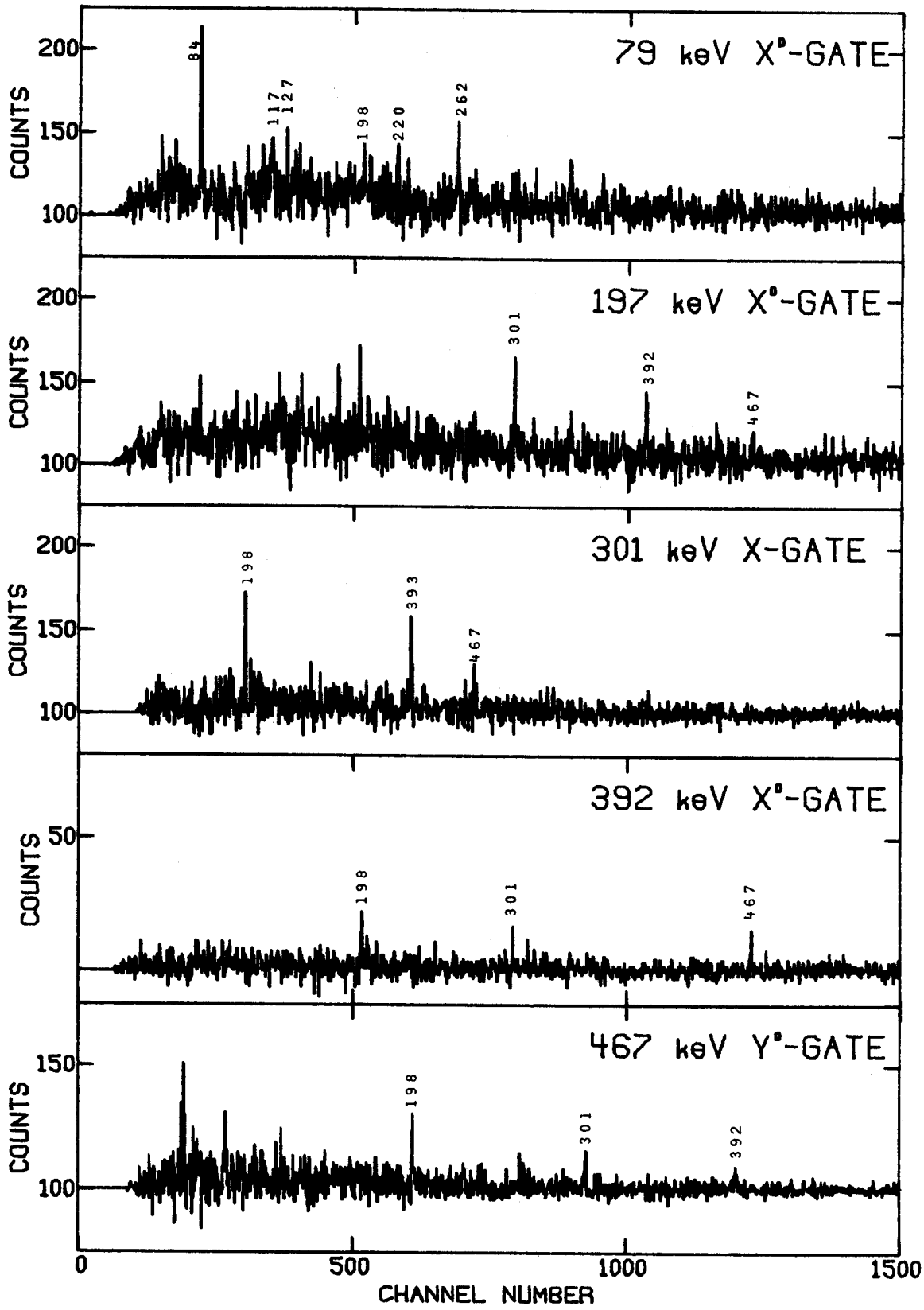

Figure C-1. Gated spectra of transitions in the $1/2^-[521]$ band.

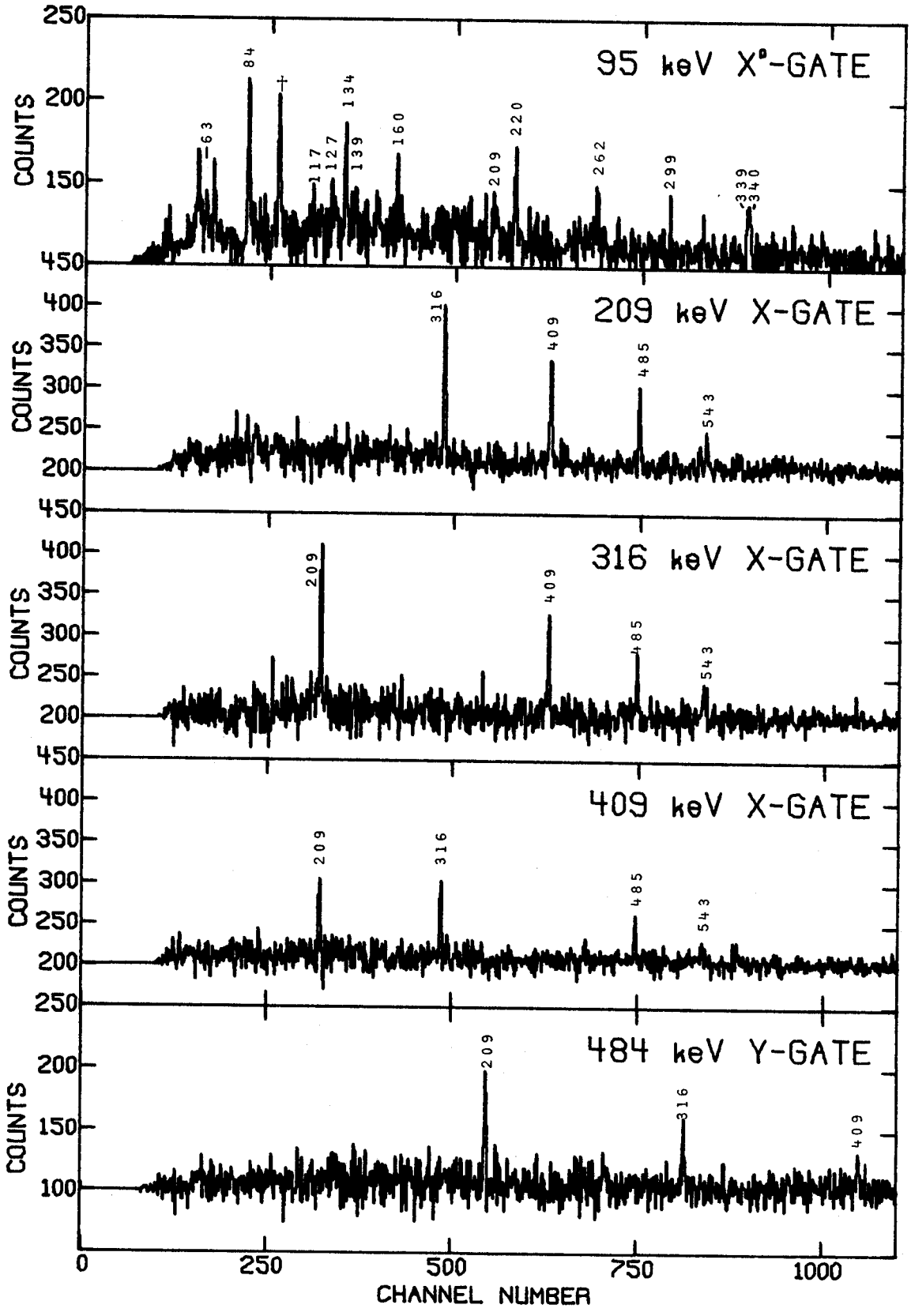

Figure C-2. Gated spectra of transitions in the $1/2^-[521]$ band.

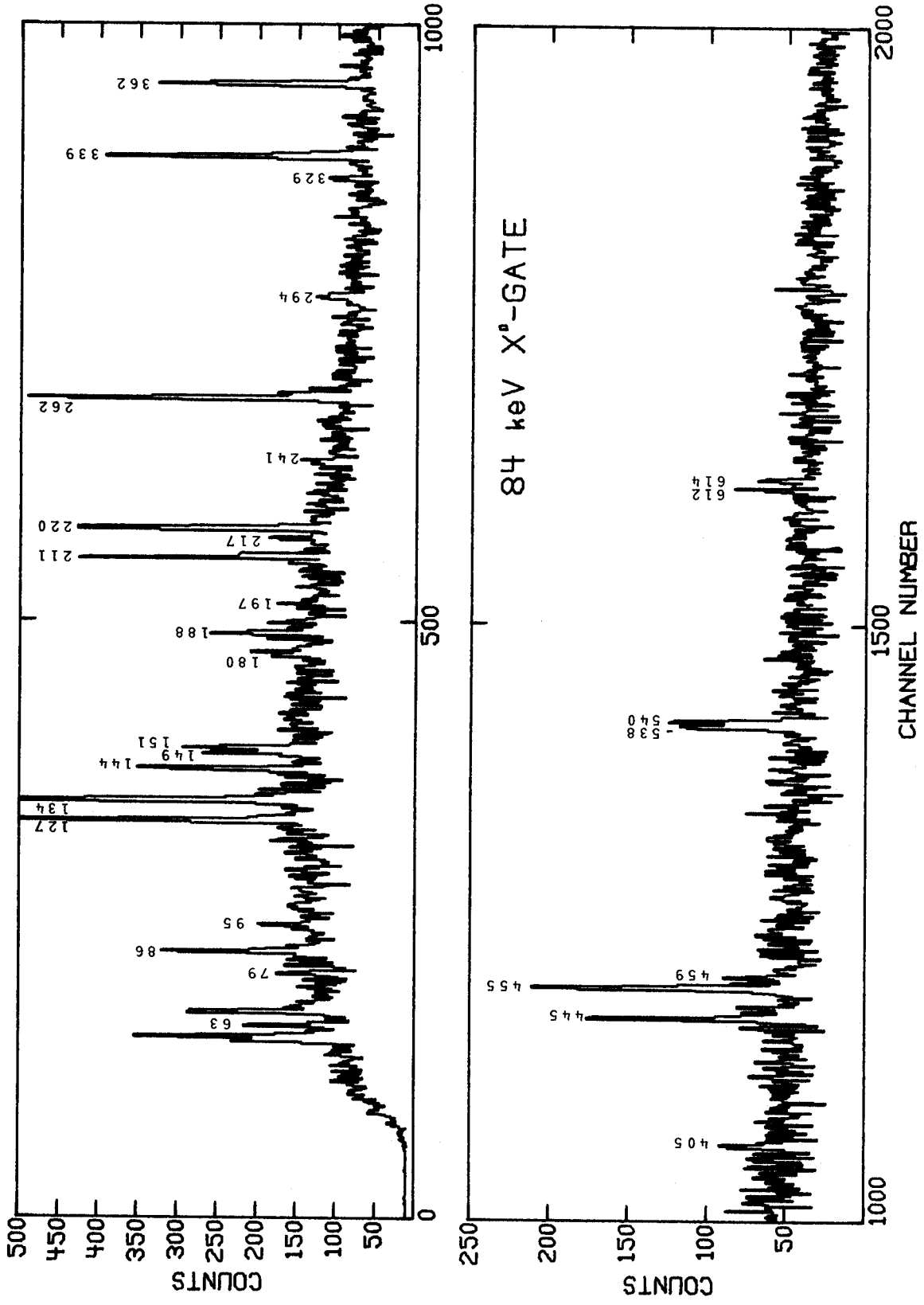

Figure C-3. Gate set on the 84-keV $E1$ interband transition from the $7/2^{+}[633]$ to the $5/2^{-}[512]$.

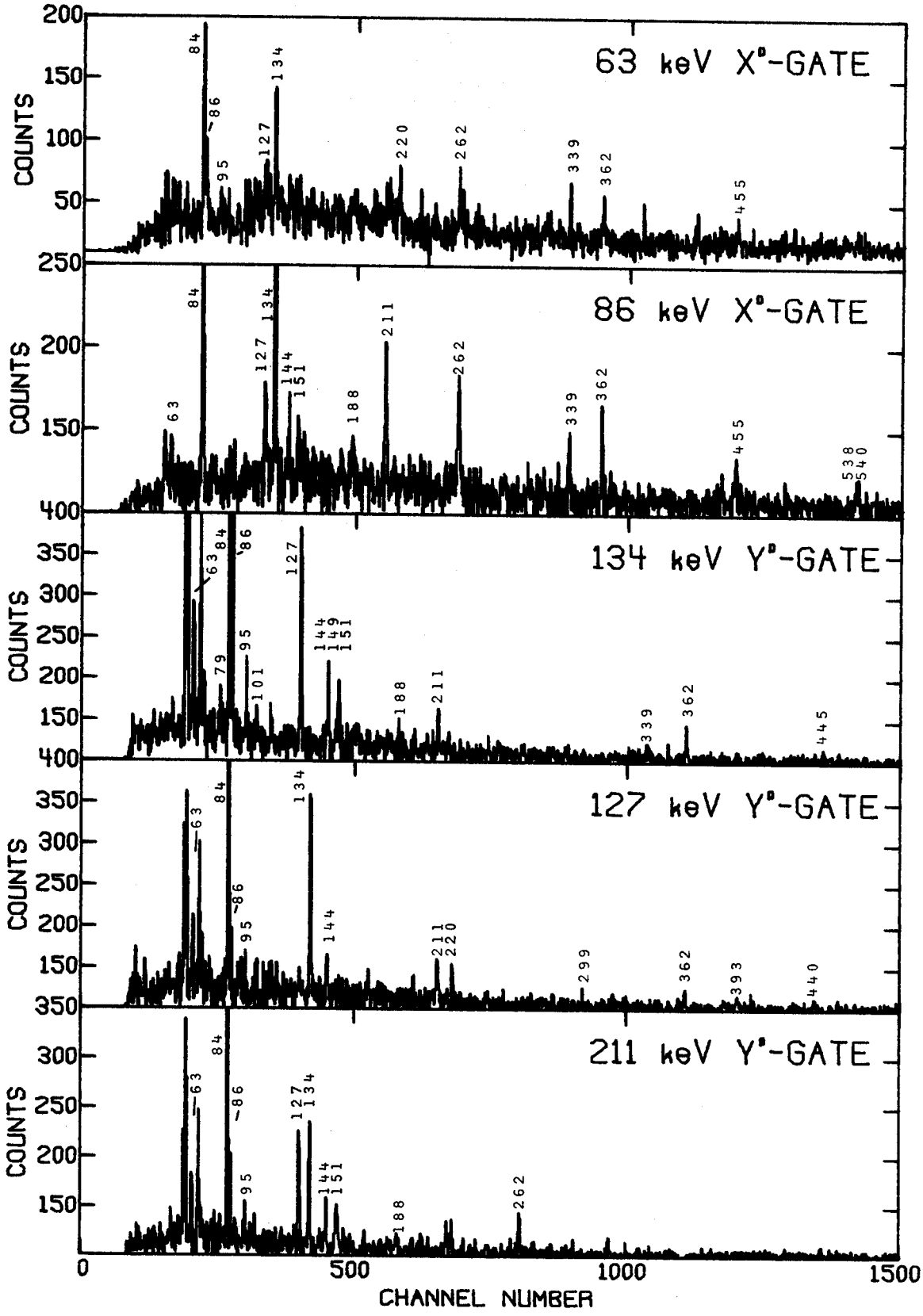

Figure C-4. Gates on the cascade transitions in the $7/2^{+}[633]$ band.

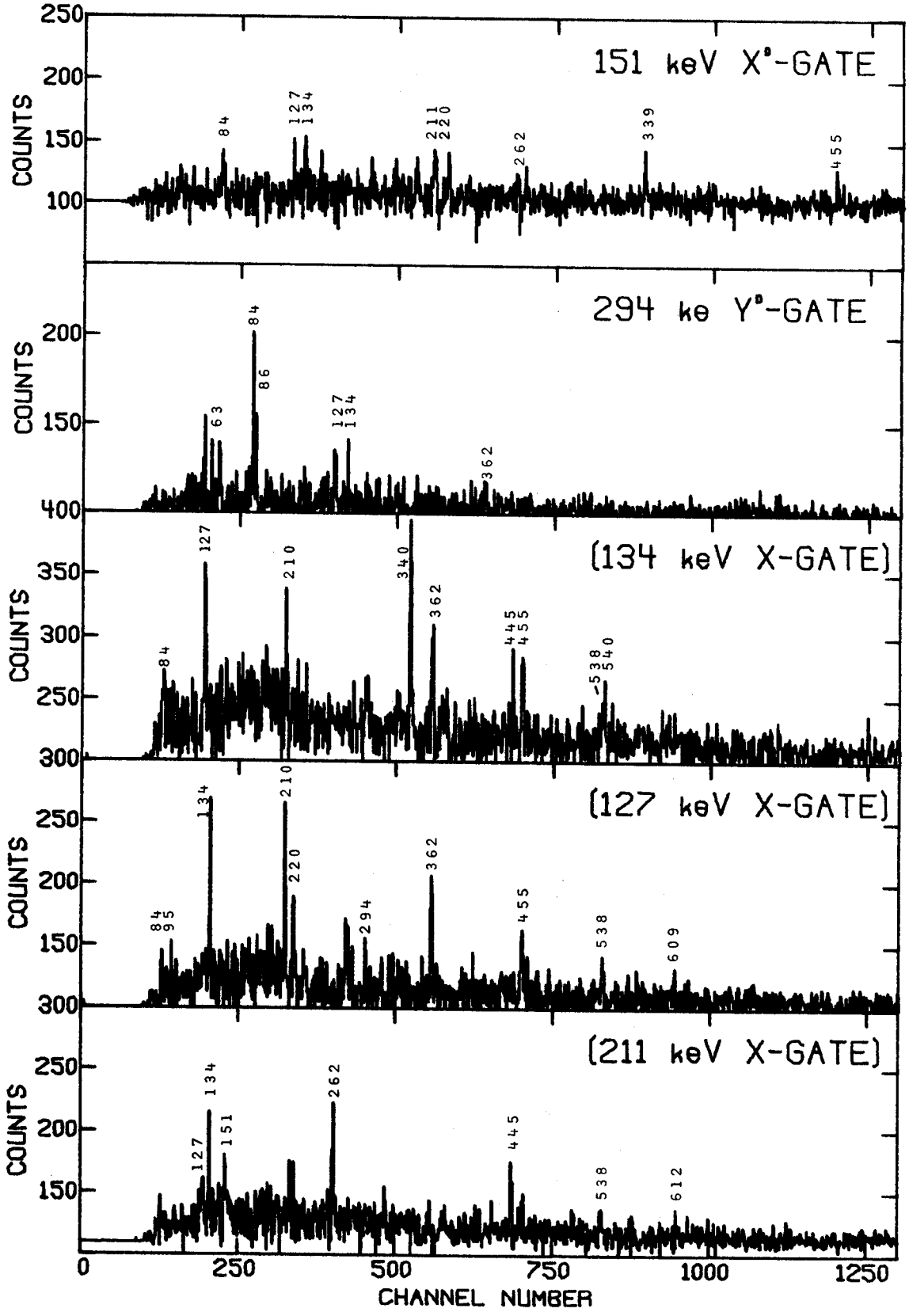

Figure C-5. Gates set on the cascade transitions in the $7/2^{+}[633]$ band.

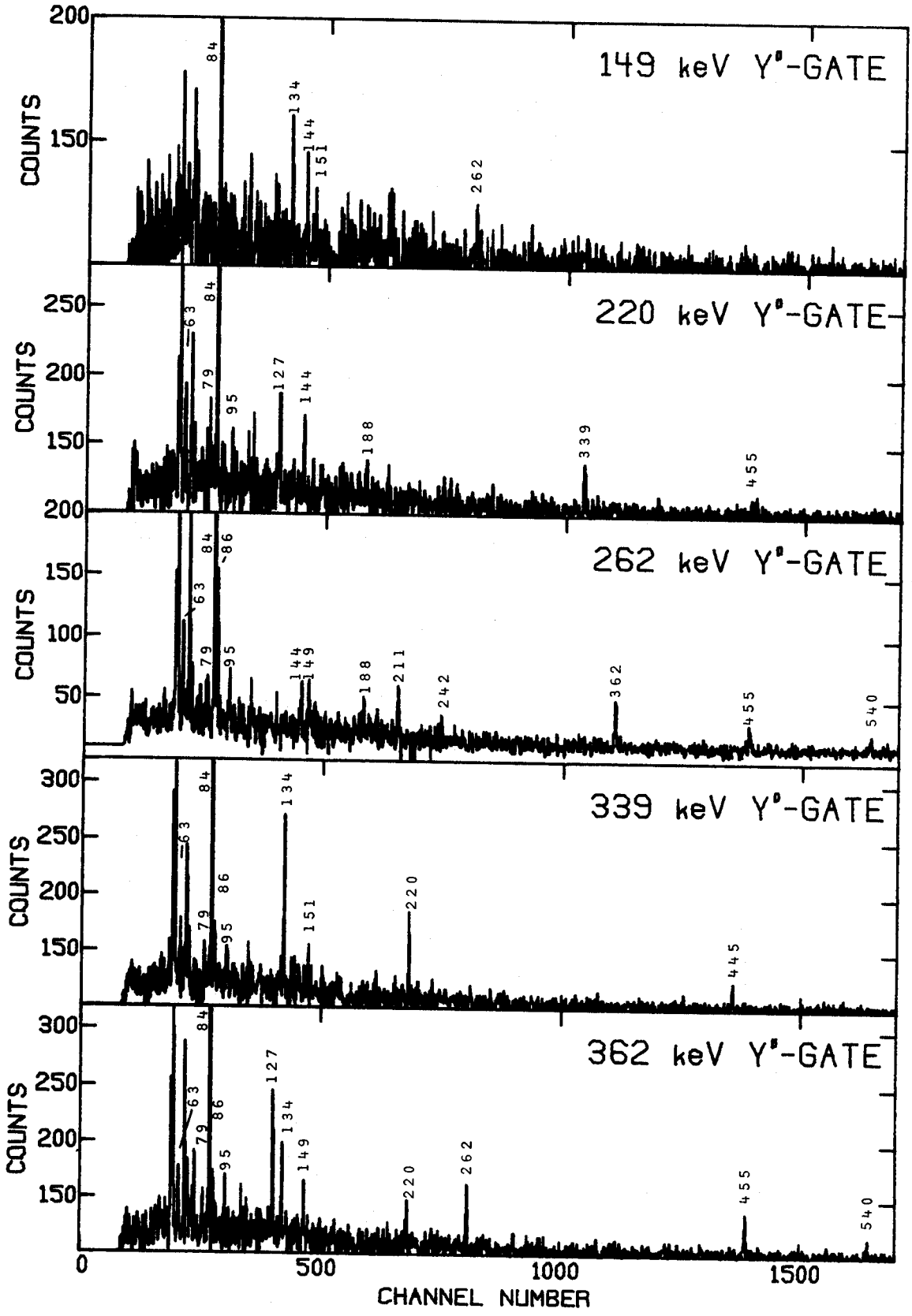

Figure C-6. Gates on the crossover transitions in the $7/2^{+}[633]$ band.

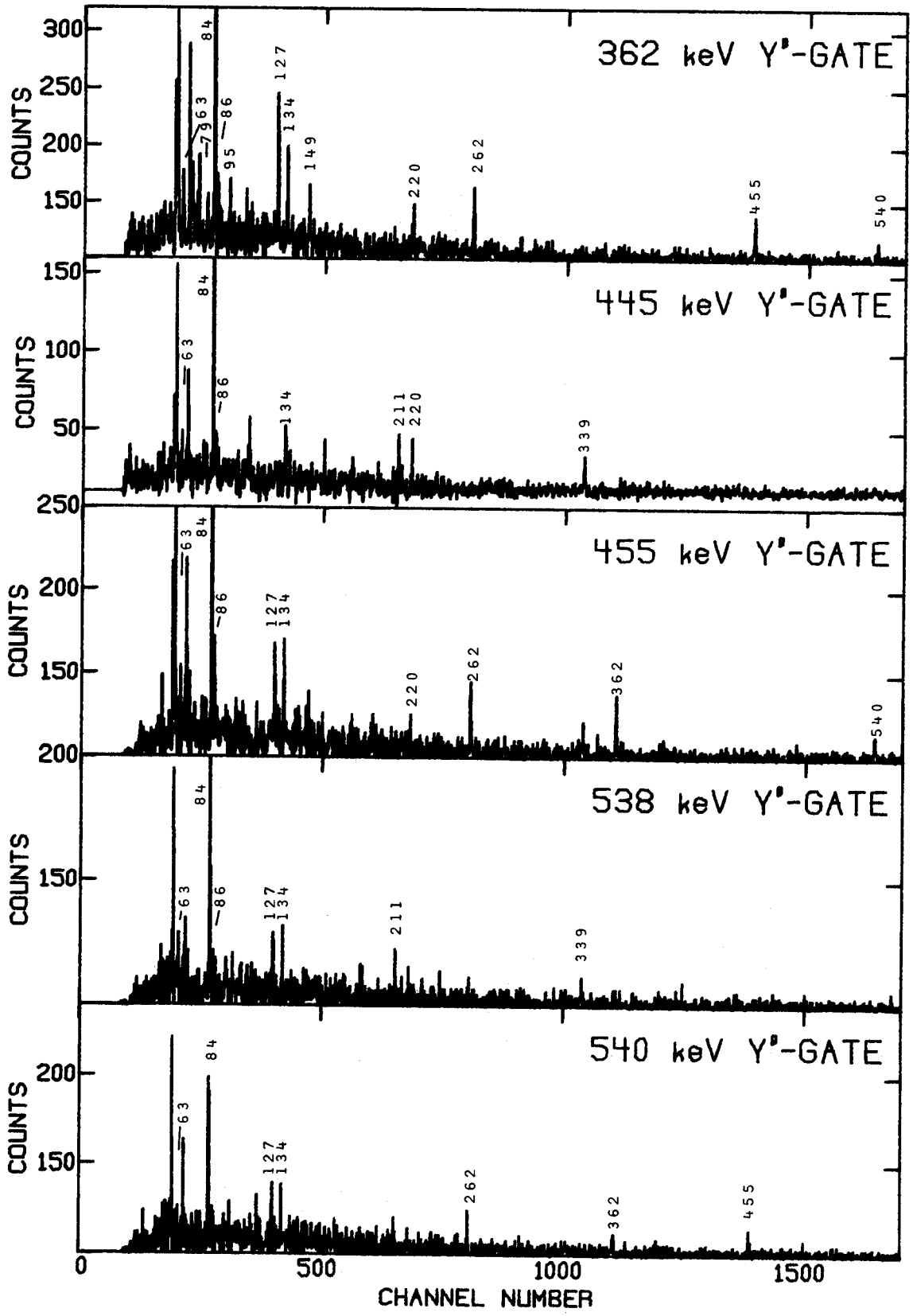

Figure C-7. Gates on some crossover transitions in the $7/2^{+}[633]$ band.

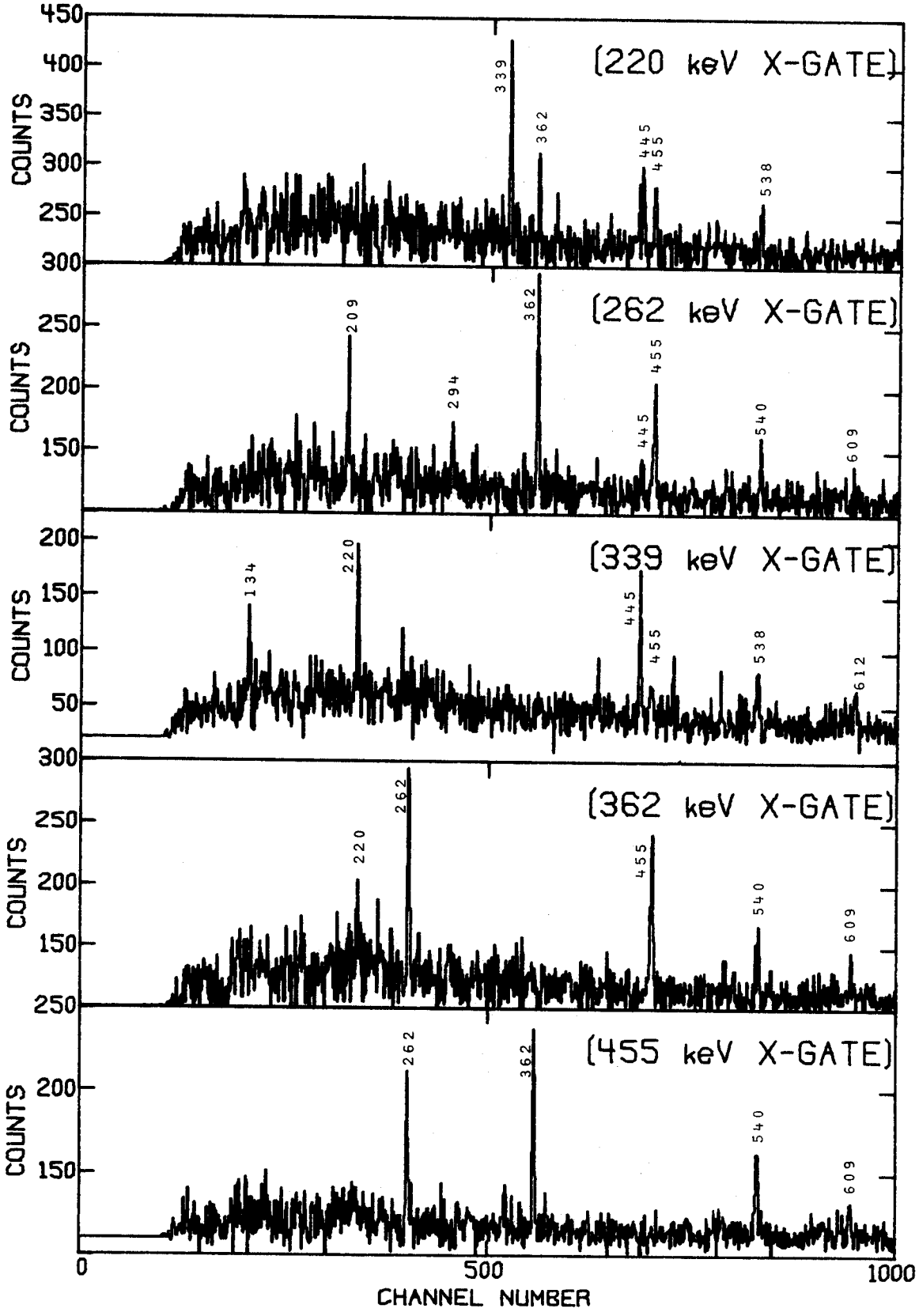

Figure C-8. Gated spectra of crossover transitions in the $7/2^{+}[633]$ band displaying high energy coincidences.

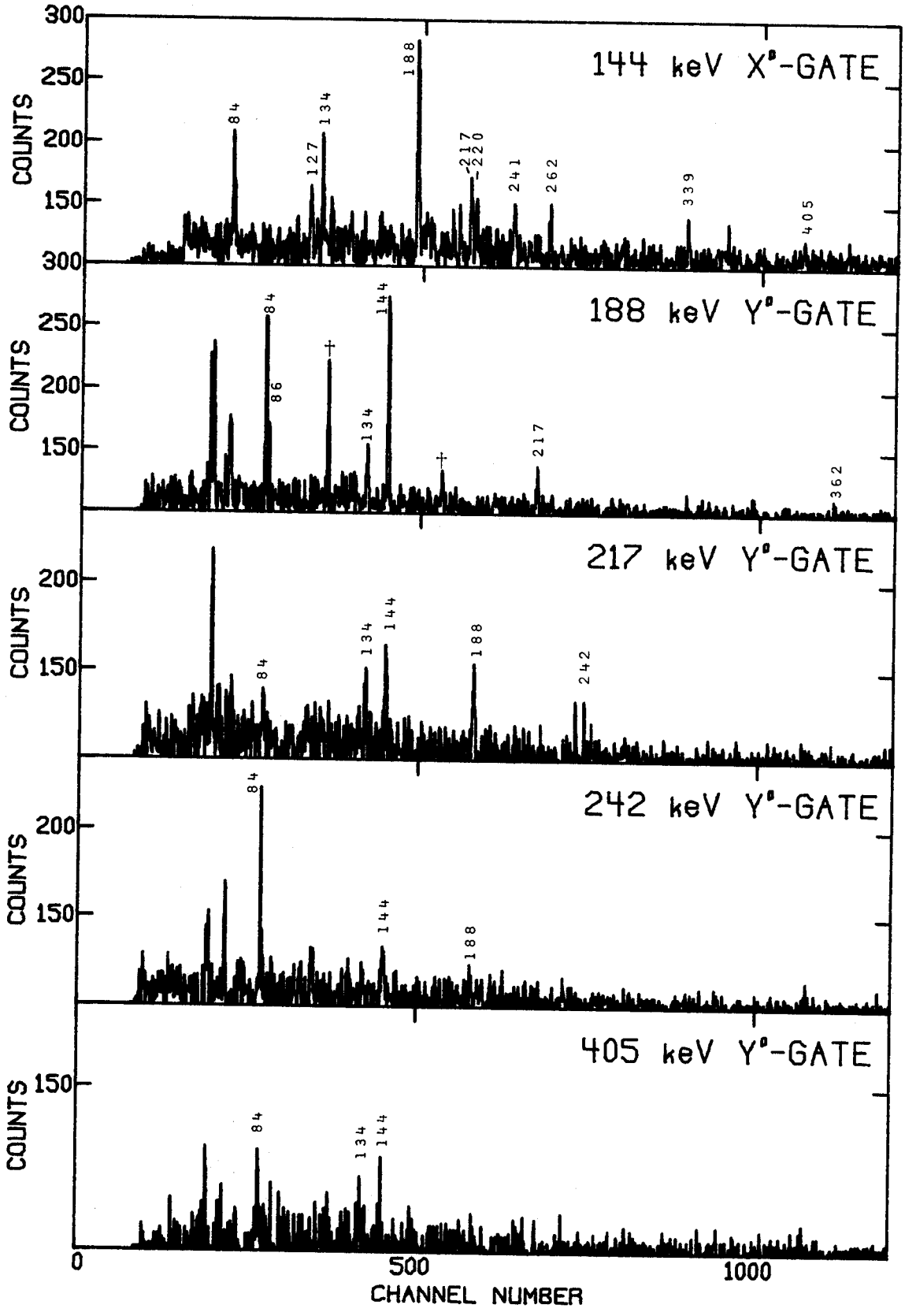

Figure C-9. Gates on transitions associated with the possible three quasiparticle band.

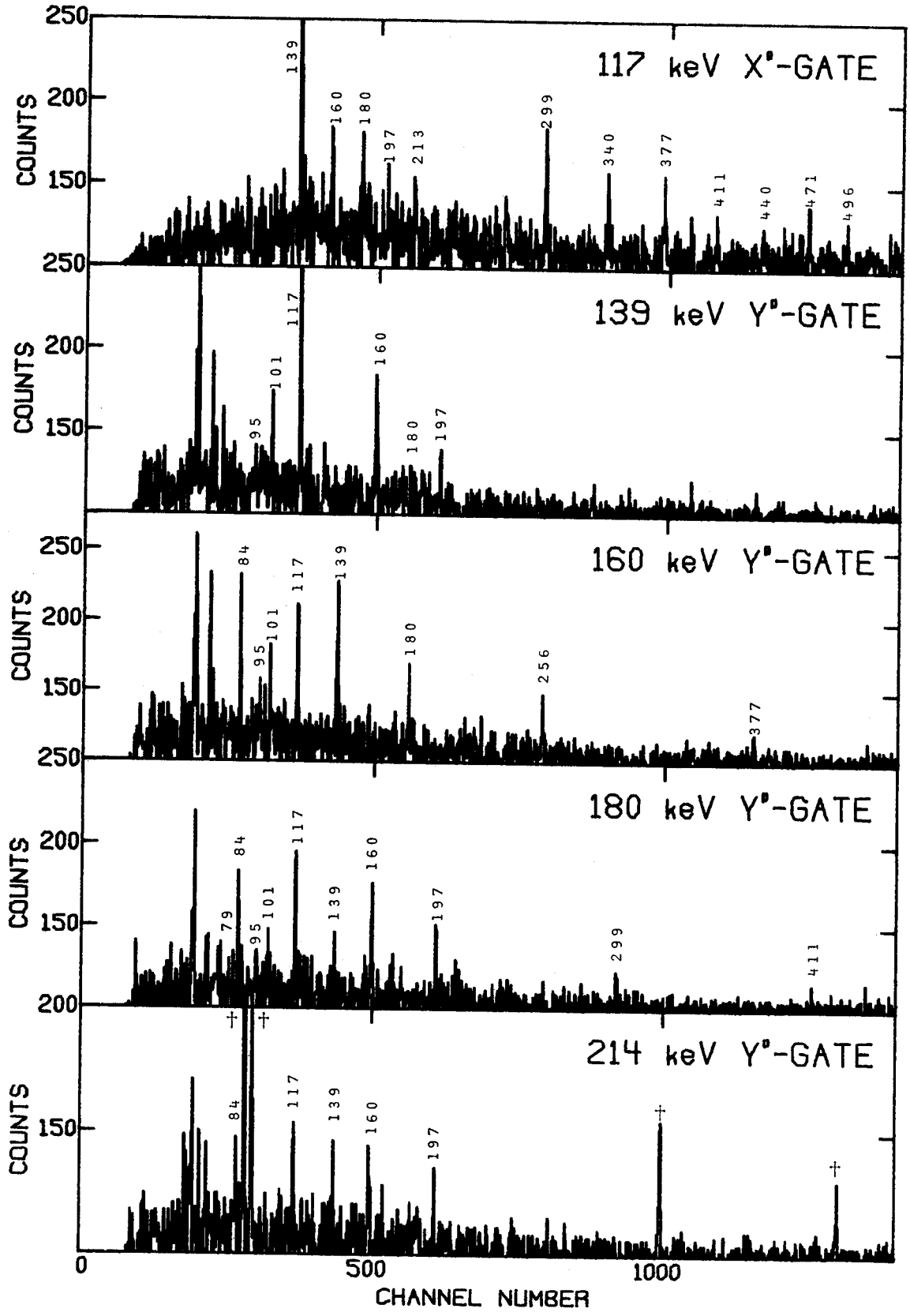

Figure C-10. Gates on cascade transitions in the $7/2^-[514]$ band.

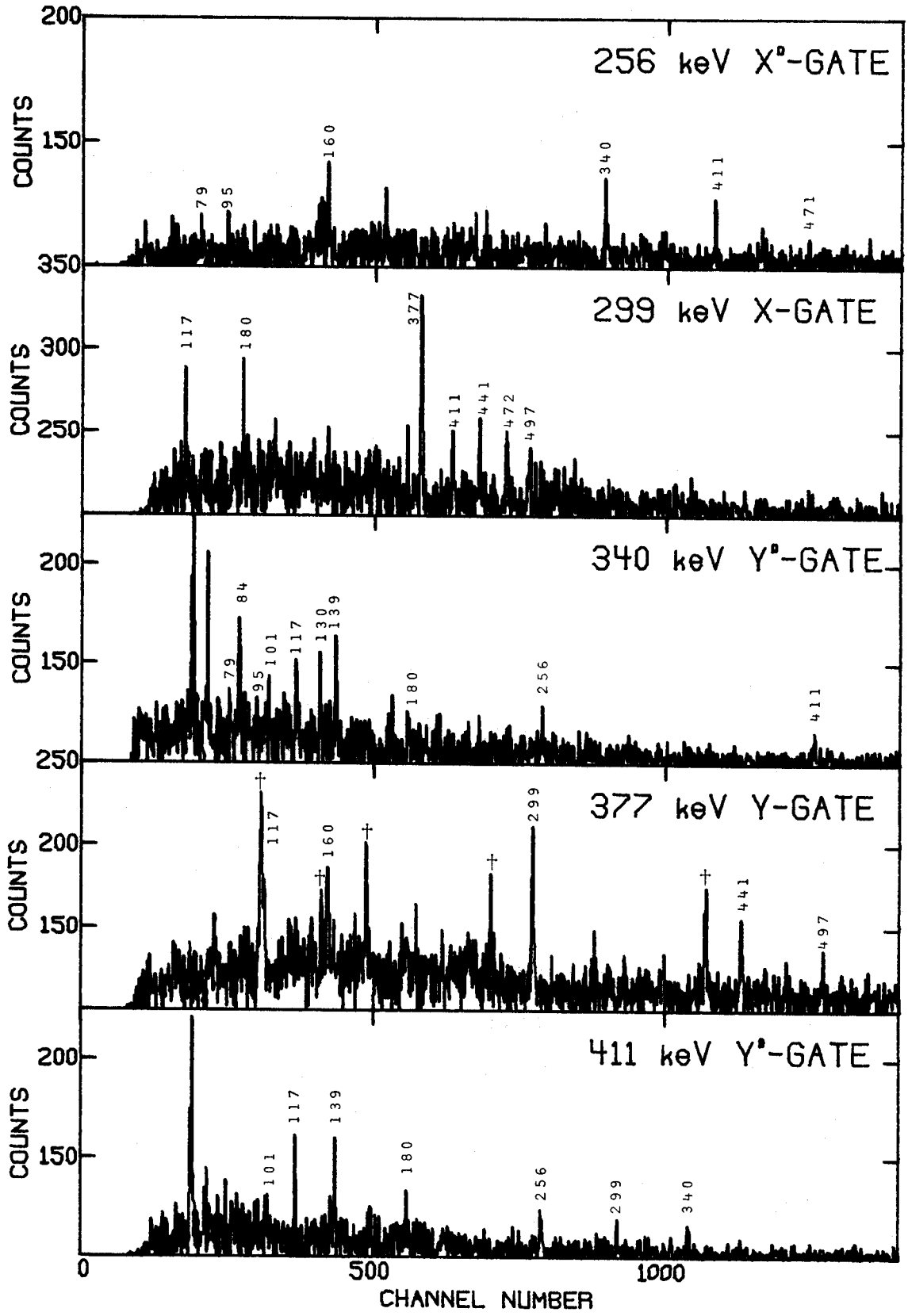

Figure C-11. Gates on some crossover transitions in the $7/2^-[514]$ band.

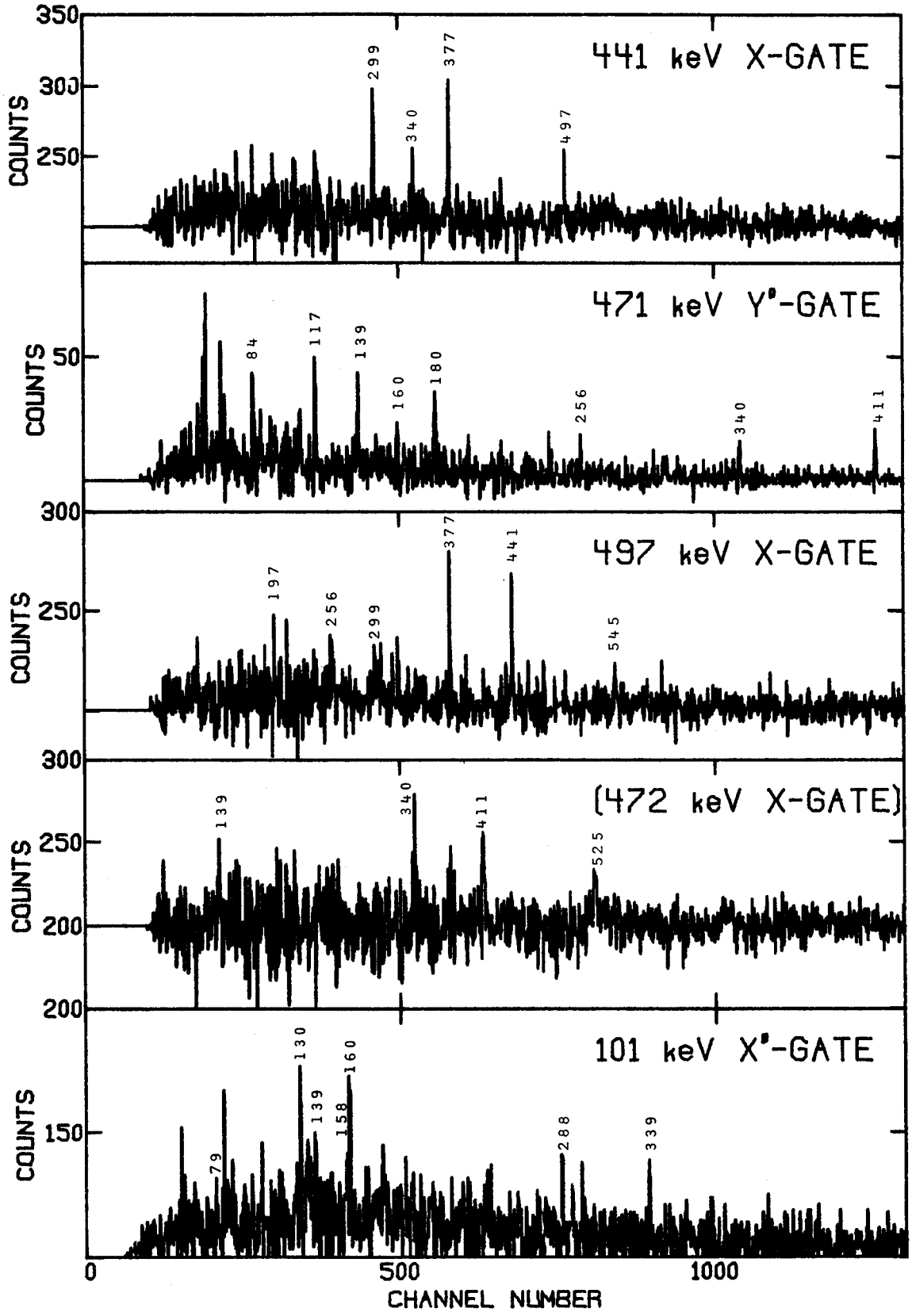

Figure C-12. Gates on some crossover transitions in the $7/2^-[514]$ band, and a gate on the 101-keV cascade transition in the $5/2^-[512]$ band.

APPENDIX D

Angular Distribution Plots of ^{177}W Transitions

The curves shown here represent fits of the data to the equation:

$$W(\theta) = \sum_{K=0,2,4} A_K P_K(\cos\theta)$$

using the program GADFIT (written by R. A. Warner for the MSU Σ-7 computer). The data were taken in the 90-180° quadrant. The values of A_2/A_0 and A_4/A_0 which were extracted from these fits are given in Table 3-1.

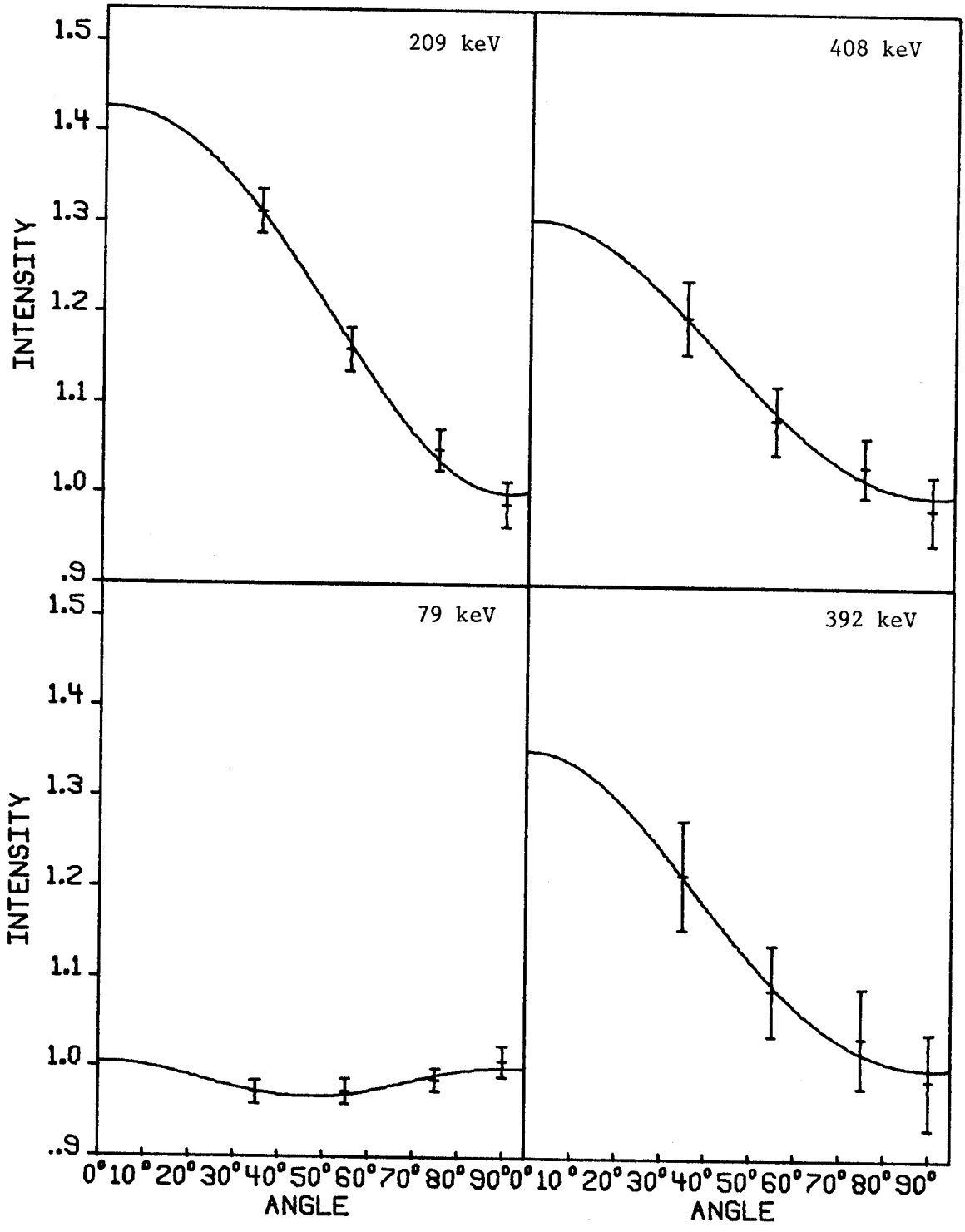

Figure D-1. Some angular distributions of the transitions in the $1/2^-[521]$ band. The 79-keV transition is $M1/E2$, the others are $E2$.

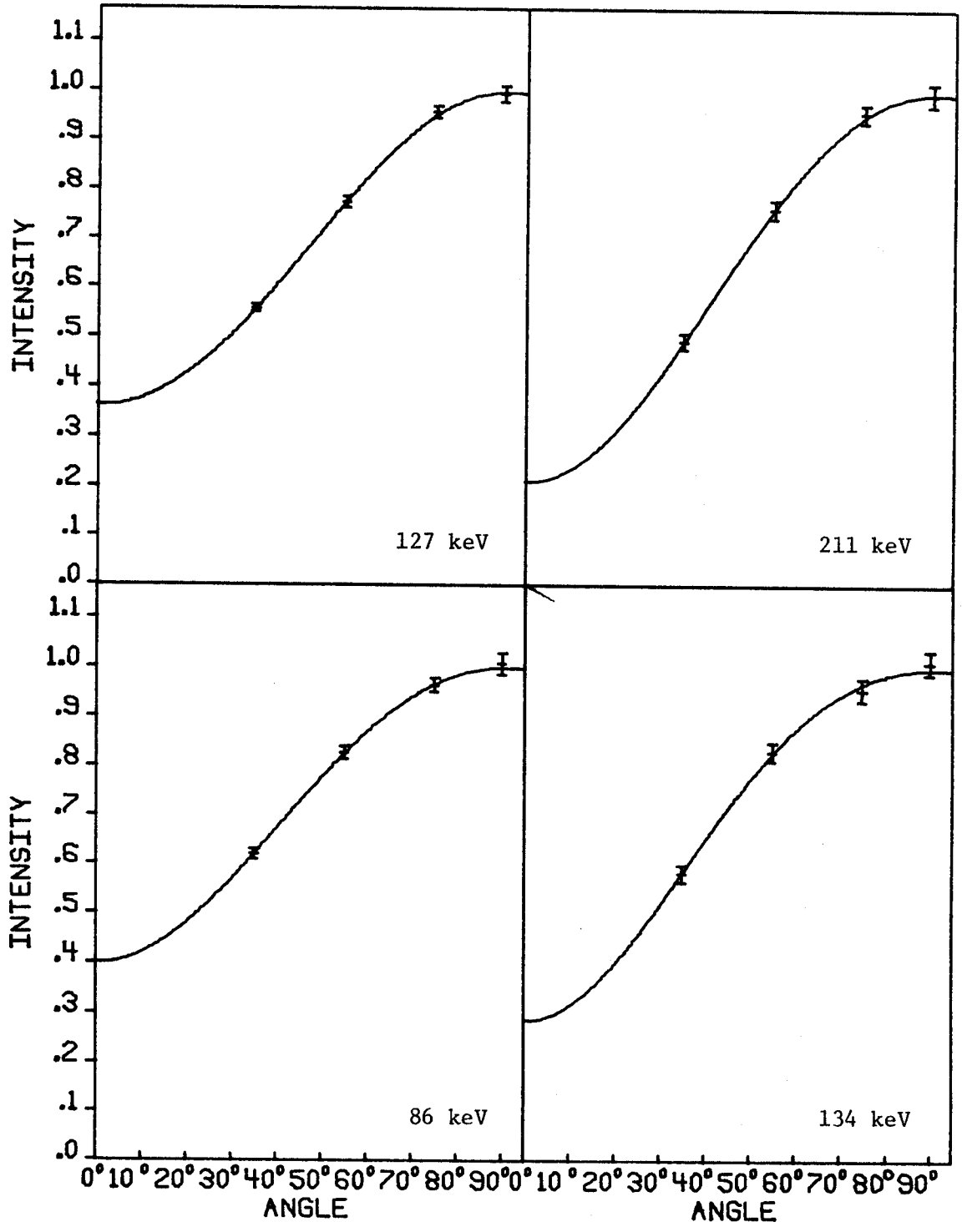

Figure D-2. Angular distributions of some cascade transitions in the $7/2^{+}[633]$ band.

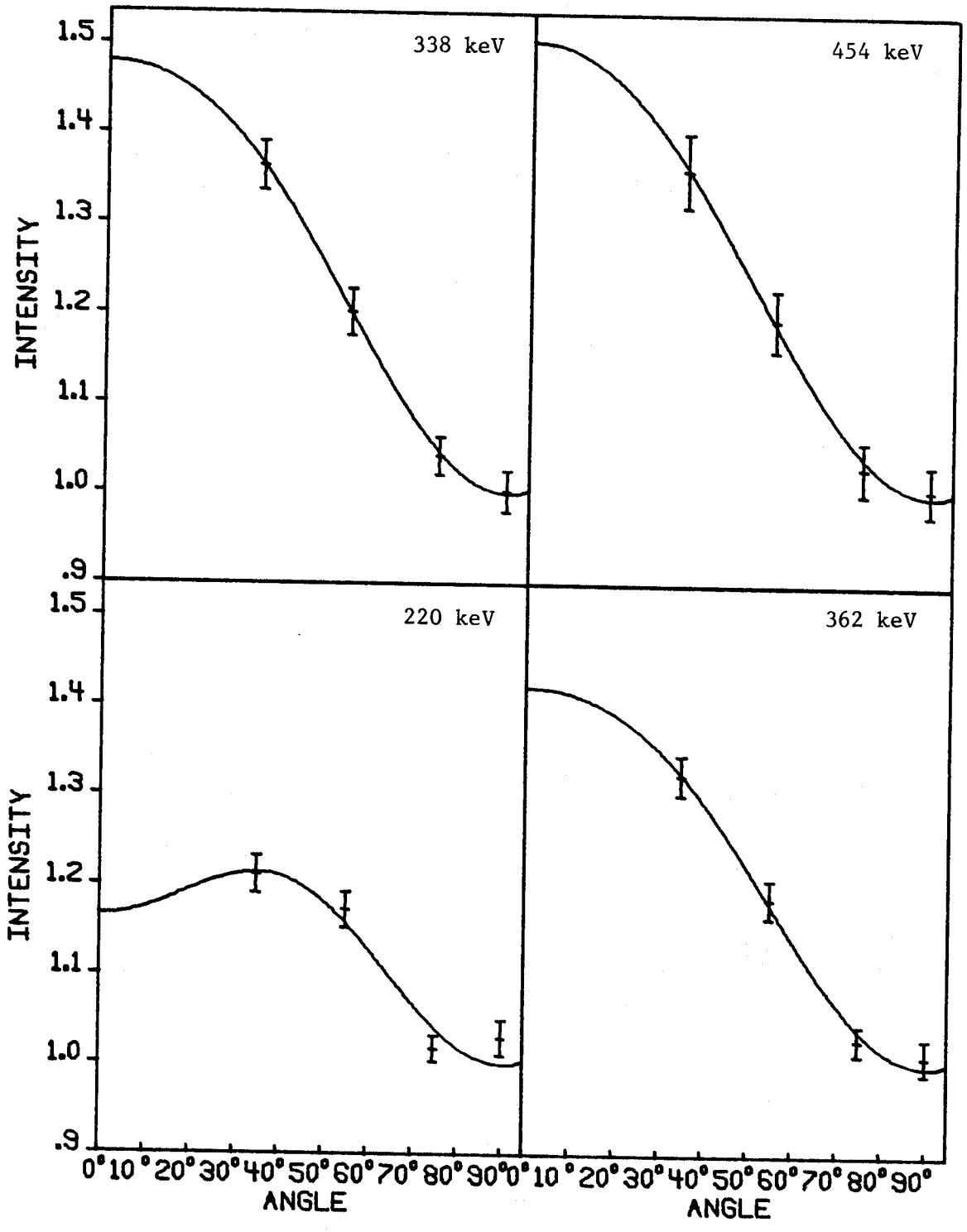

Figure D-3. Angular distributions of the $7/2^{+}[633]$ crossover transitions.

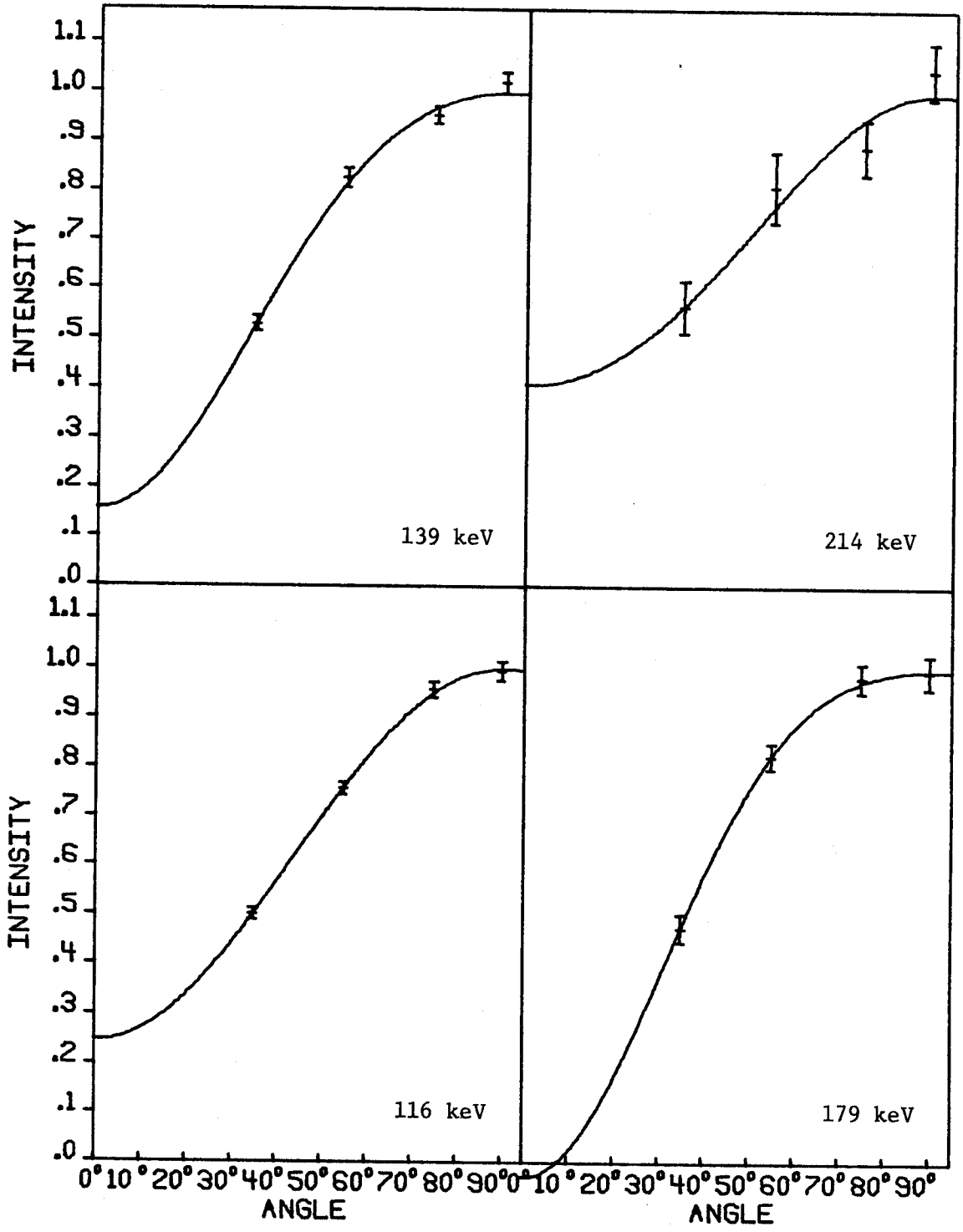

Figure D-4. Mixed multipolarity angular distributions of cascade transitions in the $7/2^-[514]$ band.

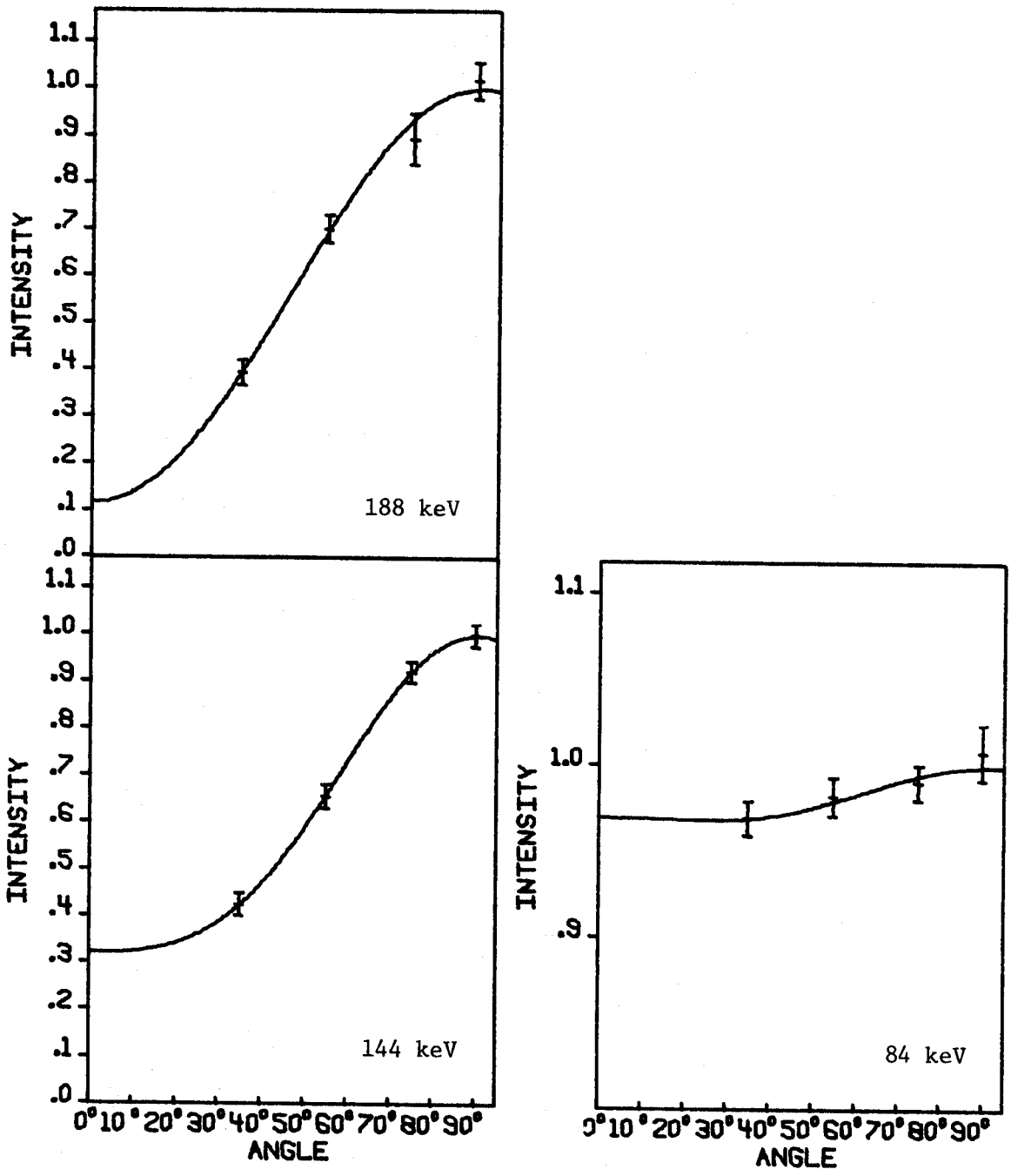

Figure D-5. Angular distributions of the interband 84-keV and 144-keV transitions, and of the 144-keV cascade member of the possible three quasiparticle band.

APPENDIX E

Level Scheme of ^{183}Os

Levels in ^{183}Os were populated in both the ^{185}Re(p,3n) and ^{182}W(α,3n) reactions. The usual techniques of in-beam gamma-ray spectroscopy - gamma-ray singles, angular distributions, excitation functions,gamma-time coincidence, and gamma-gamma-time coincidence - were employed to deduce the level scheme shown in Figure E-1. Transitions marked with an asterisk are components of closely spaced (<0.5keV) multiplets.

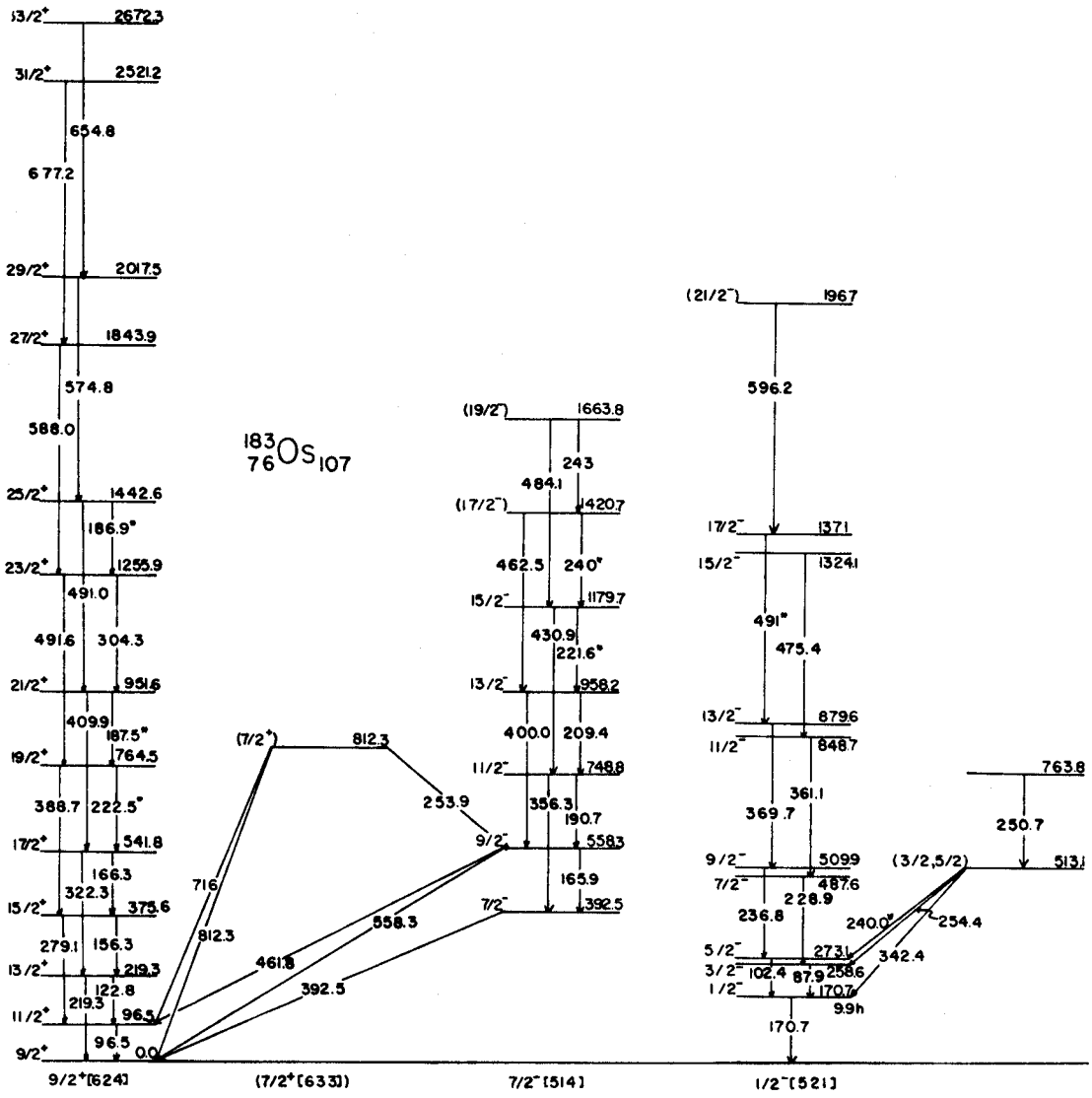

Figure E-1. Level scheme of ^{183}Os.